Center for Theoretical Physics

Polish Academy of Sciences

Few dipolar atoms

by

Rafał Ołdziejewski

A thesis submitted to the Center for Theoretical Physics of the

Polish Academy of Sciences in accordance with the requirements

for the degree of Doctor of Philosophy

in Physics

Thesis written under the supervision of

prof. dr hab. K. Rzążewski and

dr K. Pawłowski

May 2019

to my family

Summary

The thesis describes the influence of dipolar interactions on the properties of many-body systems from a theoretical point of view. Its main goal is to analyze the consequences of the interplay between the local and non-local parts of interactions between atoms. The thesis puts special attention on stronger interactions beyond the applicability of the usual mean-field approaches. The presented study focuses mainly on one-dimensional models.

In Chapter 1, we briefly review the history of studies on ultracold gases with emphasis on dipolar atoms examples. We embed the subjects of the thesis in the context of ongoing research in the field.

Chapter 2 introduces the theoretical framework needed in the later parts of the thesis. That includes discussion of some general properties of the many-body systems and two-body interactions in the ultracold limit. It recalls the well-know mean-field description of ultracold gases.

Chapter 3 presents properties of two dipolar atoms moving in a harmonic trap without an external magnetic potential. It is possible to adiabatically pump the system from the s-wave to the d-wave relative motion.

Chapter 4 compares the mean-field dark solitons and the lowest energy states for fixed total momentum of the corresponding many-body system of weakly interacting bosons. The bosonic symmetrization is responsible for emergence of solitonic features even in the limit of vanishing interactions.

Chapter 5 studies bosons interacting via attractive short-range and repulsive dipolar forces. It shows that the lowest excitations of the system may be smoothly transformed from the typical states of collective character to the celebrated roton state by simultaneous tuning short-range interactions and adjusting a trap geometry.

Chapter 6 describes a transition between droplet-like and bright soliton-like states at the border of net attractive and repulsive interactions for a small number of atoms and strong interactions. Based on that, it introduces a new version of the Gross-Pitaevski equation.

Chapter 7 presents a microscopic model of two-body wave function diagnosis based on atom-light interactions. In particular, it discusses the influence of pulse properties on the absorption of photons by two identical atoms moving in a trap.

The last Chapter 8 summarizes the thesis and outlines some possibilities of extending the presented results.

Acknowledgements

Chciałbym serdecznie podziękować moim Promotorom, prof. dr hab. Kazimierzowi Rzążewskiemu oraz dr hab. Krzysztofowi Pawłowskiemu za opiekę naukową oraz liczne wskazówki i uwagi, które znacznie poprawiły jakość niniejszej rozprawy.

Prof. Rzążewskiemu w szczególności dziękuję za szeroko otwarte drzwi do swojego gabinetu, w którym cierpliwie tłumaczył mi wszelkie niejasności związane z prowadzonymi przeze mnie badaniami. Jego liczne anegdoty na temat świata fizyków i nie tylko tworzą unikalną atmosferę pracy– pełną otwartości i życzliwości.

Dr Krzysztofowi Pawłowskiemu jestem niezmiernie wdzięczny za krytyczne uwagi dotyczące mojej rozprawy oraz niestrudzone dążenie do pełniejszego zrozumienia wszystkich wyników otrzymanych w trakcie moich badań. Krzysiek nauczył mnie, że tworzenie nauki to przygoda, w której odpowiedzialność za swoje działania ponosi się przede wszystkim przed samym sobą.

Niniejsza rozprawa przyjęłaby bez wątpienia uboższy kształt, gdyby nie udział Wojtka Góreckiego w pracach naszego zespołu. Jego analityczne zdolności, dociekliwość, zaangażowanie oraz dbałość o szczegóły na poziomie fizyki matematycznej niezmiernie wzbogacały nasze wspólne badania, a także ożywiały nasze naukowe dyskusje. Wojtkowi zawdzięczam przykład jakim członkiem zespołów naukowych czy innych społeczności chciałbym zawsze być.

Dziękuję Krzyśkowi Jachymskiemu za wprowadzenie mnie w świat kwantowych kropli oraz pokazanie mi, że prace naukowe można pisać nie tylko ze swoimi zwierzchnikami, ale również z kolegami. Moje wyobrażenia o piwie uległy nieodwracalnemu przekształceniu od kiedy Krzysiek wprowadził mnie do świata kwaśnych Lambiców i mlecznych Stoutów.

Jestem niezmiernie wdzięczny moim serdecznym kolegom ze studiów na FUWie Tomkowi Maciążkowi, Michałowi Parniakowi i Michałowi Papajowi, z którymi prowadziliśmy regularne spotkania służące "klepaniu zadanek i zarządaniu wrogimi przejęciami". Dziękuję również Michałowi Stękielowi i Maćkowi Karczmarczykowi za wspólną walkę na kursie z Fizyki Statystycznej, a także za wiele inspirujących rozmów.

Moje studia byłyby dużo mniej barwne i satysfakcjonujące, gdyby nie koledzy z Centrum Fizyki Teoretycznej, a w szczególności ekipa obiadowa. Narzekanie na niski stosunek jakość/cena jedzenia, a także luźne rozmowy na wszelkie tematy od polityki grantowej po reformę służby zdrowia stanowiły ważny punkt dnia podczas pracy w Centrum.

Dziękuję wszystkim moim kolegom i przyjaciołom spoza świata nauki za utrzymywanie mnie na powierzchni Ziemi i przypominanie, że istnieją poważniejsze problemy niż testowanie zbieżności obliczeń numerycznych. Sprawiliście, że spokojnie mogę uznać Warszawę ze dzielnicę Białegostoku.

Żadne piękne słowa nie oddadzą tego, jak bardzo jestem wdzięczny całej mojej Rodzinie za wszystko co jej zawdzięczam i co od niej dostaję. Nie mogę nie wspomnieć o moich Rodzicach, którzy wychowali mnie w absolutnym poczuciu bezpieczeństwa i wolności życiowych wyborów.

W szczególności dziękuję mojej Mamie za trudy samotnego wychowywania mnie i mojego Brata oraz za przykład człowieka wiernego swojemu sumieniu. Dziękuje mojemu Bratu za bycie moim najsurowszym krytykiem i jednocześnie największym sprzymierzeńcem.

Pragnę podziękować mojej Żonie za bycie moim zwierciadłem, moją inspiracją i moim oparciem. Twój jeden ironiczny żart na mój temat uczy mnie więcej niż niejeden kurs. Dzięki Tobie jestem nieskończenie lepszym i ciekawszym człowiekiem.

Na koniec chciałbym również podziękować Narodowemu Centrum Nauki za wsparcie finansowe – granty *Opus* nr $2015/19/B/ST2/02820$ oraz *Preludium* nr $2016/21/N/ST2/03432$.

List of Publications

The present thesis is mostly based on the following works that have appeared in print elsewhere:

1. R. Ołdziejewski, W. Górecki, K. Rzążewski, *Two dipolar atoms in a harmonic trap*, Europhys. Lett. 114, 46003 (2016) (Chapter 3)

2. R. Ołdziejewski, K. Rzążewski, *Diagnosing a two-body state of ultracold atoms with light*, Europhys. Lett. 119, 46002 (2017) (Chapter 7)

3. R. Ołdziejewski, W. Górecki, K. Pawłowski, K. Rzążewski, *Many-body solitonlike states of the bosonic ideal gas*, Phys. Rev. A 97, 063617 (2018) (Chapter 1, 2 and 4)

4. R. Ołdziejewski, W. Górecki, K. Pawłowski, K. Rzążewski, *Roton in a few-body dipolar system*, New J. Phys. 20, 123006 (2018) (Chapter 1, 2 and 5)

5. R. Ołdziejewski, W. Górecki, K. Pawłowski, K. Rzążewski, *Novel droplet-soliton phase transition in quasi-1D dipolar bose gas*, in preparation (Chapter 6)

During PhD studies the author contributed also to other publications:

1. R. Ołdziejewski, K. Jachymski, *Properties of strongly dipolar Bose gases beyond the Born approximation*, Phys. Rev. A 94, 063638 (2016)

2. K. Jachymski, R. Ołdziejewski, *Nonuniversal beyond-mean-field properties of quasi-two-dimensional dipolar Bose gases*, Phys. Rev. A 98, 043601 (2018)

3. W. Golletz, W. Górecki, R. Ołdziejewski, K. Pawłowski, *Dark solitons revealed by particle losses in the 1D Bose gas*, arXiv preprint arXiv:1905.04604 (2019)

List of Figures

Contents

Chapter 1

Introduction

The very first encounter with quantum physics blurs the classical concept of an atom almost literally. A billiard ball picture gives way to a nonintuitive wave-particle duality description. The second strike to an enthusiast of the quantum theory comes from the fact that within it all particles are indistinguishable. This gives rise to quantum particle statistics predicting bosons (integer spin particles) and fermions (half-integer spin particles).[1]

As in the classical world, but with new difficulties mentioned above, quantum physics branches into two main categories of phenomena: the one-body problem and the many-body problem. Indeed, all two-body models reduce to the former by the center of mass separation. Moreover, in some cases, the picture of a single atom immersed in the field produced by the rest of the particles well represents the most important properties of a system with a large number of particles. We call such a regime the mean-field regime. Usually, the three-body problem is already intractable analytically, not to mention the system with dozens of atoms.

The efforts in this thesis swirl around the many-body problems in the context of ultracold dipolar atoms. Owing to the recent experimental advances, it is now possible to probe these complex systems. Still, there is a lot to do from both theoretical and experimental perspectives.

1.1 Ultracold gases and Bose-Einstein condensate

Owing to wave-particle duality every particle with a momentum k is associated with a matter wave characterized by its wavelength dubbed de Broglie wavelength $\lambda_{\mathrm{dB}} = \frac{h}{k}$. For any massive body (with mass m) in an ensemble with equilibrium temperature T, it reads

$$\lambda_{\mathrm{dB}} = \sqrt{\frac{2\pi\hbar^2}{mk_{\mathrm{B}}T}} \tag{1.1}$$

The number of atoms occupying the volume element λ_{dB}^3, known as the phase space density, is $v = n\lambda_{\mathrm{dB}}^3$ with n denoting the number density. It is small for gas in the room temperature, but as we see from Eq. (1.1), decreasing temperature makes the phase space density growing. At some point, $v \sim 1$, the spatial extent of the wavepacket becomes of the same order of magnitude as the

[1] Note, that in two dimensions also anyonic statistics may appear.

average distance between atoms. Accordingly, the system stands in the gate of the realm of the degenerated quantum gas, where the quantum statistics starts to play a crucial role. We are going to focus on Bose gases leaving the introduction to the degenerate Fermi gases to extensive reviews, see for instance [1] and references therein.

(Probably) every physicist knows (or should know) about the historical origins of the Bose-Einstein statistics [2]. In the letter to Albert Einstein in 1924, Satyendra Nath Bose derived Planck's empirical formula for black-body radiation evoking to the concept of indistinguishable photons.[2] With Einstein's blessing and translation to German, the paper was published and then followed by its generalization for massive particles in the ideal gas done by Einstein. In Einstein's second paper on the subject [5], he envisaged that when the phase space density exceeds a critical value, for the ideal gas $v_{\rm cr} \approx 2.612$, almost all bosons would occupy the lowest single-particle state. Therefore, a many-body system would behave, no matter how big it would be, like a single particle. The same way as for the laser, the purely quantum effect leads to macroscopic coherence. Note, that Bose-Einstein condensation is a peculiarity of the quantum statistics only.

At first, considered as a minor theoretical curiosity at times of early quantum mechanics development, BEC was brought back into the scientific discussion by London and Tisza in the context of superfluidity [6, 7]. Over the years, BEC phenomenon was also studied in a diversity of topics in condensed matter, subatomic physics, and astrophysics, including superconductivity or neutron stars [8]. A lack of BEC experimental realization became an obstacle in further investigations.

One can reach the critical phase space density of gas only in the limit of extremely low (high) temperatures and real-space densities. Densities of the neutron stars are impossible to access in terrestrial laboratories. On the other hand, we expect a solid state rather than a gas in the ultracold limit even for a weakly interacting one as the ideal gas does not exist in nature. [3] Probability of three-body recombination process, responsible for solidification, scales as n^3, whereas two-body scattering yielding thermalization occurs with a rate proportional to n^2. A gaseous probe has to be five orders of amplitude more dilute than the air to overcome recombination. In that case, one needs to cool the probe under 1 μK to achieve the critical phase space density of BEC and to devise smartly a container of gas, because containers made of material could disrupt cooling. These tight requirements resulted in enormous advances in the field of cooling and trapping atoms [9–11]. Finally, the first BEC was observed in 1995 opening a new era in ultracold physics [12, 13]. Then, observation of Feshbach resonances [14] and mastery in using them enhanced a number of new experiments with BEC greatly. We refer the reader to excellent and comprehensive reviews devoted to the development of the field, for example [15–17], to name only few. Nowadays, the ultracold gases serve as a versatile test-bed for different theories in many other fields of physics like condense matter and also as an upgrade of technologies based on quantum mechanics like quantum metrology, quantum computers or atomic clocks [18].

[2] The concept of the indistinguishable particles was considered for the first time by Władysław Natanson in [3, 4] in 1911. However, these works did not formulate the statistic itself and did not go down in a broad scientific discourse.

[3] Even if the ideal gas had existed in reality, it would have not thermalized. To cool down a system, one needs interactions.

Although Goral et al. in [19] provided with the first theoretical description of condensate with long-range dipolar interactions in 2000, the early BEC experiments were conducted with elements that effectively interact only short-range and dipolar forces were negligible.[4] With a pioneering condensation of ^{52}Cr [23, 24] followed by ^{164}Dy [25], and ^{162}Dy and ^{160}Dy [26] and ^{168}Er [27] much of the physics was enhanced as these elements posses significant permanent magnetic moments (6-10 μ_{B}) while for instance ^{87}Rb only $1\mu_{\mathrm{B}}$. A comprehensive review on the first experiments with dipolar BEC, including observation of the first quantum ferrofluid [28], is written by Lahaye et al. [29]. A lot of work with dipolar atoms was also done in the context of optical lattices simulating different models from condensed matter, for instance in [30–32] and references therein. Precise control over the strength of short-range interactions allows studying thoroughly the interplay between them and long-range dipolar interactions. In a recent series of groundbreaking papers, self-bound dipolar droplets [33, 34], as well as roton excitation [35] followed by the detection of dipolar supersolid were reported [36–38]. Dipolar systems have still many to reveal. We need ongoing theoretical effort to properly describe those systems because they pose a lot of difficulties as dipole-dipole interactions are anisotropic and long-range. Now, we will describe them briefly following the review paper by Lahaye et al. [29].

1.2 Dipolar interactions

The general form of dipole-dipole interaction (DDI) in the absence of an external magnetic field reads:

$$U_{\mathrm{dd}}(\boldsymbol{r}) = \frac{C_{\mathrm{dd}}}{4\pi} \frac{(\boldsymbol{e}_1 \cdot \boldsymbol{e}_2)\, r^2 - 3\,(\boldsymbol{e}_1 \cdot \boldsymbol{r})\,(\boldsymbol{e}_2 \cdot \boldsymbol{r})}{r^5}, \tag{1.2}$$

where $\boldsymbol{e}_i$ denotes the orientation of dipole i and $\boldsymbol{r}$ is a vector joining two dipoles with $r = |\boldsymbol{r}|$. The strength of dipole interactions C_{dd} depends on whether dipoles are magnetic or electric. For magnetic atoms $C_{\mathrm{dd}} = \mu_0 \mu^2$ with μ_0 being the vacuum permeability and μ is a magnetic dipole moment (see [29] for values for different elements) depending on the total spin of an atom (see Chapter 3.2). For electric dipoles $C_{\mathrm{dd}} = \frac{D^2}{\epsilon_0}$ with D being electric dipole moment and ϵ_0 is the vacuum permittivity.[5]

In most experiments with ultracold physics, a strong external magnetic field is applied to the probe in order to trap particles. Atoms are polarized and $\boldsymbol{e}_1 = \boldsymbol{e}_2$ accordingly. In that scenario, the DDI can be written as

$$U_{\mathrm{dd}}(\boldsymbol{r}) = \frac{C_{\mathrm{dd}}}{4\pi} \frac{1 - 3\cos^2\theta}{r^3}, \tag{1.3}$$

where θ is the angle between the direction of polarization and the relative position of the particles. In Fig. 1.1 a) and b) from [29] we see a schematic view of dipolar interactions showing its anisotropic nature. Mathematically DDI are long-range in 3D and non-local in lower dimensions (for detailed discussion see [39]).

[4] However, the dipolar interactions, even comparably small, turned to be crucial in understanding the physics of the ^{87}Rb F = 1 spinor BEC [20–22].

[5] In this Thesis, we focus solely on magnetic atoms. See [29] to learn more about polar molecules, Rydberg atoms etc.

In a constrained geometries polarized dipoles may be ordered in any configuration between two limiting configurations: repulsive side-by-side configuration with $\theta = \frac{\pi}{2}$ and attractive head-to-tail configuration with $\theta = 0$ (see Fig. 1.1 c) and d) respectively). We remind, that for $\theta \approx 54^\circ$ the DDI vanish.

We will see in Chapter 3, that the DDI couple internal (spin) and external (orbital) degrees of freedom. A celebrated example of this is the Einstein-de Haas effect. In the original version of the experiment [40], the authors observed how a ferromagnetic cylinder suspended on a thin string rotated around its own axis after the applied magnetic field had changed. The system reacted to the field change by changing the orientation of the magnetic moments in the atoms (the projection of the spin component changed). The rotation of the system is a simple result of the total momentum conservation. In Chapter 3 we will return to this phenomenon in the context of ultracold gases.

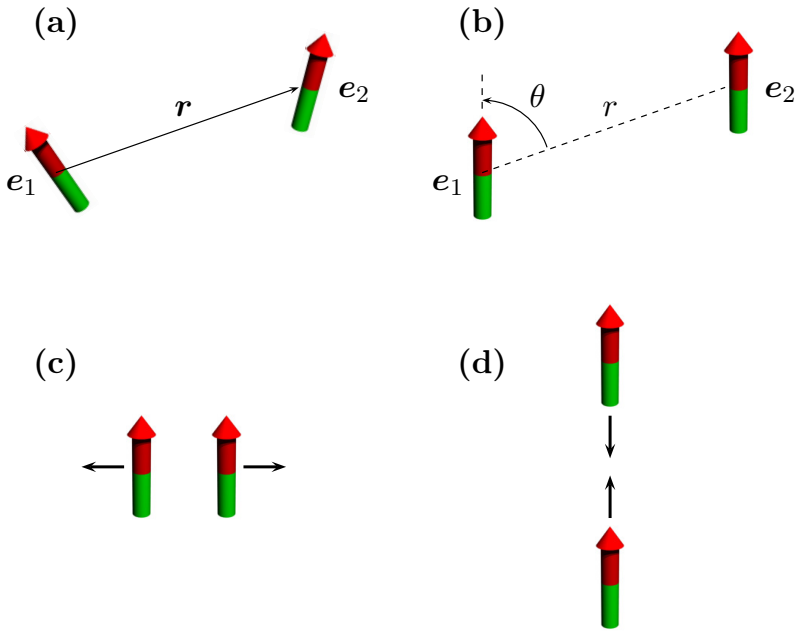

Figure 1.1: Dipole-dipole interactions. a) Non-polarized case. b) Polarized case. c) Repulsive side-to-side configuration. d) Attractive head-to-tail configuration. All rights reserved [29]

1.3 Ultracold gas in lower dimensions

As we pointed out earlier dipolar BECs introduced a new twist to the field of ultracold gases. A plethora of experiments and theoretical results in three dimensions both for dipolar and alkali gases do not drain all possibilities. Now, we restrict the dynamics of an ultracold gas to one dimension.[6] In experiments, one can tightly confine the gas in chosen directions (see also Chapter 2.2.2). In the next section, we will discuss three physical phenomena, which are particularly important in the context of this Thesis.

[6]In one dimension there is no actual BEC according to the modern definition of the BEC state for interacting gases given by Penrose and Onsager in 1956 [41]. However in general, in the limit of ultra-low temperatures and weak interactions, the one-dimensional many-body system fulfills criteria for the mean-field description with the GPE.

The most common way to describe a BEC in the vicinity of zero-temperature is by the integro-differential Gross-Pitaevskii equation (GPE) [42, 43]

$$i\hbar\partial_t\psi_{\mathrm{GPE}}(x,t) = \left(-\frac{\hbar^2\partial_x^2}{2m} + N\int dx'\, U_{\mathrm{eff}}(x-x')|\psi_{\mathrm{GPE}}(x',t)|^2\right)\psi_{\mathrm{GPE}}(x,t), \tag{1.4}$$

where U_{eff} is an effective potential in the ultracold regime with both local and non-local interactions described in Chapter 2.2. In the context of atoms it is the so called mean-field (MF) description of the weakly interacting bosons [44]. We will briefly derive this equation in Chapter 2.5.1. The mean-field description of an ultracold system in one dimension provides with an inexhaustible wealth of theoretical outcomes and experimental hints about the properties of ultracold gases. It would be almost impossible to list them all in the finite framework of this thesis. However, we compactly introduce and discuss topics that will arise in the later Chapters.

Soliton It is hard to list all important features, discoveries and applications associated with solitons. These mathematical objects, certain types of solutions of nonlinear integrable differential equations, were found in many areas of Science, ranging from physics to biology and medicine. There is a number of known equations supporting the solitonic solutions. In physics, very important

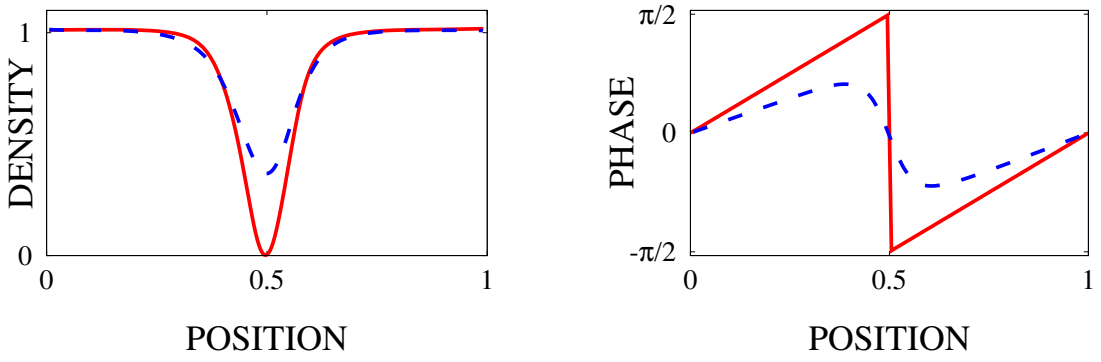

Figure 1.2: Sketch of density (left) and phase (right) of dark solitons in a box with periodic boundary conditions. The solid red lines correspond to the extreme situation of a black soliton - its density vanishes at the center, whereas the phase has a π jump. The blue dashed lines correspond to an example of a gray soliton with the minimal density 0.36. Position is in the box units (see Chapter 4).

examples are the Korteweg-de Vries equation [45], Sine-Gordon equation [46, 47] and the GPE. Here, we focus on the contact interacting gas where $U_{\mathrm{eff}}(x) \sim \delta(x)$ wih the corresponding GPE:

$$i\hbar\partial_t\psi_{\mathrm{GPE}} = \left(-\frac{\hbar^2\partial_x^2}{2m} + gN\,|\psi_{\mathrm{GPE}}|^2\right)\psi_{\mathrm{GPE}} \tag{1.5}$$

where g is the coupling strength (see Chapter 2.2.1). This equation has also proved to be useful to describe the electric field of light in the non-linear media [48].

The solitonic solutions of Eq. (1.5) were derived already in the 70s by A. Shabat and V. Zakharov [49, 50]. We recall the main finding for the positive coupling strength, $g > 0$. In this case the spatial density in the soliton has a single characteristic notch. Within the area of the notch

the phase of ψ_{GPE} is quickly changing. In the extreme situation, the density in the middle of the soliton is zero and the phase has a π jump. The width of the soliton is given by the healing length $\xi = 1/\sqrt{gn}$. The properties of dark solitons are illustrated in Fig. 1.2. Shortly after cooling atoms down to the Bose-Einstein condensate regime, also the solitons have been generated [51–53]. In the present days solitons are routinely produced with the phase imprinting method in many laboratories around the world. In this Thesis, we will discuss the Lieb-Liniger model underlying the dark solitons in a BEC phenomenon in Chapters 2.3.1 and 4.

Recent findings of groups from Poland and Great Britain [54–56] shows that some solutions of the GPE with dipolar interactions also displays features of dark solitons. However, the GPE in this scenario is not integrable, which affects vastly the dynamics and properties of the system.

In the attractive case with $g < 0$ a solution to Eq. 1.5 takes a form of bright solitons. They have a sech-shaped profile and they are more common in nature than dark solitons. As in the dark soliton case, there exists a dipolar analog of the usual bright soliton with many similar properties. We refer the reader to [57] for a very comprehensive introduction to solitons in ultracold gases.

Rotons In the contact interacting ultracold gas low-lying excitations described by the Bogoliubov approximation feature phonons and free-particle only. A bit different situation takes place with a dipolar gas where the roton minimum may appear. Before we refer to the rotons in an ultracold gas, we present a brief history of this excitation in the context of experiments with ultracold Helium.

In the 30s of the last century, Allen and Misener [58] and Kapitza [59] discovered unusual properties of the Helium-II followed by first theoretical attempts in explaining them [6, 7]. The qualitative theory of superfluidity is due to Landau [60–62]. He deduced from the measurement of the specific heat [63] and the second sound velocity [64] that the excitations in the Helium-II must have a peculiar spectrum [62] with the local minimum dubbed "roton". Later Feynman alone [65] and with Cohen [66] formulated the very first, yet semiquantitative microscopic model explaining the origin of this local minimum. Finally, in Helium the roton was observed experimentally [67], but rather unsatisfactory agreement between theory and measurement suggested that the exact nature of the rotonic excitation was still missing. It was finally understood many years later by means of subtle ansatzes for the roton's wave function [68, 69]. The existence and properties of the roton were also discussed in depth in studies of excitations of thin liquid-helium films [70–72]. It should be emphasized that liquid Helium-II is a strongly correlated (with a small condensate fraction) system, where roton's characteristic momentum scales as the interatomic distance. There are still active studies of the roton state in this regime [73].

At the beginning of XXI century the roton-maxon spectrum was predicted in completely different physical system – trapped dipolar gas of polarized ultracold atoms. The nature of the roton in ultracold gases is very different than the one in Helium (see [74] for detailed discussion). Here it is induced by the interplay between the long-range forces and a steep external potential in the polarization direction [75, 76]. Without an external potential the system is unstable, as the dipoles would first tend to the head to tail configuration and then they will just fall on each other due to the attractive part of the dipolar interaction. The system may be stabilized by the steep external potential, which blocks the motion in the direction of the dipoles' polarization. Roton emerges

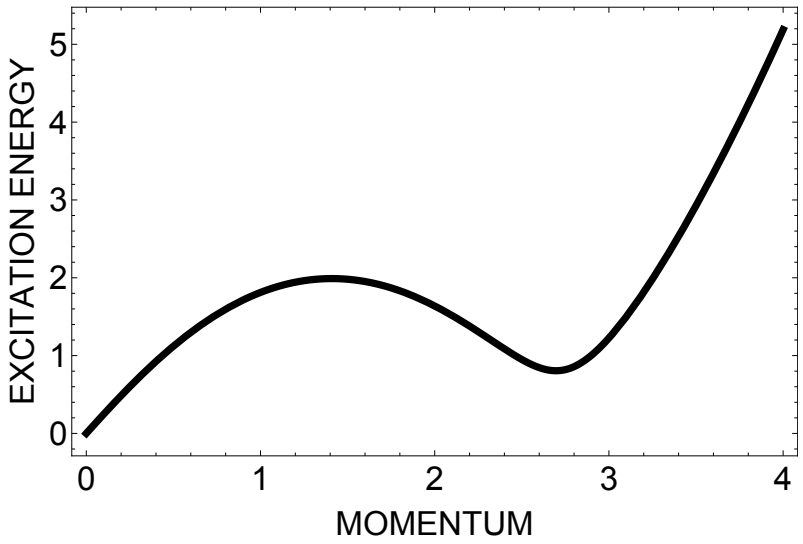

Figure 1.3: Sketch of a typical dispersion relation with a roton minimum in a trapped ultracold dipolar gas. The position and depth of the minimum can be tuned in the experiments [38]. Energy and momentum in the box units introduced in Chapter 5.

for parameters close to collapse, for which dipoles are close to overcome the trapping forces. In this situation atoms cluster into 'clumps', regularly separated by a period corresponding to inverse of the roton momentum [77]. This happens for relatively weak interactions, for which the system is in the Bose-Einstein condensate state. Therefore, one can use the mean field or Bogoliubov description and find the roton state as a Bogoliubov quasi particle [75–94]. The dispersion curve of such systems is related to a specific k-dependence of an effective interaction potential rather than to strong correlations. Possibility of changing the particles polarization as well as almost free tuning of the short range interactions combined with the trap geometry modifications enables unprecedented flexibility in the study of the roton spectrum in dipolar gases ending with a recent experimental confirmation of the phenomenon [35].

Droplet Recent experiments with highly magnetic dipolar atoms discovered a new self-bound liquid state for atom number densities that are 10^8 lower than in a helium liquid. The existence of such dilute droplets was suggested earlier in the context of Bose-Bose mixture [95]. In the very first experiments, the three-dimensional condensate with long-range magnetic dipolar interactions and tunable short-range interactions was quenched into the unstable regime from the MF perspective i.e. attractive and repulsive forces were of the same order and almost canceled out each other. A gas formed a spatially ordered collection of stable droplets with a higher density than usual condensate [96–98]. These quantum droplets are self-bound i.e. they are stable even without any external trapping potential [33, 34, 99, 100]. One has to include beyond mean field Lee-Huang-Yang (LHY) correction, which scales as $n^{3/2}$, into the GPE which provides an additional effectively repulsive term preventing the gas from collapsing to describe the droplet theoretically. The LHY correction for dipoles is much stronger and includes some additional subtleties compared to contact interactions [78, 101–103]. Note, that in the dipolar community there is an ongoing discussion

whether LHY corrections account for all properties of droplets. In a new paper [104], the authors argue about that hypothesis.

In the case of Bose-Bose mixtures droplets were also predicted in lower dimensions [105] on the same footing of LHY corrections, which has a different form for 1D and 2D systems. For dipolar atoms, the calculations are not as straightforward. In two dimensions the LHY term is nonuniversal [106], whereas for one dimension it was calculated numerically for some parameters of the system [107]. Additionally, an analog of droplets stabilized by LHY term exists in the so-called Tonks-Girerdeau limit [108] (See Chapter 6), where the contact interactions are infinitely strong.

1.4 Many-body physics

It is possible to study many-body systems in modern experiments with ultracold gases distributed between the wells of an optical lattice [16]. This way, with a help of tunable parameters of interaction, using the Feshbach resonances [14, 109], and the properties of the lattice itself, one can access in a controlled way vital models of condense matter physics - for a recent review see [31]. Usually, such systems interact strongly. One needs an actual many-body description encoding the information about all the correlations between particles, instead of the MF theory accounting for mutual correlations between particles only partially by nonlinearity in a corresponding GPE.

Modern experiments entered also into the one-dimensional realm due to the cigar-shaped traps. As the role of interactions in one dimension is special and tools from higher dimensions do not necessarily apply for stronger interactions, theorists have been developed different techniques and concepts [110]. Many one-dimensional problems were solved by means of Bethe Ansatz (for a review see [111, 112] and references therein). The historically earliest example is the famous Lieb-Liniger model [113, 114] comprising of N contact interacting bosons moving on the circle (see Chapter 2.3.1). Their seminal analytical solution predicts two branches of elementary excitations, which was also observed experimentally [115, 116]. There is the puzzling link between the mean-field solitons introduced in Section 1.3 and solutions of the underlying many-body Lieb-Liniger model. More than a decade after the seminal paper of Lieb, a coincidence between the dispersion relations of dark solitons and of so called type-II elementary excitations from the many body description [117, 118] has been noticed. The further relations between type-II eigenstates and solitons were presented in [119–127].

Little is known about the classification of the exact many-body eigenstates in one-dimensional dipolar gas. For (quasi)-1D model with bosons interacting only by repulsive dipolar interactions the lowest energy states resemble rather type- II excitations known from the Lieb-Liniger model [128]. The picture gets vague even more if one adds the short-range interactions to the final mix. Particularly interesting questions appear about the relationship between many-body eigenstates for such a system and the corresponding approximated theory.

1.5 Thesis overview

The main goal of this thesis is to contribute to the better understanding influence of dipolar interactions on the many-body systems in constrained geometries. A lot of condensed matter theories simulated in one-dimensional optical lattices deals with a very small number of particles trapped in a single well. We will put special attention to stronger interactions that require an extended description beyond the usual mean-field approaches. In the end, we will also check the applicability of the standard measurement methods used for large systems in the case where only a few atoms are present in a probe. Without doubts, the dipolar and many-body physics abounds in many interesting phenomena and only a few topics are studied in this dissertation. We organize the work in the following way:

- In this chapter, we present a brief review of ultracold physics with emphasis on dipolar examples. We start with some basic facts about BEC. Then, we shortly discuss dipolar interactions and their consequences. We mainly focus on one-dimensional examples. Finally, we briefly recap some many-body aspects important from the perspective of this thesis.

- Chapter 2 introduces the basic concepts and methods used in the later course of this thesis. We discuss some general properties of the many-body system and two-body interactions, mainly in the context of one-dimensional problems. Finally, we recall the mean-field description of ultracold gases.

- In Chapter 3, we investigate two dipolar atoms moving in a harmonic trap without an external magnetic field. In particular, we study the anisotropic characteristic of dipolar forces. Namely, we show that the internal spin-spin interactions between the atoms couple to the orbital angular momentum causing an analog of the Einstein-de Haas effect. It is possible to adiabatically pump our system from the s-wave to the d-wave relative motion. We also observe anti-crossings of energy levels.

- Chapters 4-6 focuses on atoms moving on the circumference of a circle. In particular, we devote Chapters 5-6 to the study of the interplay between local and non-local interactions for different polarization of dipoles in that geometry. We dedicate Chapter 4 for comparison between mean-field dark solitons and the lowest energy states for fixed total momentum of the many-body system of weakly interacting bosons for either contact or purely dipolar interactions. Solitonic features like phase jumps and density notches emerges even in the limit of vanishing interactions. We show that these properties are simply effects of the bosonic symmetrization whose consequences we study in dynamics and systems where interactions are relevant.

- In Chapter 5, we study bosons interacting via attractive short-range and repulsive dipolar forces (side-to-side configuration) both in weakly interacting regime as well as the regime beyond the range of validity of the Bogoliubov approximation. We show that the lowest energy states with fixed total momentum can be smoothly transformed from the typical states of collective character to states resembling single-particle excitations, in particular, the

celebrated roton state. We realize transition by simultaneous tuning short-range interactions and adjusting a trap geometry.

- Chapter 6 concentrates on studying the ground-state of N bosons interacting via repulsive short-range and attractive dipolar forces (head-to-tail configuration). Notably, we observe a transition between droplet-like and bright soliton-like states at the border of net attractive and repulsive interactions for a small number of atoms and stronger interactions. In the second part, we propose a new version of the GPE without LHY corrections for larger systems. We provide with a diagram showing novel droplet-soliton transition.

- In Chapter 7, we investigate a very simple microscopic model of two-body wave-function diagnosis based on atom-light interactions. We study an absorption of a weak pulse by two identical atoms moving in a trap. Especially, we study the influence of pulse properties on the results. We report a significant impact of pulse duration on the resulting one-photon and two-photon absorption probabilities.

- Chapter 8 recaps the thesis pointing out its main achievements. In the end, we discuss future perspectives concerning the results presented in this dissertation.

Chapter 2

Theoretical framework and methods

In this Chapter we introduce basic theoretical concepts and analysis methods used in this thesis. We start with a few general properties of a many-body bosonic system. Then, we shortly discuss two-body interactions- short-range potential in an ultracold limit and dipole-dipole forces in a 1D space. After that, we turn our attention to atoms moving on a circumference of a ring as it is the main geometry considered in this thesis. We recall the seminal Lieb-Liniger (LL) model and shortly discuss the ideal gas spectrum afterward. Finally, we present methods used in this thesis to access spatial properties of a many-body system on a ring.

In the second part of this Chapter, we briefly discuss the mean-field description of ultracold bosons. We recall the famous Gross-Pitaevskii equation (GPE) describing a macroscopically occupied orbital. Some of the energetically low excitations of the ultracold gas are aptly characterized by the well-known Bogoliubov approximation. Here, we present a version of it with the conservation of particles number.

2.1 General properties of many-body systems with two-body interactions

2.1.1 Many-body Hamiltonian in second quantization

We examine bosonic systems, which consist of N atoms. Any state vector describing such system is symmetric under exchange of any two particles. In the framework of second quantization, one uses a Fock state representation instead of a full many-body wave-function $\psi_N(\boldsymbol{x}_1, ..., \boldsymbol{x}_N)$ with $\boldsymbol{x}_i$ standing for the position of an i-th particle. A single Fock state is usually expressed as $|\{n\}_i\rangle = |n_0, n_1, ...\rangle$ where n_i is an occupation number of a single particle state $\phi_i(\boldsymbol{x})$ from a proper single-particle basis $\{\phi_i(\boldsymbol{x})\}$. We study only models in which the number of atoms is conserved, $\sum_{i=0} n_i = N$. All vectors $|\{n\}_i\rangle$ form an orthonormal basis $\{|\{n\}_i\rangle\}$ for a symmetric subspace with fixed N of the Fock space. In this language, a general bosonic state with N particles is a superposition of Fock states, namely:

$$|\Psi\rangle = \sum_i c_i |\{n\}_i\rangle \tag{2.1}$$

with c_i standing for the expansion coefficients.

We assume systems considered in this thesis dilute and ultracold. Therefore, we can restrain interactions in our analysis to only two-body level[1] and only use a simplified version of the interaction potential. The presence of ultra-low temperatures also justifies our interest in the lowest eigenstates of the system in the later parts of the thesis.

In this case, the many-body Hamiltonian in second quantization can be expressed in space representation as

$$\hat{H} = \int d\boldsymbol{x} \hat{\psi}^\dagger(\boldsymbol{x}) \hat{H}_1 \hat{\psi}(\boldsymbol{x}) + \frac{1}{2} \int d\boldsymbol{x} \int d\boldsymbol{x}' \, \hat{\psi}^\dagger(\boldsymbol{x}) \hat{\psi}^\dagger(\boldsymbol{x}') U(\boldsymbol{x} - \boldsymbol{x}') \hat{\psi}(\boldsymbol{x}') \hat{\psi}(\boldsymbol{x}), \tag{2.2}$$

where $\hat{\psi}(\boldsymbol{x})$ ($\hat{\psi}^\dagger(\boldsymbol{x})$) are the standard Bose field anihilation (creation) operators defined as

$$\hat{\psi}(\boldsymbol{x}) = \sum_i \phi_i(\boldsymbol{x}) \hat{a}_i \tag{2.3}$$

$$\hat{\psi}^\dagger(\boldsymbol{x}) = \sum_i \phi_i^*(\boldsymbol{x}) \hat{a}_i^\dagger \tag{2.4}$$

with $\hat{a}_i$ ($\hat{a}_i^\dagger$) bosonic anihilation (creation) operators. We remind that the Bose field operators obey the following commutation relation

$$\left[\hat{\psi}(\boldsymbol{x}), \hat{\psi}^\dagger(\boldsymbol{x}) \right] = \delta(\boldsymbol{x} - \boldsymbol{x}'). \tag{2.5}$$

The single particle Hamiltonian can be written in general as

$$H_1(\boldsymbol{x}) = -\frac{\hbar^2}{2m} \nabla^2 + U_1(\boldsymbol{x}), \tag{2.6}$$

where m stands for a single particle mass and $U_1(\boldsymbol{x})$ for the external (including trapping) potential. In this thesis we mainly study the interplay between short-range and long-range interactions, therefore two-body interaction potential can be decomposed as $U(\boldsymbol{x} - \boldsymbol{x}') = U_{\mathrm{SR}}(\boldsymbol{x} - \boldsymbol{x}') + U_{\mathrm{LR}}(\boldsymbol{x} - \boldsymbol{x}')$. We return in shortly to discuss specific forms of potentials considered in this work.

2.1.2 Average energy

We want to express the average energy of any state of the system $|\Psi\rangle$ described by Eq. 2.2. We assume the absence of any external potential, $U_1(\boldsymbol{x}) = 0$, that holds for most of the cases in this thesis. By straightforward calculation of $\langle \psi | \hat{H} | \psi \rangle$, one can show that it equals to

$$\left\langle \hat{H} \right\rangle = -\frac{\hbar^2}{2m} \int d\boldsymbol{x} \langle \hat{\psi}^\dagger(\boldsymbol{x}) \nabla^2 \hat{\psi}(\boldsymbol{x}) \rangle + \frac{1}{2} \int d\boldsymbol{x} d\boldsymbol{x}' \, G_2(\boldsymbol{x}, \boldsymbol{x}') U(\boldsymbol{x} - \boldsymbol{x}'), \tag{2.7}$$

where

$$G_2(\boldsymbol{x}, \boldsymbol{x}') := \langle \Psi^\dagger(\boldsymbol{x}) \Psi^\dagger(\boldsymbol{x}') \Psi(\boldsymbol{x}') \Psi(\boldsymbol{x}) \rangle$$

[1] Note, that even in this regime sometimes it is necessary to include three-body or even more complicated interactions into the considerations, for example near the collapse of BEC.

is the second-order correlation function. The first term in Eq. (2.7) has more familiar interpretation in the momentum space, where it can be written as:

$$\frac{\hbar^2 N}{2m}\int d\boldsymbol{k} k^2 P(\boldsymbol{k})$$

with $P(\boldsymbol{k}) = \frac{1}{N}\langle \hat{a}^\dagger_{\boldsymbol{k}}\hat{a}_{\boldsymbol{k}}\rangle$, calculated in momentum space, standing for a probability of finding an atom with a momentum $\boldsymbol{k}$. From the above we see the important role of $G_2(\boldsymbol{x},\boldsymbol{x}')$ and $P(\boldsymbol{k})$ in a quantum state characterization.

2.2 Two-body interactions

Actual interparticle interaction potential, depends on many microscopical details e.g. type of atomic element, the internal quantum state of an atom or type of confinement trapping atoms, to name only a few. Depending on scientific community the most popular choices include Aziz potential, Lenard-Jones potential, van der Waals potential, hard-sphere potential, gaussian potential and many different.

In this thesis, we mainly focus on physical phenomena introduced by dipolar forces between atoms with a permanent magnetic (electric) moment themselves or by the interplay between them and short-range interactions. We briefly present both of them in the following subsections.

2.2.1 Short-range interactions

We are entitled to consider only interactions on a binary level due to the diluteness of an ultracold gas. In standard experiments with quantum gases, a peak number density is typically around $n \sim 10^{20}\ \mathrm{m}^{-3}$ (five orders of magnitude smaller than in the air). A typical distance between particles l is larger than the characteristic range of interactions r:

$$r \ll l = n^{-\frac{1}{3}} = \left(\frac{N}{V}\right)^{-\frac{1}{3}} \tag{2.8}$$

where V is the total volume of a system. We assume non-zero interactions only if any two atoms in an ensemble approach each other a distance smaller than r. Moreover, in the ultracold gases regime i.e. the low energy regime, the typical single particle momentum k is very small, namely:

$$k \ll \frac{\hbar}{r} \tag{2.9}$$

Outcomes of the scattering theory describing accurately properties of two-body interactions simplify under the above conditions. For all models of local (not dipolar etc.) interparticle interactions the only nonvanishing contribution to the scattering amplitude comes from the s-wave channel and it is characterized by a single k-independent parameter, the scattering length a_s. Then, instead of using the actual potential one can consider a delta function pseudo-potential

$$U_\mathrm{ps}(\boldsymbol{x}) = g_\mathrm{3D}\delta(\boldsymbol{x}), \tag{2.10}$$

where

$$g_{3\mathrm{D}} = \frac{4\pi\hbar^2 a_{\mathrm{s}}}{m}. \tag{2.11}$$

In the literature, one can find many different studies on different systems with interactions given by Eq. 2.10 eg. the Lieb-Liniger model that we describe later in this Chapter. Before that, we want to mention a few remarks about this useful, yet simplified effective potential model.

1. Note, that the scattering length fully determines low energy properties of the true potential. It shows whether the net local interactions are repulsive ($a_{\mathrm{s}} > 0$) or attractive ($a_{\mathrm{s}} < 0$). One can, in principle, calculate the unique value of the scattering length for any real atom/molecule. It is called the background scattering length a_{bg}. It requires to include all details of true potential making its calculations a difficult and a demanding task. Note, that there exist species with $a_{\mathrm{bg}} < 0$, eg. Lithium. The scattering length also depends on the dimensionality of the system.

2. The real advantage of ultracold gases as a tool to test concepts from different fields of physics is associated with the existence of the phenomenon known as the Feshbach resonances predicted theoretically in the 70s. It allows tuning a_s in experiments to any desired value including flipping its sign. Starting from 1998 applying the Feshbach resonance is a standard implement in the experiments with quantum gases.

3. In the case of 3D problems within the many-body approach, eg. the exact diagonalization, Eq. (2.10) would fail in the prediction of the system properties. The best known example was given in the case of two ultracold atoms in the seminal paper by Bush et al. [129]. One has to use the regularized version of Eq. (2.10). In lower dimensions, one does not need such regularization.

4. Atoms scattering in the presence of an external confinement introduces corrections to the scattering length and the confinement induced resonance [130, 131]. The scattering length becomes a function of confinement parameters. In Chapters 5 and 6, we only include very simple correction to the value of the scattering length that is given by the normalization factor of the wave function Ansatz in the direction of tight confinement.

5. The scattering theory shows that in the case of dipolar interactions all partial waves, not only s-wave, contribute to the scattering amplitude. Thus, the pseudopotential from Eq. 2.10 cannot be used. The above unhide the long-range nature of dipole-dipole interactions.

2.2.2 Dipolar pseudo-potential

In Chapters 4-6 we discuss the case of polarized atoms for which the dipolar potential takes the form from Eq. (1.3):

$$U_{\mathrm{dd}}(\boldsymbol{x}_1 - \boldsymbol{x}_2) = \frac{C_{\mathrm{dd}}}{4\pi} \frac{1 - 3\cos^2\theta}{|\boldsymbol{x}_1 - \boldsymbol{x}_2|^3}, \tag{2.12}$$

where θ is the angle between the direction of polarization and the relative position of the particles. We also confine atoms by a tight harmonic potential:

$$U_1(x,y,z) = \frac{1}{2}m\omega_\perp\left(y^2+z^2\right) \tag{2.13}$$

The space in $\hat{x}$ direction is assumed to be infinite. Then, assuming that in $\hat{y}$ and $\hat{z}$ direction any two atoms are in the ground state of the harmonic oscillator, a two-body wave function reads:

$$\Psi\left(\boldsymbol{x}_1,\boldsymbol{x}_2\right) = \phi_0(z_1)\phi_0(z_2)\phi_0(y_1)\phi_0(y_2)\Psi(x_1,x_2), \tag{2.14}$$

where ϕ_0 is the Gaussian wave function:

$$\phi_0(y) = \left(\frac{1}{\pi l_\perp^2}\right)^{1/4}\exp\left(-y^2/(2l_\perp^2)\right) \tag{2.15}$$

with $l_\perp = \sqrt{\hbar/(m\omega_\perp)}$ being the transverse oscillator width. The necessary condition underlying this approximation is that both, the thermal energy $k_\mathrm{B}T$ and the interaction energy in $\hat{x}$ dirtection, are much below the energy of the first excited state in the transverse direction. Under the above approximation, we can reduce full three-dimensional dipolar potential (as well as contact potential) to the effective one-dimensional dipolar potential. Formally, it can done by integrating out 'freezed' degrees of freedom:

$$U_\mathrm{dd}(x_1-x_2) = \int dy_1dy_2dz_1dz_2\,\phi_0(z_1)\phi_0(z_2)\phi_0(y_1)\phi_0(y_2)U_\mathrm{dd}(\boldsymbol{x}_1-\boldsymbol{x}_2) \tag{2.16}$$

The expression given by Eq. (2.16) can be calculated in several steps including switching to centre of mass and relative coordinates, using polar coordinates and a proper change of variables [56, 132–134]. Finally, the effective potential in real space is expressed by

$$U_\mathrm{dd}(x) = \tilde{C}_\mathrm{dd}\left(u_\mathrm{dd}\left(x/l_\perp\right) + \frac{8}{3}\delta(x/l_\perp)\right) \tag{2.17}$$

where

$$u_\mathrm{dd}(u) = 2|u| - \sqrt{2\pi}(1+u^2)e^{u^2/2}\mathrm{Erfc}\left(|u|/\sqrt{2}\right) \tag{2.18}$$

with a condition $\int \frac{1}{4}u_\mathrm{dd}(u)du = 1$ and

$$\tilde{C}_\mathrm{dd} = \frac{C_\mathrm{dd}\left(1+3\cos\left(2\theta\right)\right)}{32\pi l_\perp^3} \tag{2.19}$$

Hereafter, we absorb the contact interaction term from Eq. (2.17) to short-range pseudo-potential from the previous subsection 2.2.1, i.e. $U_\mathrm{dd}(x) = \tilde{C}_\mathrm{dd}u_\mathrm{dd}\left(x/l_\perp\right)$. In Fig. 2.1 from [54] we present the most important features of $u_\mathrm{dd}(x)$ ($C_\mathrm{dd} > 0$). For large distances x it behaves like $\frac{1}{x^3}$ and its characteristic range (width at half maximum) scales like $l_\perp$. Note, that from the mathematical point of view the effective dipolar potential in 1D is non-local rather than long-range.

The Fourier transform $\mathcal{F}[\cdot]$ of the Eq. (2.17) reads [57]:

$$V_\mathrm{dd}(k) = 4\tilde{C}_\mathrm{dd}\left(\frac{k^2l_\perp^2}{2}e^{k^2l_\perp^2/2}\mathrm{E}_1\left(\frac{k^2l_\perp^2}{2}\right) - \frac{1}{3}\right), \tag{2.20}$$

where $\hbar k$ is the momentum associated with the $\hat{x}$ direction and $E_1(x)$ is the exponential integral.

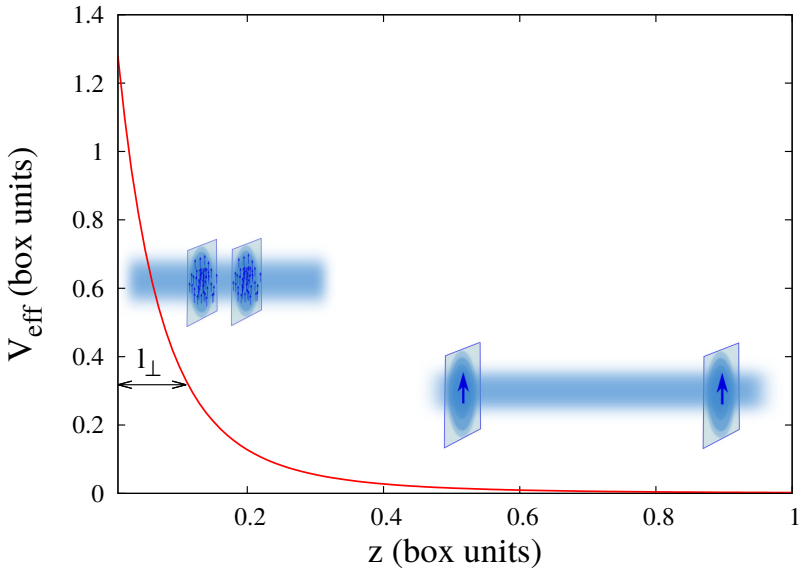

Figure 2.1: Effective potential in position representation. Here, $V_{\text{eff}} \propto u_{\text{dd}}$. For large distances x it behaves like $\frac{1}{x^3}$ and its characteristic range (width at half maximum) scales like $l_\perp$. (Copyright IOP Publishing. Reproduced by permission of IOP Publishing. All rights reserved [54])

2.2.3 The effective potential. Realistic vs. periodic

As we replace the ring with a box with periodic boundary condition, the effective interaction potential used in Chapters 4-6 is only approximate model of the physical interactions. In reality particles trapped in the ring-shaped potential would interact via interaction potential depending on the shortest distance between them, the length of a chord. We explain the qualitative differences, between the physical interaction potential and our model in Fig. 2.2. Below we give details how our model $U_{\text{eff}}(x)$ arises, and compare it with the real potential. We use the symbol U for the potentials in the position representation and V for potentials in the momentum space. Below we denote $U_{1\text{D}} = U_{\text{SR}} + U_{\text{dd}}$.

In a real experiment, when space needs to be finite, atoms are trapped in the ring shaped potential (as we want to avoid breaking translational invariance). Therefore they interact via potential depending on the length of the chord (see left panel in Fig. 2.2):

$$U_{\text{ring}}(x) = U_{1\text{D}}\left(\frac{L}{\pi}\sin\left(\frac{\pi x}{L}\right)\right) \tag{2.21}$$

In this thesis, from technical reasons, we model such situation by a box of length L with periodic boundary conditions. We introduce effective potential, which includes interaction with all imaginary copies of system:

$$U_{\text{eff}}(x) = \sum_{n\in\mathbb{Z}} U_{1\text{D}}(x + nL) \tag{2.22}$$

Therefore, the effective potential in momentum representation is $V_{\text{eff}}(k) = \int_0^L e^{-ikx}U_{\text{eff}}(x)dx$ (which satisfies $V_{\text{eff}}(k) = \mathcal{F}(U_{1\text{D}})(k)$ as well).

In all cases of this thesis, our approximation of the effective potential is well justified. A sufficient condition is $l \ll L$. In Chapter 5.A we will show a comparison between both approaches.

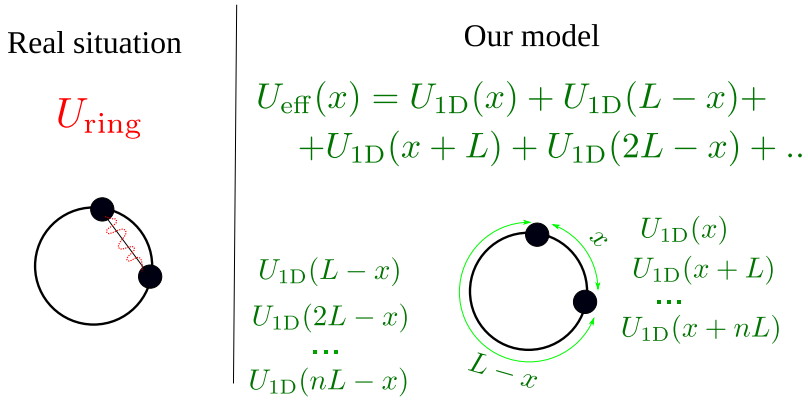

Figure 2.2: Schemes to discuss the relations between the real potential (left panel) and our approximation (right panel). Physically, the interaction U_{ring} between two atoms depends on the shortest distance between them, i.e. the length of a chord. From technical reasons we approximate the ring with a box with periodic boundary conditions. In consequences the atoms in our model interact along the short and long arcs connecting them. As we use in computation the Fourier transform there are small contributions to the interactions energy coming from the copies of our system shifted by the multiple of the length of the circle L. The resulting potential is denoted as U_{eff}. As discussed below, the differences between the real interaction potential U_{ring} and our model U_{eff} are very small.

2.3 Atoms moving on a circumference of a ring

In this thesis, we mostly deal with finite size systems. One of the most common choice of a boundary for a problem is Periodic Boundary Conditions (PBC). In (quasi)-1D systems this may be seen as equivalent to a ring not only for the ideal gas case or point-like interactions but also to nonlocal interactions, in particular, dipole-dipole forces as in this thesis. The PBC implies translational invariance of the system, therefore the total momentum of the system consisting of N atoms

$$\hat{K} = -i\hbar \sum_{i=1}^{N} \frac{\partial}{\partial x_i} \tag{2.23}$$

commutes with the Hamiltonian. Hence, all eigenstates may be numbered by the value of their total momentum $\hat{K}$. We denote i-th eigenstate with the total momentum K and with N atoms as:

$$|\Psi^i_{NK}\rangle = |N, K, i\rangle, \tag{2.24}$$

In analogy with nuclear physics [135, 136] and following [119, 120] we call the lowest energy states of a given total momentum of the system ($i = 0$), the yrast states.

Below, we present a short introduction to many-body ring systems put in a specific context of this thesis.

2.3.1 The Lieb-Liniger model

The famous Lieb-Liniger model [113, 114] describes particles moving on a circle of length L and interacting with each other by delta potential. The Hamiltonian reads

$$\hat{H} = -\frac{\hbar^2}{2m}\sum_{i=1}^{N}\frac{\partial^2}{\partial x_i^2} + g\sum_{1\leq i<j\leq N}\delta\left(x_i - x_j\right) \tag{2.25}$$

and we consider here only $g > 0$ cases. The eigenstates of Eq. (2.25) can be found by the Bethe Ansatz and by imposing PBC on the system as was done originally in [113]. Let $\{k\} = k_1, ..., k_N$ be an ordered set of N quasimomenta. Then, the Bethe Ansatz in our case can be written as

$$\Psi_{NK}^{i}(\vec{x}) = \sum_{P} A_P \mathrm{e}^{i\sum_j k_{P_j} x_j} \tag{2.26}$$

where $\vec{x} = (x_1, ..., x_N)$ denotes a position vector of N particles. The summation in Eq. (2.26) extends over all permutations P of set $\{k\}$ and A_P are superposition coefficients depending on P. The quasimomenta k_i are real (for $g > 0$) and $\forall_{i\neq j} k_i \neq k_j$. They fully determine the eigenvalues of energy $E = \frac{\hbar^2}{2m}\sum\limits_{i=1}^{N} k_i^2$ with a constraint imposed by the total momentum $K = \hbar\sum\limits_{i=1}^{N} k_i$ conservation. With all that, one can derive a set of transcendental equations of the following form:

$$k_j L = 2\pi I_j + \sum_{n=1}^{N}\theta\left(k_j - k_n\right), \tag{2.27}$$

where $\theta\left(x\right) = -2\arctan\left(\frac{x}{g}\right)$, and I_j are integers (half-integers) if the number of particles N is odd (even) and $\forall_{i\neq j} I_i \neq I_j$. Notice, that one set of $\{I\}_i$ parametrizes exactly one eigenstate. Hereafter, we always assume that $I_1 < I_2 < ... < I_N$ as well as $k_1 < k_2 < ... < k_N$. As we see Eq. (2.27) decomposes for an ideal gas situation with a well-known solution for a single-particle momentum[2] and phase shifts due to the scattering events introduced by interactions. The ground state of the system is given by a set [111]:

$$\{I_{GS}\} = \left\{\frac{-N-1}{2}, \frac{-N-3}{2}, ..., \frac{N-1}{2}\right\}. \tag{2.28}$$

In his seminal work [114], Lieb pointed out that all excitations of the system are combinations of members of two families of elementary excitations. We call an excitation type-I if one takes the highest (lowest) value I_N (I_1) and increase (decrease) it by p where p stands for an integer. This operation results in a new set $\left\{I_j^I\right\}$ determining a new set of quasi momenta $\left\{k_j^I\right\}$. The system acquires $\Delta p = k_{N+p} - k_N$ ($\Delta p = k_{N-p} - k_1$) of momentum and $\Delta E = \left(\Delta p\right)^2 + \frac{2\pi N}{L}\left|\Delta p\right|$ of energy. As an example we choose I_N and $p = 1$, which gives:

$$\left\{I_j^I\right\} = \left\{\frac{-N-1}{2}, \frac{-N-3}{2}, ..., \frac{N-3}{2}, \frac{N-1+2p}{2}\right\}. \tag{2.29}$$

In the limit $\frac{Ng}{L} \to 0$ such excitations are equivalent to Bogoliubov quasi-particles [114].

[2]Note, that for the ideal gas scenario the integers I_j from a set $\{I\}$ do not necessarily have to be distinct, as well as real single-particle momenta.

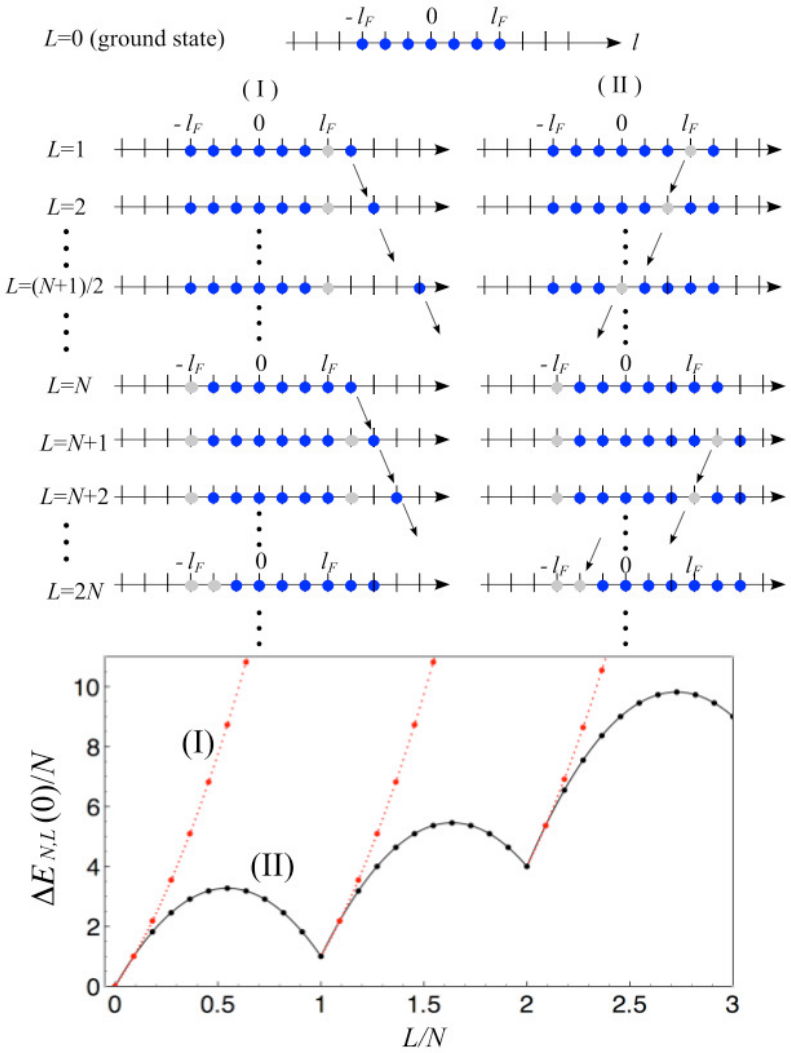

Figure 2.3: Schematic presentation of two branches of elementary excitations for the Lieb-Liniger model for $g \to \infty$ and $N = 7$ (top) and its energies as a function of K for $g \to \infty$ and $N = 11$. In this figure, the total momentum of the system K is denoted by L, a set of integers $\{I_j\}$ by $\{l_j\}$ with I_N changed for l_F. The momentum and energy units are $\frac{2\pi\hbar}{R}$ and $\frac{\hbar^2}{2mR^2}$, where R is the size of the system. (Copyright (2011) by American Physical Society [120])

The second family of elementary excitations, called type-II excitations or hole excitations, comes from changing I_j $(1 < j < N)$ to I_{N+1}. As a result, the system gains $\Delta p = k_N - k_j$ if $\frac{N+1}{2} < j < N$ ($\Delta p = k_1 - k_j$ if $1 < j < \frac{N+1}{2}$) of momentum and $\Delta E = \frac{2\pi N}{L} |\Delta p| - (\Delta p)^2$ of energy. As an example we choose I_{N-1} $(j = N - 1)$ resulting in:

$$\left\{I_j^{II}\right\} = \left\{\frac{-N-1}{2}, \frac{-N-3}{2}, ..., \frac{N-5}{2}, \frac{N-1}{2}\frac{N+1}{2}\right\}. \tag{2.30}$$

In the limit $\frac{Ng}{L} \to 0$ they correspond to dark solitons from Gross-Pitaevskii equation, not only by matching its dispersion relation [118], but also by matching its spatial properties [120, 124, 125].

We use Fig. 5 from [120] (see Fig. 2.3) to explain two types of elementary excitations graphically and to show a typical spectrum of the finite-size system. For small K two elementary

branches are close to each other. These part of the spectrum corresponds to the phonon quasiparticles. We also notice, that whenever $K = p \cdot N$, where K has an integer value (in $\frac{2\pi\hbar}{L}$ units) and p denoting an integer, the spectrum starts to resemble itself for $K < N$. For finite systems on the ring it suffices to consider the eigenstates only up to $K/N = 1/2$. This comes from the presence of the so called *umklapp* process [114]. Any eigenstate with a total momentum $K' = p \cdot N + K$ (where $p \in \mathbb{Z}, -\frac{N}{2} \leq K \leq \frac{N}{2}$) may be understood as the state with a total momentum K with a shifted center-of-mass momentum. Note that such shifting does not change the internal structure of the state.

2.3.2 Noninteracting gas of bosons

We investigate the system in the simplest case of the ideal gas, $g = 0$. In this case, every Fock state in the plane wave basis

$$\{\phi_j(x)\} = \frac{1}{\sqrt{L}} e^{\frac{i2\pi j}{L}x} \tag{2.31}$$

is already an eigenstate of the Hamiltonian (2.25). The energy of the Fock state $|n\rangle = |n_{-\infty}...n_k...n_\infty\rangle$ equals

$$E(n) = \frac{2\pi^2\hbar^2}{L^2} \sum_{k=-\infty}^{\infty} n_k\, k^2, \tag{2.32}$$

In analogy with the previous subsection, we may distinguish two characteristic types of excitations.The first ones are the elementary excitations obtained from the ground state $|n_0 = N\rangle$ by taking a single atom to momentum K, so the total momentum is carried by a single particle. The spectrum is given by the parabola $E = \frac{2\pi^2}{L^2}K^2$, which agrees with the Bogoliubov approximation in a limiting case of vanishing interactions. This picture also corresponds with the Lieb-Liniger type-I elementary excitations.

The another important branch consisting of the lowest energy states at a given momentum, i.e. the yrast states, can be constructed as follows. One has to identify which set of integers n_k minimizes the kinetic energy (2.32), but under constrained total momentum $K = \sum_{k=-\infty}^{\infty} k\, n_k$. As a result, the yrast state with momentum K is a state with K atoms occupying the plane wave with momentum $k = 1$, namely the orbital $\frac{1}{\sqrt{L}} e^{i2\pi x/L}$, and the rest of them remain in the state $\frac{1}{\sqrt{L}}$ corresponding to $k = 0$:

$$|N,\, K,\, 0\rangle := |n_0 = N - K, n_1 = K\rangle. \tag{2.33}$$

The spectrum of the yrast states equals $E = \frac{2\pi^2}{L^2}K$. The Eq. (2.33) tells us, that the yrast states are rather **the collective** excitations as obtained by exciting simultaneously K atoms.

These two branches, depicted in Fig. 2.4, are nothing else but the two branches of excitations found by E. Lieb [114] but in the limit $g \to 0$, both named elementary excitations in the literature. Apparently this nomenclature looses sense in the limit $g \to 0$, where the type II excitations are collective.

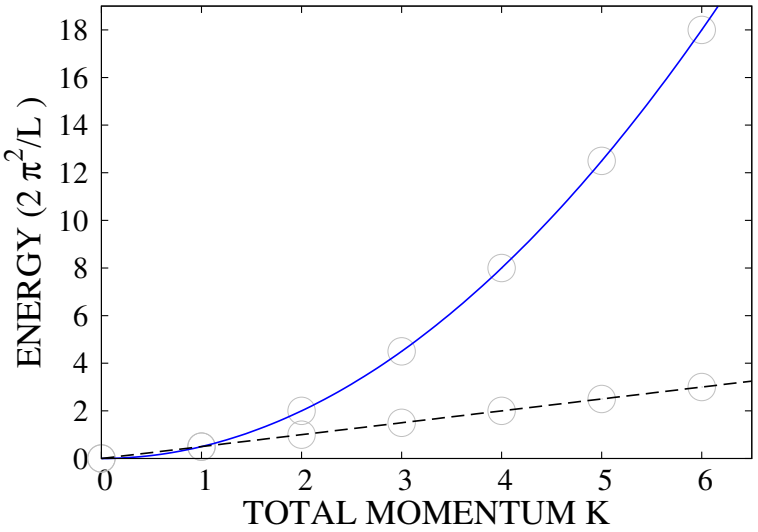

Figure 2.4: The two branches of excitations of the ideal gas: the upper branch (blue solid line), with energy given by $E = \frac{2\pi^2}{L^2}K^2$ corresponds to the single-particle excitations. The lower branch (black dashed line), with energy-momentum relation $E = \frac{2\pi^2}{L^2}K$ comes from the yrast states. Momentum, as defined in the text, is dimensionless.

2.4 Accessing spatial properties of a many-body system on a ring

The main difficulty in describing a many-body system pertains finding its eigenstates. Including interactions, this is a demanding task even for a model within classical physics, let alone a quantum one with indistinguishable particles. Using the second quantization framework one can simplify a problem distinctly. For a relatively small number of particles, an exact diagonalization technique can be used to find numerically exact solutions if an analytical solution is not known. In this thesis, when we discuss $N > 2$ problems, we use the Lanczos algorithm [137] for exact diagonalization. We construct Hamiltonian matrices in a plane wave basis introduced in a previous section by Eq. (2.31). We adjust, to ensure convergence of our solutions, a cut-off for a specific problem described in this thesis in a way presented in [138]. Finally, we obtain an i-th eigenstate of fixed total momentum K and number of particles N given by Eq. (2.24). Formally, its spatial representation is denoted by

$$\Psi^i_{NK}(\vec{x}) \equiv \langle \vec{x} | \Psi^i_{NK} \rangle, \tag{2.34}$$

where $\vec{x} = (x_1, ..., x_N)$ is a position vector of N particles. In general, such a many-body wave-function consists of $N!$ terms limiting possibilities of its spatial analysis.

2.4.1 Conditional single-body wave function

How to extract properties of a single-body wave-function from the many-body eigenstates in the ring geometry? The naive approach would be to reduce the many-body density matrix by tracing out $N - 1$ atoms. This approach would fail – all eigenstates would be projected to exactly

the same single-body uniform density, as a result of the translational invariance. The Authors of the paper [124] have shown another procedure, in the spirit of [139], which reveals the spatial structures hidden in the eigenstates. One obtains a conditional single-body wave-function by means of drawing remaining $N-1$ particle-positions. The position of the first particle $\bar{x}_1$ is drawn from the uniform distribution, $P(x_1) = 1/L$. Then the position of the second one $\bar{x}_2$ is drawn from the conditional distribution, obtained by setting the first argument of the many-body wave-function as the parameter with the value $\bar{x}_1$ and tracing out the particles $x_3,\, x_4,\, \ldots, x_N$, i.e. from the distribution $P(x_2) \propto \int |\psi\left(\bar{x}_1,\, x_2,\, \ldots, x_N\right)|^2 \,\mathrm{d}\, x_3 \,\mathrm{d}\, x_4 \ldots \,\mathrm{d}\, x_N$. The procedure is repeated until the conditional single-particle wave-function is reached:

$$\psi_{\mathrm{con}}^{\bar{x}_1,\, \bar{x}_2,\, \ldots,\, \bar{x}_{N-1}}(x_N) \propto \psi(\bar{x}_1,\, \bar{x}_2,\, \ldots, \bar{x}_{N-1}, x_N) \tag{2.35}$$

Then, the probability distribution function of the last particle reads

$$P(x_N) \propto |\psi_{con}^{\bar{x}_1,\, \bar{x}_2,\, \ldots,\, \bar{x}_{N-1}}(x_N)|^2 \tag{2.36}$$

Note, that within the conditional wave function we have an access to high order correlation functions. The only problem with this approach stems from the fact that calculating the marginal distributions is an extremely demanding task even in the cases, where the analytical formulas for $\Psi_{NK}^{i}(\vec{x})$ are known [124].

2.4.2 Probing a multivariate probability distribution

In a measurement performed on the gas of N atoms one obtains in fact an image of the N-th order correlation function [140]. We reconstruct the experimental-like measurement by drawing N positions from the probability density $|\psi(x_1, \ldots,\, x_N)|^2$ of a given eigenstate as the N-body distribution. Instead of the marginal distributions introduced in the previous subsection, we use the Metropolis algorithm, based on the Markovian walk in the configuration space [141], to perform such drawings. In each 'measurement' we have N points, as experimentalists have on CCD cameras. We repeat this procedure many times, collecting configurations $\{\vec{x}\}_i = \left\{\vec{x}_1^i, ..., \vec{x}_N^i\right\}$ from each (i-th) shot. Due to the translational symmetry, the center of mass is a random variable with the rotationally uniform distribution. To reveal any hidden correlations one has to appropriately align the samples. We do it by rotating samples such that their centers of mass point in the same direction. Because the problem has the topology of the ring, one can move to the 2-dimensional plane. Then, the center of mass should be understood as a vector. We sketch it in Fig. 2.5. The center of mass 2D coordinates are given by:

$$\begin{aligned} X_{\mathrm{CM}} &= \frac{L}{2\pi N} \sum_{j=1}^{N} \cos\left(\frac{2\pi x_j}{L}\right), \\ Y_{\mathrm{CM}} &= \frac{L}{2\pi N} \sum_{j=1}^{N} \sin\left(\frac{2\pi x_j}{L}\right) \end{aligned} \tag{2.37}$$

To find a 'ring' center of mass x_{CM} one should find the intersection of a circle depicted in Fig. 2.5 and a ray with a direction determined by the center of mass vector.

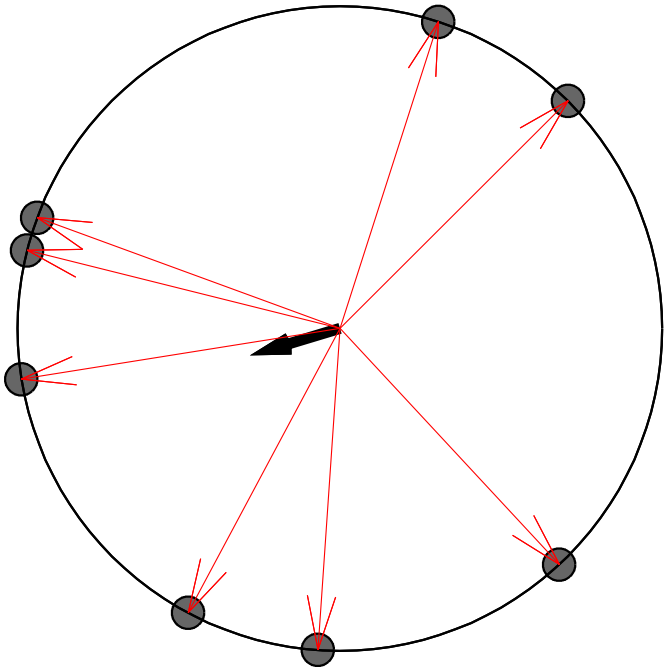

Figure 2.5: Illustration of the definition of the center of mass (black thick arrow), being here a vectorial sum of vectors (thin red arrows) pointing to the particles. The box with the periodic boundary condition is here interpreted as a circle.

2.5 Mean-field and Bogoliubov approximations

Although in this thesis we focus on actual many-body physics, i.e. we try to find and analyze eigenstates of a many-body system in a full manner, we sometimes compare our findings with approximate theories of ultracold many-body systems. In the next subsections, we shortly introduce the mean-field approach and the Bogoliubov approximation that is a first step beyond the mean-field.

2.5.1 Mean-field approximation

Usually, a single Fock with almost all bosons occupying a single-particle state is the ground state of an ultracold bosonic system. The appearance of a product state allows applying a so-called mean-field theory. Within it, the time-dependent Bose field operators $\hat{\psi}(\boldsymbol{x}, t)$ can be written as:

$$\hat{\psi}(\boldsymbol{x}, t) = \left\langle \hat{\psi}(\boldsymbol{x}, t) \right\rangle + \hat{\phi}(\boldsymbol{x}, t) \tag{2.38}$$

The mean value of the Bose field operator is just a classical field $\psi(\boldsymbol{x}, t)$ with a norm $\int d\boldsymbol{x} |\psi(\boldsymbol{x}, t)|^2 = N_0$ where N_0 is the number of atoms in a macroscopically occupied orbital. The term $\hat{\phi}(\boldsymbol{x}, t)$ describes fluctuations of the Bose field operator around its mean value. The fluctuations have both quantum and thermal origin and they characterize all atoms outside the macroscopically occupied single-particle state.

In the limit of zero temperature and weak interactions, we may assume that the quantum depletion of a ground state is negligible, namely $N_0 \to N$. Then, we can ommit the fluctations term in Eq. (2.38). In this limit, also short-range interactions take their effective form with $U_{\mathrm{SR}}(\boldsymbol{x}) \to U_{\mathrm{ps}}(\boldsymbol{x})$.

The above assumptions make the energy, given by Eq. (2.2), a functional of $\rho(\boldsymbol{x}, t) = |\psi(\boldsymbol{x}, t)|^2$. We want to find variationally $\psi(\boldsymbol{x}, t)$ minimizing its value, so that fulfills $\frac{\delta E[\rho]}{\delta \psi^*(\boldsymbol{x},t)} = 0$. We additionaly impose the normalization condition $\int d\boldsymbol{x}|\psi(\boldsymbol{x}, t)|^2 = N$. Finally, we obtain an equation, called Gross-Pitaevski equation, for a single-particle orbital describing the whole system by:

$$i\hbar\frac{\partial\psi_{\mathrm{GPE}}(\boldsymbol{x}, t)}{\partial t} = \left(-\frac{\hbar^2}{2m}\nabla^2 + U_1(\boldsymbol{x}) + \int d\mathbf{x}' U_{\mathrm{eff}}(\boldsymbol{x} - \mathbf{x}') \left|\psi(\mathbf{x}', t)\right|^2\right)\psi_{\mathrm{GPE}}(\boldsymbol{x}, t) \quad (2.39)$$

This equation was presented for the first time for contact interactions in the context of vortex lines by E. P. Gross [43] and L. P. Pitaevskii [42] independently in 1961. Inclusion of the dipolar interactions was done in 2000 by Góral et al. [19]. In Chapter 1, we discussed briefly the most important predictions made by Eq. (2.39) in the context of this thesis.

Imaginary Time Evolution We present a very helpful tool called Imaginary Time Evolution (ITE) for finding mainly ground states of Eq. (2.39). We always can decompose any eigenstate as a sum of elements of a basis

$$\psi_{\mathrm{GPE}}(\boldsymbol{x}, t) = \sum_{k=1} e^{-iE_k t/\hbar}\psi_k(\boldsymbol{x}) \quad (2.40)$$

where E_k denotes an eigenvalue of state $\psi_k(\boldsymbol{x})$ and $E_k > E_{k-1}$. We introduce the imaginary time, namely by replacing $t \to -i\tau$. With that, Eq. (2.40) becomes

$$\psi_{\mathrm{GPE}}(\boldsymbol{x}, -i\tau) = e^{-E_1\tau/\hbar}\sum_{k>1} e^{-(E_k-E_1)\tau/\hbar}\psi_k(\boldsymbol{x}). \quad (2.41)$$

We see that as τ increases the ground state decays the slowest and remains significant even for larger times. Note, that one has to properly normalize the state after each step as the ground state also vanishes (see [57] and references therein for more information).

In this thesis we use ITE in Chapter 6 to find bright solitons and droplet-like solutions. Both of them are ground states. Note, that one can use ITE also to find an excited state of GPE to some extension, but it needs slight modifications [57].

2.5.2 Number conserving Bogoliubov approximation

The well known Bogoliubov approximation stretches beyond the mean-field theory. It describes energetically low excitations by the concept of quasiparticles. In this thesis, we mainly focus on small systems where the usual Bogoliubov approximation with indefinite particles' number would be unjustified. In Chapter 5 we will use a number conserving version of the Bogoliubov approximation introduced and explained thoroughly in the work of Y. Castin and R. Dum [142]. As

we use the plane waves we would like to write the Bogoliubov approximation in the particle basis. For that, we deploy the following Ansatz [15] for the Bogoliubov vacuum ($K = 0$) in a system with N atoms:

$$|N,0\rangle_B \propto \left(\left(\hat{a}_0^\dagger\right)^2 - 2\sum_{k>0}^{\infty} \frac{v_k}{u_k} \hat{a}_k^\dagger \hat{a}_{-k}^\dagger \right)^{N/2} |\mathrm{vac}\rangle, \tag{2.42}$$

where $|\mathrm{vac}\rangle$ is the particle vacuum and

$$u_k, v_k = \left(\sqrt{\epsilon_k / E_k} \pm \sqrt{E_k / \epsilon_k} \right) / 2 \tag{2.43}$$

with $E_k = k^2/2$ and the Bogoliubov spectrum is given by:

$$\epsilon_k = \sqrt{\frac{k^2}{2}\left(\frac{k^2}{2} + 2\frac{N}{L} V_{\mathrm{eff}}(k)\right)}, \tag{2.44}$$

where $V_{\mathrm{eff}}(k)$ is a Fourier transform of the effective potential $U_{\mathrm{eff}}(x)$. A single Bogoliubov excitation with a total momentum K is expressed by:

$$|N,K\rangle_B \propto \left(u_K \hat{a}_0 \hat{a}_K^\dagger + v_K \hat{a}_0^\dagger \hat{a}_{-K} \right) |N,0\rangle_B \tag{2.45}$$

Chapter 3

Two dipolar atoms in a harmonic trap

We observe a remarkable progress in experiments with ultra cold quantum gases with only a few atoms in a trap. These experiments are performed with cold atoms distributed between the wells of an optical lattice. Many of them are prepared in the Mott insulator phase [143–145] where a well defined, small number of atoms is confined in each well. Another set of a few atoms in a trap experiments is offered by the setting available in Heidelberg and Innsbruck labs [32, 146] where in the case of the latter highly magnetic erbium atoms are used. Detailed properties of such systems crucially depend on the properties of atom-atom interaction. This interaction is best tested if exactly two atoms are present. Early analytic predictions for contact interacting atoms [129] were positively verified in precise spectroscopic experiments [147].

The dipolar interaction couples spin degree of freedom with the orbital angular momentum. This leads to the well known Einstein - de Haas effect [40]. To observe this effect with chromium atoms, where dipole - dipole interaction is just a perturbation, properly resonant magnetic field strength must be used [148]. Of course, direct coupling to the orbital angular momentum is possible for sufficiently strong dipole-dipole interactions. For the large systems, it was predicted using a conventional mean field approach [149]. A simple case of two aligned dipoles was also considered in this context [150].

It is the purpose of this chapter to present exact analysis of the role of dipole-dipole interactions for two atoms trapped in a harmonic potential without any external magnetic field. The simplicity of the harmonic potential allows separating the center of mass degree of freedom. What is more, utilizing this symmetry we may construct the energy eigenstates using the angular momentum algebra. What remains is the set of coupled radial Schrödinger equations linking components of the wave function corresponding to orbital angular momenta differing by two units. Finally, we present our results observing the Einstein-de Haas effect [40] analog.

3.1 Center of mass and relative motion coordinates

Let us consider two identical atoms (fermions or bosons) of mass m moving in an anisotropic harmonic trap with an angular frequency $\boldsymbol{\omega} = (\omega_x, \omega_y, \omega_z)$. The atoms mutually interacts by a translationally invariant potential $U(\mathbf{r}_1 - \mathbf{r}_2)$, where $\mathbf{r}_1 = (x_1, y_1, z_1)$ and $\mathbf{r}_2 = (x_2, y_2, z_2)$ are the position vectors of the two atoms. The Hamiltonian of such a system can be written in a compact form as:

$$H = -\frac{\hbar^2}{2m}\nabla_1^2 - \frac{\hbar^2}{2m}\nabla_2^2 + \frac{1}{2}m\boldsymbol{\omega}^2 \cdot \left(\mathbf{r}_1^2 + \mathbf{r}_2^2\right) + U(\mathbf{r}_1 - \mathbf{r}_2), \tag{3.1}$$

where $\boldsymbol{\omega}^2 = \left(\omega_x^2, \omega_y^2, \omega_z^2\right)$ and $\mathbf{r}_i^2 = \left(x_i^2, y_i^2, z_i^2\right)$. Note that both the kinetic energy and the external potential energy have the quadratic form. Therefore, above Hamiltonian can be separated into a center-of-mass part and a relative motion part, $H = H_{CM} + H_{rel}$ with:

$$\begin{aligned} H_{\mathrm{CM}} &= -\frac{\hbar^2}{2m}\nabla_R^2 + \frac{1}{2}m\boldsymbol{\omega}^2 \cdot \mathbf{R}^2 \\ H_{\mathrm{rel}} &= -\frac{\hbar^2}{2m}\nabla_r^2 + \frac{1}{2}m\boldsymbol{\omega}^2 \cdot \mathbf{r}^2 + U(\sqrt{2}\mathbf{r}), \end{aligned} \tag{3.2}$$

which can be diagonalized separately. Here $\mathbf{R} = \frac{1}{\sqrt{2}}(\mathbf{r}_1 + \mathbf{r}_2)$ is the center of mass coordinate and $\mathbf{r} = \frac{1}{\sqrt{2}}(\mathbf{r}_1 - \mathbf{r}_2)$ stands for the relative motion coordinate. We introduce somewhat unusual factor of $\sqrt{2}$ for the symmetry. The eigenstates and corresponding eigenvalues of H_{CM} are the well known quantum harmonic oscillator solutions. The only possible new phenomena may be found in the relative motion part of Hamiltonian, which is a subject of our studies in next sections.

3.2 Isotropic trap without an external magnetic potential

In this section we turn our attention to two identical dipolar atoms (composite bosons or fermions) of a spin (a total angular momentum of an atom) $f_1 = f_2$. We constrain our considerations to the case of an isotropic harmonic trap with $\boldsymbol{\omega} = (\omega, \omega, \omega)$. In a following subsections we use harmonic-oscillator units, in which $\hbar\omega$ is a unit of energy and the characteristic size of the ground state of the trap $\sqrt{\frac{\hbar}{m\omega}}$ is a length unit.

3.2.1 Model

An interaction potential $U(\mathbf{r})$ is a sum of a short range $U_{\mathrm{sr}}(\mathbf{r})$ and a long range magnetic dipole - dipole interaction $U_{\mathrm{dd}}(\mathbf{r})$ potentials, $U = U_{\mathrm{SR}} + U_{\mathrm{dd}}$. The magnetic dipole - dipole interaction potential $U_{\mathrm{dd}}(\mathbf{r})$ can be expressed in the following form:

$$U_{\mathrm{dd}}(\mathbf{r}) = \frac{\mu_0(\mu_B g_j)^2}{4\pi\left|\mathbf{r}\right|^3}\left[\mathbf{F}_1 \cdot \mathbf{F}_2 - 3\left(\mathbf{F}_1 \cdot \mathbf{n}\right)\left(\mathbf{F}_2 \cdot \mathbf{n}\right)\right] \tag{3.3}$$

where $\mathbf{n} = \frac{\mathbf{r}_1 - \mathbf{r}_2}{|\mathbf{r}_1 - \mathbf{r}_2|}$, μ_0 stands for the vacuum magnetic permeability, μ_B indicates the Bohr magneton, g_j is the Landé g - factor and $\mathbf{F}$ is the total angular momentum of an atom (spin vector). Thus for the atomic spin quantum number f half integer we have fermions and for f integer we have bosons.

We model $U_{\mathrm{SR}}(\mathbf{r})$ as a spherically symmetric barrier written as [151]:

$$U_{\mathrm{SR}}(\mathbf{r}) = \begin{cases} 0 & \text{for } r > b = 100\, a_0 \\ \infty & \text{for } r \leq b = 100\, a_0, \end{cases} \tag{3.4}$$

where $r = |\mathbf{r}|$ and a_0 is the Bohr radius. The scattering length a for a scattering process of a single particle on an infinite spherically symmetric potential barrier is equal to the radius of the barrier i.e. $b = a$. Later in this work, a value of b is determined by the numerical calculations for the dysprosium atoms [152]. For different U_{SR} models see i.e. [129, 150, 151, 153–155]).

After introducing our model for $U(\mathbf{r})$ the relatvie motion part of Hamiltonian H_{Rel} takes the final form as:

$$H_{rel} = -\frac{1}{2}\nabla_r^2 + \frac{1}{2}r^2 + U_{\mathrm{SR}}(\sqrt{2}r) + \frac{g_{\mathrm{dd}}}{r^3}\left[\mathbf{F}_1 \cdot \mathbf{F}_2 - 3\left(\mathbf{F}_1 \cdot \mathbf{n}\right)\left(\mathbf{F}_2 \cdot \mathbf{n}\right)\right] \tag{3.5}$$

The strength of the dipole - dipole interaction is characterized by the $g_{\mathrm{dd}} = \frac{\mu_0(\mu_B g_j)^2}{8\sqrt{2}\pi}$. Note that $\sqrt{\frac{\hbar^5}{m^3\omega}}$ is a unit of g_{dd}.

3.2.2 Solution

In order to investigate the relative motion of the two atoms we observe that the total angular momentum is conserved:

$$[\mathbf{F} + \mathbf{L}, H_{\mathrm{rel}}] \equiv [\mathbf{J}, H_{\mathrm{rel}}] = 0 \tag{3.6}$$

where $\mathbf{J}$ stands for the total angular momentum of the relative motion which is a sum of the total spin operator $\mathbf{F} = \mathbf{F}_1 + \mathbf{F}_2$ and the orbital momentum operator of the relative motion of the atoms $\mathbf{L}$. The spherical symmetry of the system means that it is convenient to solve the relative motion problem in a total angular momentum basis. An Eigenfunction of the system in this basis reads:

$$\begin{aligned} \Psi_n^{jm_j}(\mathbf{r}) &= \sum_{l,f} a_n^{jm_jlf} \psi_n^{jm_jlf}(\mathbf{r}) = \sum_{l,f} a_n^{jm_jlf} \phi_n^{jlf}(r) \left|jm_jlf\right\rangle \\ &= \sum_{l,f} a_n^{jm_jlf} \phi_n^{jlf}(r) \sum_{\substack{m_l,m_f \\ m_l+m_f=m_j}} C^{jm_j}_{lm_lfm_f} \left|lfm_lm_f\right\rangle \end{aligned} \tag{3.7}$$

Here j denotes the total angular momentum quantum number and m_j the magnetic total angular momentum number, l and m_l stand for the orbital momentum and the magnetic orbital momentum quantum numbers respectively. The total spin and its projection values are indicated by f and m_f and $C^{jm_j}_{lm_lfm_f}$ denotes Clebsch - Gordan coefficients [156]. For a given j and m_j the consecutive Eigenfunctions are enumerated by the $n = 0, 1, ...$ number and $a_n^{jm_jlf}$ indicate constant coefficients.

The choice of our basis allows us to reduce a complicated three dimensional problem to the set of the radial Shrödinger equations for ϕ_n^{jlf} with given j, l, f. Any coupling between the equations may only come - in the case of spherically symmetric trap - from the dipolar part of the relative motion Hamiltonian. We are now interested in the result of acting with the U_{dd} operator on a single

state $\psi_n^{jm_jlf}(\mathbf{r})$. In order to calculate this it is convenient to rewrite the dipole - dipole interaction potential in terms of the ladder operators:

$$\begin{aligned} U_{\mathrm{dd}} = \frac{g_{\mathrm{dd}}}{r^3}\Big[&\frac{1}{2}\left(F_{1+}F_{2-} + F_{1-}F_{2+}\right) + F_{1z}F_{2z} - 3\left(F_{1+}n_- + F_{1-}n_+ + F_{1z}n_z\right) \\ &\times \left(F_{2+}n_- + F_{2-}n_+ + F_{2z}n_z\right)\Big] \end{aligned} \tag{3.8}$$

with:

$$\begin{aligned} n_+ &= \frac{x+iy}{2r} = -\sqrt{\frac{2\pi}{3}}Y_1^1(\theta,\varphi) \\ n_- &= \frac{x-iy}{2r} = \sqrt{\frac{2\pi}{3}}Y_1^{-1}(\theta,\varphi) \\ n_z &= \frac{z}{r} = \sqrt{\frac{4\pi}{3}}Y_1^0(\theta,\varphi) \\ F_+ &= F_x + iF_y \\ F_- &= F_x - iF_y \end{aligned} \tag{3.9}$$

Here $Y_l^{m_l}(\theta,\varphi)$ denotes a standard spherical harmonic in the spherical coordinates. Using (3.8), (3.9), spin operators properties and the well - known formula for the product of two spherical harmonics (see for instance [157]) it can be shown that:

$$U_{\mathrm{dd}}\psi_n^{jm_jlf}(\mathbf{r}) = \frac{g_{\mathrm{dd}}}{r^3}\sum_{l',f'}\alpha_{ll'ff'}\psi_n^{jm_jl'f'}(\mathbf{r}) \tag{3.10}$$

with the following selection rules:

$$\begin{aligned} l' &= l + \Delta l & \Delta l &= 0, \pm 2 \\ f' &= f + \Delta f & \Delta f &= 0, \pm 2 \end{aligned} \tag{3.11}$$

The above result might be understood by the fact that the dipole - dipole interaction operator is symmetric with respect to the exchange of the two particles. Thus it does not change a symmetry of the given $\psi_n^{jm_jlf}(\mathbf{r})$. A value of the scalar coefficient $\alpha_{ll'ss'}$ is expressed by a product of Clebsh - Gordon coefficients determined by the standard angular momentum algebra.

Knowing (3.10) we are able to find the radial Schrödinger equation for the $\chi_n^{jlf}(r) \equiv r\phi_n^{jlf}(r)$ by the straightforward calculation:

$$-\frac{1}{2}\frac{d^2}{dr^2}\chi_n^{jlf}(r) + \frac{1}{2}r^2\chi_n^{jlf}(r) + \frac{l(l+1)}{2r^2}\chi_n^{jlf}(r) + \frac{g_{\mathrm{dd}}}{r^3}\sum_{l',f'}\alpha_{ll'ff'}\chi_n^{jl'f'}(r) = E_n^j\chi_n^{jlf}(r) \tag{3.12}$$

where E_n^j is an eigenvalue. The short range potential $U_{\mathrm{SR}}(r)$ used in this chapter is incorporated in the boundary conditions, namely by $\chi_n^{jlf}(r) = 0$ for $r \leq b$.

As can be seen in (3.12) in order to find a $\chi_n^{jlf}(r)$ one has to solve a system of the radial Schrödinger equations for a fixed total angular momentum number j. Note that the number of equations in the system is determined by the maximum value of the total spin: $f_{\max} = f_1 + f_2$.

3.2.3 Main results

Solving the system of the radial Schrödinger equations introduced in the previous subsection completes the full characteristic of an eigenstate $\Psi_n^{jm_j}(\mathbf{r})$ with any j, m_j and n. In particular, we are interested in the case with the total angular momentum $j = 0$, because it turns out that the ground state of the system is $j = 0$ state for all $f_1 = f_2 > \frac{1}{2}$.

From the angular momentum algebra we also deduced that for an eigenstate with $j = 0$ the total spin number is equal to the orbital quantum number i.e. $l = f$. Thus for such states the corresponding coefficient matrix $\alpha_{ll'ff'}$ reduces to the $\alpha_{ll'}$ matrix. We calculate them for the various atomic spin values i.e. $f_1 = f_2 = \frac{1}{2}, 1, \frac{3}{2}$ and $\frac{21}{2}$. Our results can be found in the Appendix 3.A.

Knowledge of the $\alpha_{ll'ff'}$ coefficients allows us to solve numerically the system of the radial Schrödinger equations of the form presented in (3.12). We use the multi-parameter shooting method. We set the $b = 0.04$ in the harmonic oscillator units. For the dysprosium-like atoms it corresponds to the trap frequency $\omega \approx 2\pi\ 3.2$ kHz and consequently to $g_{\mathrm{dd}} = 0.0006$ in the harmonic oscillator units. Our system admits two control parameters that may be changed by experimenters. Note that the g_{dd} in the harmonic oscillator units depends on the trap frequency as $\sqrt{\omega}$, so it is tunable. One may also change the scattering length a_{s} by the optical Feshbach resonances [158–161], so that the b value in the harmonic oscillator units may be kept constant while one changes the trap frequency.

In Fig. 3.1 we present the eigenvalues E_n^0 with $n = 0, 1, 2$ as a function of g_{dd} for atoms with different spins. For atoms with the spin $f_1 = f_2 = 1,\ \frac{3}{2}$ and $\frac{21}{2}$ we consider only solutions for the even orbital angular momentum quantum number l. In the case of odd l results are qualitatively the same[1].

For spin $\frac{1}{2}$ atoms the energy values rise very slowly as g_{dd} rises. The radial part of $\psi_n^{0011}(\mathbf{r})$ is simply the $\phi_n^{011}(r)$, so the expected value of the orbital angular momentum operator $\langle L^2 \rangle$ is constant and equal $\langle L^2 \rangle = 2$ for all n. In fact, we checked that for $\frac{1}{2}$ atoms the ground state of the relative motion is the lowest state for $j = 1$. To understand this a bit surprising finding, we refer to the results from the Appendix 3.A. In this case, the crucial thing is that for spin $\frac{1}{2}$ particles the coefficient matrices are of dimension one. It means, that there is no coupling between different l states and the sum in Eq. (3.12) reduces to a single term. Then, it can be shown, that for $j = 0$ only the triplet state has the non-zero positive coefficient indicating the repulsive character of the dipolar interactions. On the other hand, the only non-zero valued coefficient for $j = 1$ state is negative and dipole - dipole interaction is attractive.

For the higher spin values we observe more complex behaviour. First of all, the energy values for $n = 0,\ 1$ and 2 are highly dependent on the value of g_{dd}. For low values of g_{dd} eigenvalues vary slightly, then for higher values they decrease rapidly. We observe also the presence of anti - crossings between consecutive lines $E_n^0(g_{\mathrm{dd}})$ accompanied by changes of the $\langle L^2 \rangle$. This is due to changes in the structure of the radial part of eigenstates. From the (3.12) we notice that the radial part of an eigenstate is a linear combination of the $\phi_n^{0ll}(r)$ where in this case $l \in \{0, 2, .., 2 \cdot f_1\}$.

[1] Note that one has to assure a proper bosonic (fermionic) symmetry of the total wave function, which is a product of the center of mass wave function and the relative motion wave function. For instance, an even l relative motion state has to be combined only with the center of mass state with the even (odd) parity for bosons (fermions).

As the g_{dd} rises the weight of each $\phi_n^{0ll}(r)$ function varies i.e. values of a_n^{00ll} coefficient varies. For instance, we see that for low g_{dd} the ground state consists of almost only the s - state ($\phi_0^{000}(r)$), whereas as we increase the trap frequency, contributions of the functions with higher l grow. The ground state starts to "rotate". This feature resembles the Einstein - de Haas effect [40], although it is caused only by the internal spin - spin interactions between two atoms without any influence of external fields.

Moreover, as values of a_n^{00ll} for $l > 0$ grow and a_n^{0000} decreases also mutual orientation between the atoms starts to favour attractive regions of the DDI over repulsive regions. For the spin $f_1 = f_2 = \frac{1}{2}$ atoms, such a behaviour is impossible as all three angular parts of the eigenstates are multiplied by the same $a_n^{0000}\phi_n^{000}(r)$ expression which is almost being unchanged as g_{dd} rises. This fact explains qualitative difference between the dependence of the eigenvalues on g_{dd} for spin $\frac{1}{2}$ and higher spin values.

To understand deeper the underlying spatial mechanism, which is responsible for a steep decrease of energy for higher spins we use an example of the $f_1 = f_2 = 1$ case, which is the simplest one where the effect occurs. As for $j = 0$ the total spin f cannot be higher than 2, the only possible values of orbital angular momentum are 0 and 2. Let us consider a situation, when $m_f = 0$ (thus also m_l=0), what means that spins are antiparallel. One can notice that for state with well defined orbital angular momentum $l = 2$, the value of average energy of dipole-dipole interaction is positive and for $l = 0$ it is equal to zero (because of the shape of spherical harmonics). Attractive interaction can dominate only when the system is in appropriate superposition of states with $l = 0$ and $l = 2$ (see Fig. 3.2). This statement appears to be true in general - for $j = 0$ the value of energy of states with the well defined orbital angular momentum l is always positive (or equal to zero for $l = 0$). This is the reason, why decrease of the energy does not appear for $f_1 = f_2 = \frac{1}{2}$ - as the maximum spin is $f = 1$, for given parity of spin function there is only one possible orbital angular momentum.

Fig. 3.1 also illustrates that the bigger atomic spin is, the lower trap frequency is needed to observe above effects. In addition, the effect of changes in the expected value of orbital angular momentum is stronger for larger atomic spin values. It seems that at least it is possible to check our model experimentally using the system of the dysprosium atoms with the $\frac{21}{2}$ spin.

The nature of anti - crossings in Fig. 3.1 can be explained by Landau - Zener theory [162, 163] as depicted in Fig. 3.3. As an example we used $\frac{3}{2}$ spin atoms. A composition of the eigenstate corresponding to the eigenvalue $E_n(g_{\mathrm{dd}})$ is not conserved along given energy line, but it propagates along straight lines upward or downward. This type of effect was already observed by Kanjilal et al., although for a simpler system consisting of two aligned dipoles [150].

3.2.4 Results for different barrier width and one control parameter

In the previous subsection we manipulated the trap frequency ω and the scattering length a to tune g_{dd} and keep b value constant at the same time. Here, we discuss how the results for eigenvalues depend on the hardcore potential width b. As an example we use spin $\frac{3}{2}$ atoms. For different values of the atoms spin we obtain similar behaviour. In Fig. 3.4 we plot eigenvalues of

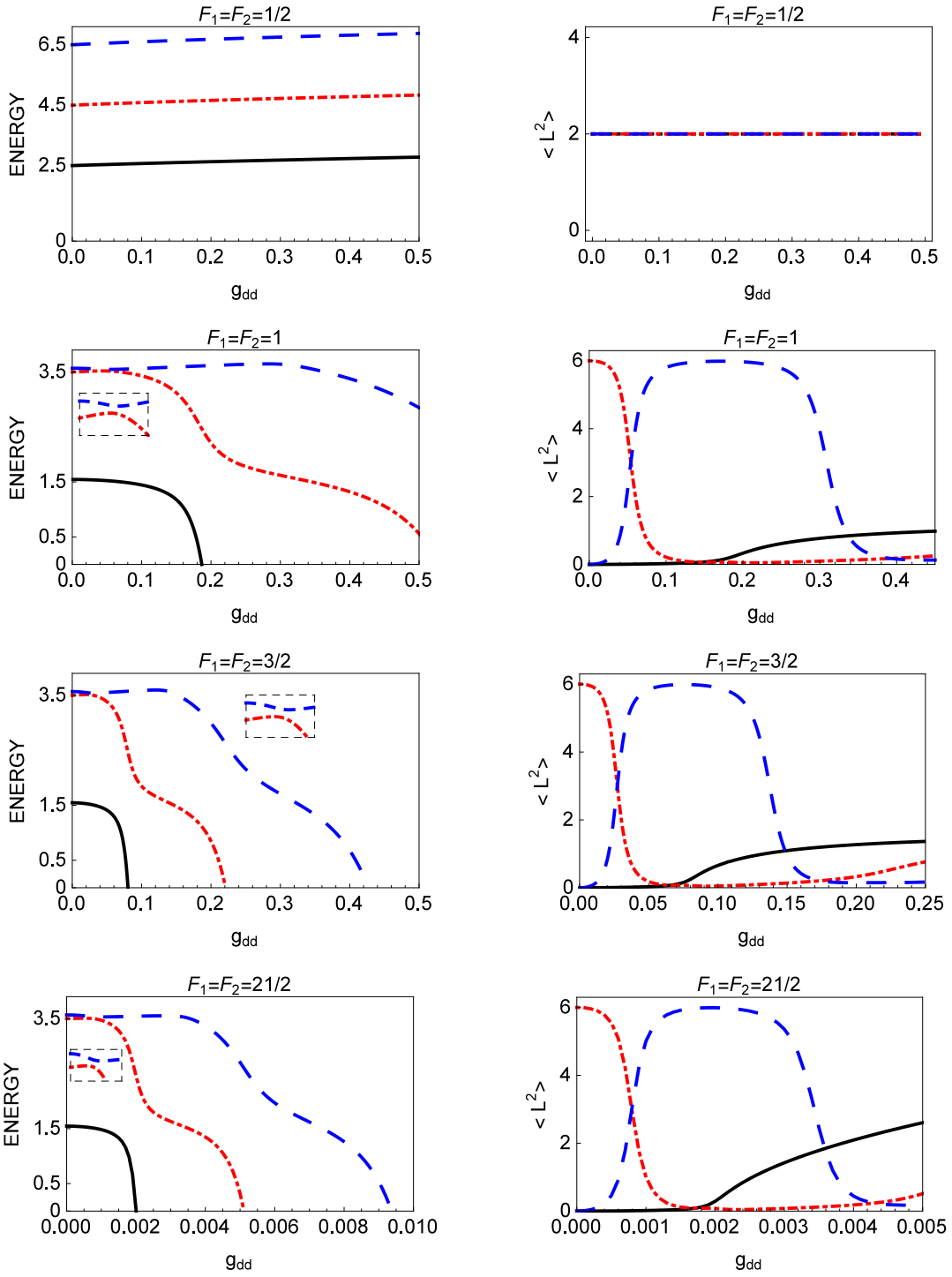

Figure 3.1: Energy E_n^0 vs g_{dd} and expected value of orbital angular momentum operator $\langle L^2 \rangle$ for the $n = 0,\ 1,\ 2$ and atoms of spin $f_1 = f_2 = \frac{1}{2},\ 1,\ \frac{3}{2},\ \frac{21}{2}$. The black solid line represents the ground state, the red dashed dotted line and blue dashed line indicate first and second excited states respectively. The insets magnify the anti - crossing area. Note different horizontal scale for $f_1 = f_2 = \frac{21}{2}$.

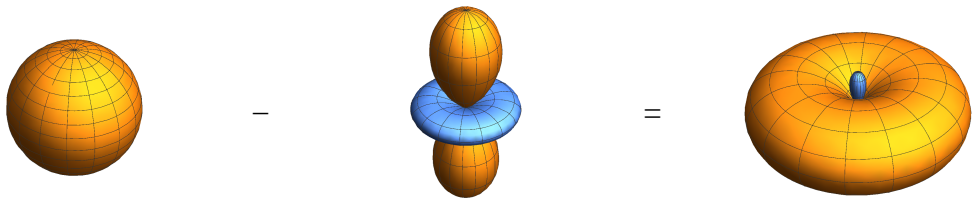

Figure 3.2: Shape of the angular parts of the wave functions for $m_f = 0$ and $m_l = 0$. The blue region indicates the negative value of Y_2^0. As spins are antiparallel, for the states with the well defined orbital angular momentum repulsion dominates. To reveal the attractive interaction, a superposition of the states is needed.

the lowest three states as a function of g_{dd} for three different b values. The results are qualitatively the same. We notice that the lower b is, the faster anti-crossings occur in the energy levels. This can be explained be the fact that as b value rises the contact interactions are getting stronger. This means that also g_{dd} has to be bigger in order to observe effects caused by the dipole-dipole interactions.

The analogue of the Einstein - de Haas effect also occurs if b is not kept constant as g_{dd} rises i.e. trap frequency rises. In Fig. 3.5 we plot eigenvalues and $\langle L^2 \rangle$ of the lowest tree states as a function of $\sqrt{\omega}$. We observe anti-crossings of the energy levels and corresponding changes in $\langle L^2 \rangle$ which are very similar to those obtained in the main text. Nevertheless, it should be pointed out that in this case the effect is rather tenuous and thus harder to observe than in the case with constant b. Consequently, to make the effect more visible, the plot is generated for g_{dd} value much higher than g_{dd} of typical atoms of $\frac{3}{2}$ spin.

3.2.5 Conclusions

Motivated by experiments under development [26, 32, 96, 164] we based our calculations on dysprosium parameters. Our model of the dipole - dipole interactions between two atoms reveals a non-trivial dependence of two atoms in a harmonic trap system on the trap frequency. We showed that increasing ω the system undergoes an analog of Einstein - de Hass effect. Such a behaviour is a result of spin - spin interaction and its coupling to the orbital angular momentum. We show a possibility of adiabatically pumping our system from the s-wave to the d-wave relative motion. The effective spin-orbit coupling occurs at the Landau - Zener anti-crossings of the energy levels. Our results may be checked experimentally for the dysprosium atoms. Of course, proposed model is oversimplified in this case as dysprosium atoms are not exactly spherically symmetric [152].

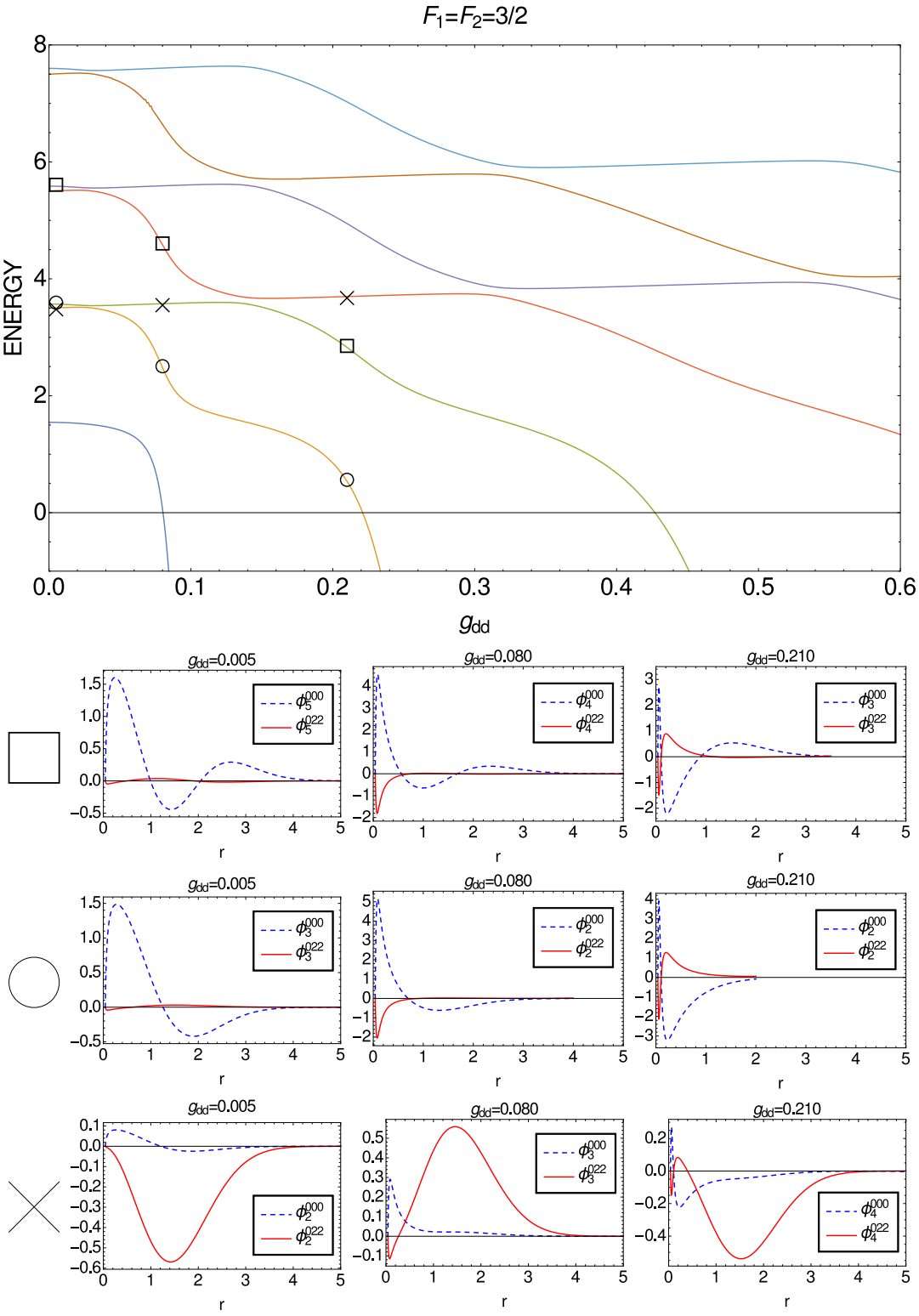

Figure 3.3: Composition of eigenstates for different eigenvalues E_n^0 for the $\frac{3}{2}$ spin atoms. The blue dashed lines indicate radial functions $\phi_n^{000}(r)$ with the orbital quantum number $l = 0$ for the given value of $g_{\rm dd}$ vs radial variable r and the red solid lines represent radial functions ϕ_n^{022} for the given $g_{\rm dd}$ with the orbital quantum number $l = 2$ vs radial variable r. Square, circle and cross stay for sets of eigenstates with the same composition of $\phi_n^{0ll}(r)$ functions.

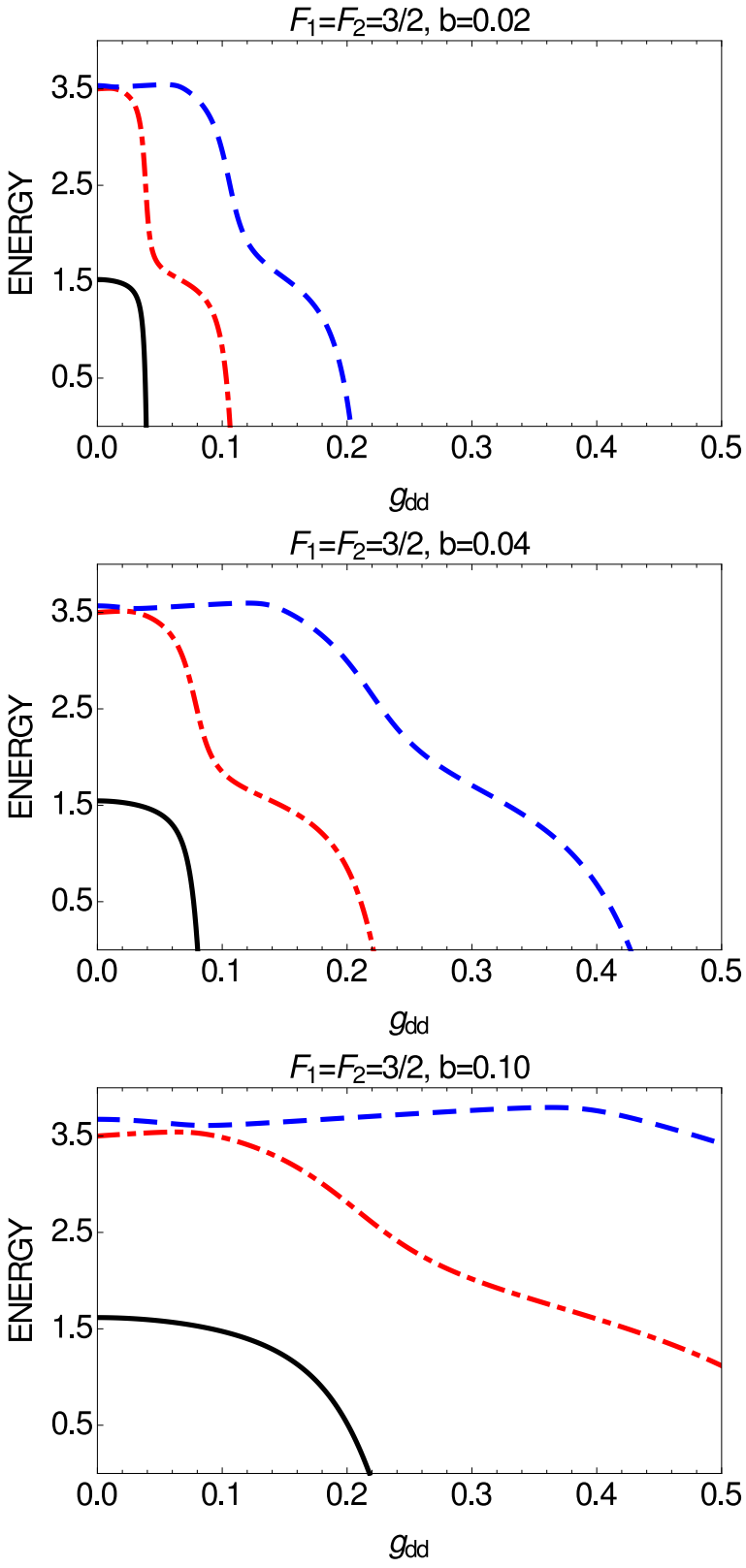

Figure 3.4: Energy E_0^n vs $g_{\rm dd}$ for the $n = 0,\ 1,\ 2$ and spin $\frac{3}{2}$ atoms for different hardcore potential barrier width b.

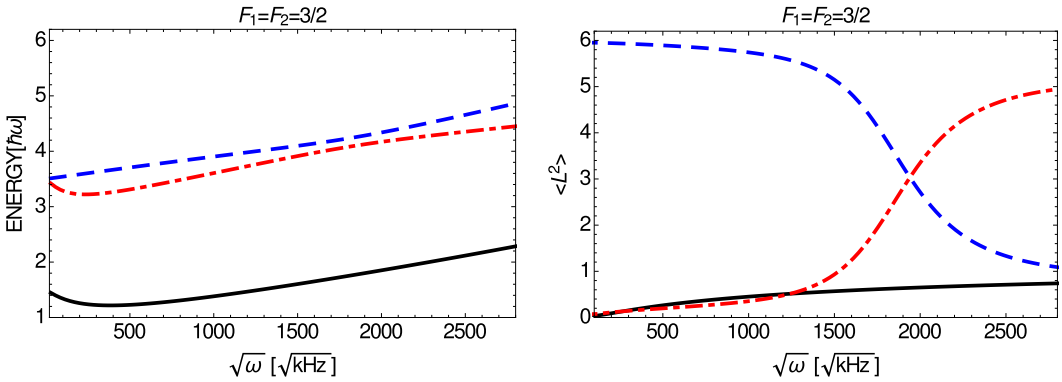

Figure 3.5: Energy E_0^n vs $\sqrt{\omega}$ and expected value of orbital angular momentum operator $\langle L^2 \rangle$ for the $n = 0,\ 1,\ 2$ and spin $\frac{3}{2}$ atoms for different hardcore potential barrier width b.

Appendix

3.A The coupling coefficients

Here, we present the values for $\alpha_{ll'}$ coefficients for the various atomic spin values i.e. $f_1 = f_2 = \frac{1}{2}, 1, \frac{3}{2}$ and $\frac{21}{2}$. We introduce the $\boldsymbol{\alpha}^p_{f_1}$ matrices of the $\alpha_{ll'}$ coefficients where f_1 is the single atom spin and $p = e, o$ indicates even or odd parity of the l and l'.

Spin $\frac{1}{2}$ For the spin $\frac{1}{2}$ particles $\boldsymbol{\alpha}^p_{\frac{1}{2}}$ are scalars. For the singlet state we obtain:

$$\boldsymbol{\alpha}^e_{\frac{1}{2}} = 0 \tag{3.13}$$

which means that the singlet state is not affected by the dipole - dipole interactions. The corresponding matrix for the triplet states is:

$$\boldsymbol{\alpha}^o_{\frac{1}{2}} = 1 \tag{3.14}$$

and the dipole - dipole interaction is repulsive. The above results allow one to investigate the contact interactions between the two $\frac{1}{2}$ spin atoms and the dipole - dipole interactions in parallel. For $j = 1$ the only non vanishing coefficient is α_{1111} equal to:

$$\alpha_{1111} = -\frac{1}{2} \tag{3.15}$$

thus in this case the dipole - dipole interaction is attractive.

Spin 1 The coefficient matrix for the even orbital angular momentum quantum numbers $l, l' = 0, 2$ can be written as:

$$\boldsymbol{\alpha}^e_1 = \begin{pmatrix} 0 & \sqrt{2} \\ \sqrt{2} & 2 \end{pmatrix} \tag{3.16}$$

For the $l, l' = 1$ we obtain:

$$\boldsymbol{\alpha}^o_1 = 2 \tag{3.17}$$

Spin $\frac{3}{2}$ The coefficient matrix for the even orbital angular momentum quantum numbers $l, l' = 0, 2$ can be expressed by:

$$\boldsymbol{\alpha}^{e}_{\frac{3}{2}} = \begin{pmatrix} 0 & 3 \\ 3 & 3 \end{pmatrix} \tag{3.18}$$

For the $l, l' = 1, 3$ we obtain:

$$\boldsymbol{\alpha}^{o}_{\frac{3}{2}} = \begin{pmatrix} \frac{17}{5} & \frac{9}{5} \\ \frac{9}{5} & \frac{18}{5} \end{pmatrix} \tag{3.19}$$

Spin $\frac{21}{2}$ The coefficient matrix for the even orbital angular momentum quantum numbers $l, l' = \{0, 2, ..., 18, 20\}$ can be written as:

$$\boldsymbol{\alpha}^{e}_{\frac{21}{2}} = \begin{pmatrix} 0 & 6\sqrt{322} & 0 & 0 & 0 & 0 & 0 & 0 & 0 & 0 & 0 \\ 6\sqrt{322} & \frac{489}{7} & \frac{18\sqrt{1235}}{7} & 0 & 0 & 0 & 0 & 0 & 0 & 0 & 0 \\ 0 & \frac{18\sqrt{1235}}{7} & \frac{5030}{77} & \frac{180\sqrt{357}}{11\sqrt{13}} & 0 & 0 & 0 & 0 & 0 & 0 & 0 \\ 0 & 0 & \frac{180\sqrt{357}}{11\sqrt{13}} & \frac{735}{11} & \frac{84\sqrt{203}}{\sqrt{221}} & 0 & 0 & 0 & 0 & 0 & 0 \\ 0 & 0 & 0 & \frac{84\sqrt{203}}{\sqrt{221}} & \frac{1332}{19} & \frac{540\sqrt{806}}{19\sqrt{119}} & 0 & 0 & 0 & 0 & 0 \\ 0 & 0 & 0 & 0 & \frac{540\sqrt{806}}{19\sqrt{119}} & \frac{32615}{437} & \frac{2178\sqrt{17}}{23\sqrt{35}} & 0 & 0 & 0 & 0 \\ 0 & 0 & 0 & 0 & 0 & \frac{2178\sqrt{17}}{23\sqrt{35}} & \frac{1846}{23} & \frac{182\sqrt{14}}{\sqrt{145}} & 0 & 0 & 0 \\ 0 & 0 & 0 & 0 & 0 & 0 & \frac{182\sqrt{14}}{\sqrt{145}} & \frac{2695}{11} & \frac{360\sqrt{4921}}{31\sqrt{319}} & 0 & 0 \\ 0 & 0 & 0 & 0 & 0 & 0 & 0 & \frac{360\sqrt{4921}}{31\sqrt{319}} & \frac{20536}{217} & \frac{918\sqrt{26}}{7\sqrt{407}} & 0 \\ 0 & 0 & 0 & 0 & 0 & 0 & 0 & 0 & \frac{918\sqrt{26}}{7\sqrt{407}} & \frac{9405}{91} & \frac{570\sqrt{7}}{13\sqrt{37}} \\ 0 & 0 & 0 & 0 & 0 & 0 & 0 & 0 & 0 & \frac{570\sqrt{7}}{13\sqrt{37}} & \frac{1470}{13} \end{pmatrix} \tag{3.20}$$

Note that the above is the tri-diagonal band matrix as was pointed in the Eq. (7) of the main article.

It can be also proved that $a_{00} = 0$ for the arbitrary chosen $f_1 = f_2$.

Chapter 4

Many-body weakly interacting bosonic gas

In Chapter 1.3, we briefly mentioned the correspondence between the yrast states of N point-like interacting bosons moving on the circumference of a circle described by the Lieb-Liniger model and dark solitons solutions from the corresponding GPE. In addition, we remind that even for a small number of particles the GPE dark soliton orbital emerges as a single-particle conditional wave function as long as one stays within the mean-field (GPE) assumptions [124].

Recently, it was found that some solutions of the dipolar GPE exhibit very similar features as their contact interacting counterparts [54–56], namely characteristic density notches and phase jumps. However, these dark soliton-like excitations differ significantly from that known from the Lieb-Liniger model. An open question appears naturally if many-body solutions of a dipolar counterpart of the Lieb-Liniger model- in particular, the yrast states- correspond analogously to the dipolar GPE solutions.

In this chapter, we remind the Reader the Lieb-Liniger model (see Chapter 2.3.1) and its dipolar analog. Then, we study the yrast states in both cases and compare them with the mean-field solitons following the procedure described in the paper [124]. In particular, we find that the structure of the corresponding many-body eigenstates is very simple and close to the case without interaction. We show that even in the limit of vanishing interaction the yrast states possess features typical for solitons like the phase jumps and the density notches. These properties are simply effects of the bosonic symmetrization and are encoded in the Dicke states hidden in the yrast states [165]. Then, we study soliton-like states motion, extracted from the many-body eigenstates, time-independent states. Finally, we discuss to what extent the conclusions derived for the non-interacting case may be also applied to the interacting gas.

4.1 Model

We consider N bosons moving on the circumference of a circle of length L. We examine both the Lieb-Liniger (LL) interactions and the non-local part of the quasi-1D dipole - dipole (DD)

interactions for atoms polarized perpendicularly to the direction of the motion (its model can be found in Chapter 2.2.2; $\theta = \frac{\pi}{2}$). Our quasi-1D system is governed by Hamiltonian:

$$\hat{H}_{\mathrm{LL(dd)}} = -\frac{\hbar^2}{2m}\sum_{i=1}^{N}\frac{\partial^2}{\partial x_i^2} + \sum_{1\leq i<j\leq N} U_{\mathrm{LL(dd)}}\left(x_i - x_j\right), \tag{4.1}$$

where x_i is a position of ith boson. From now on we set $\hbar = m = 1$. The Lieb-Liniger point-like potential reads:

$$U_{\mathrm{LL}}(x) = g\delta\left(x_i - x_j\right), \tag{4.2}$$

where in the reality the constant g depends on the 3D scattering length and the dimensionality (see Chapter 2.2.1). The non-local part of the quasi-1D dipolar potential is given by (Chapter 2.2.2):

$$U_{\mathrm{dd}}(x) = g_{\mathrm{dd}}\frac{\left(-2|u| + \sqrt{2\pi}(1+u^2)e^{u^2/2}\mathrm{Erfc}\left(|u|/\sqrt{2}\right)\right)}{4l_\perp} \tag{4.3}$$

The strength of dipole-dipole interactions is $g_{\mathrm{dd}} = \frac{C_{\mathrm{dd}}}{4\pi l_\perp^2}$ (see Chapter 2.2.2).

4.2 Solutions

The systems governed by the above Hamiltonian are translationally invariant. Therefore, the total momentum operator $\hat{K} = \frac{L}{2\pi i}\sum_{i=1}^{N}\frac{\partial}{\partial x_i}$ commutes with Hamiltonian $\hat{H}_{\mathrm{LL(dd)}}$, $\left[\hat{K}, \hat{H}_{\mathrm{LL(dd)}}\right] = 0$. Hence, the value of a total momentum K is a good quantum number and all the eigenstates can be ordered by it. Note that we express the total momentum in units $(2\pi/L)$ so it is an integer. We are interested in the lowest energy eigenstates with a given total momentum, an yrast state.

The exact solutions of $\hat{H}_{\mathrm{LL}}$ are obtained with the help of Bethe ansatz and well-known for more than 50 years by now (see Chapter 2). On the other hand, a problem with long-range interactions is not, to best of our knowledge, tractable analytically. To compare and handle the above two models on an equal footing we perform numerical calculations (see Chapter 2).[1] We choose the Fock basis $|n_{-k_{\max}}, \ldots, n_k, \ldots, n_{+k_{max}}\rangle$, with n_k atoms occupying the orbital $\frac{1}{\sqrt{L}}e^{i2\pi kx/L}$ with an integer k. We use the cut-off for maximal momentum k_{max} sufficiently high to ensure convergence. To find an yrast state $|N,\, K,\, 0\rangle$ with a total momentum K and number of atoms N we use the exact diagonalization with the Lanczos algorithm [137].

As an example for our calculations we choose $N = 8$, $g = 0.08$ (the same as in [124]), $g_{dd} = 0.08$ and $\sigma = l_\perp/L = 0.1$. Here, we use the box units with L as a length unit and $\frac{mL^2}{\hbar}$ as a unit of time. The strength of dipolar interactions are chosen to fulfill $\int U_{\mathrm{LL}}(x)dx = \int U_{\mathrm{dd}}(x)dx$. We are interested in the yrast state with $K = N/2$ that for the Lieb-Liniger model corresponds to the black soliton. Our computation performed in the Fock basis gives us immediate access to the structure of the eigenstate. It turns out that the many-body yrast state is dominated by the single Fock state $|n_0 = \frac{N}{2}, n_1 = \frac{N}{2}\rangle$ with atoms equally distributed between the orbitals with momenta

[1] Note that even knowing the exact solutions of the Lieb-Liniger model it is much more efficient to solve it numerically.

$k = 0$ and $k = 1$ in both cases described by $\hat{H}_{\mathrm{LL(dd)}}$. The fidelity of this single Fock state and the total state exceeds 99.5% in both cases.

As discussed earlier in Chapter 2.4.1 one way to extract single-body properties from a many-body eigenstate requires to find the conditional single-particle wave function of Nth particle $\psi_{\mathrm{con}}^{\bar{x}_1,\bar{x}_2,\ldots,\bar{x}_{N-1}}(x_N)$ where positions of remaining $N-1$ particles are drawn from the multi-dimensional probability distribution given by squared modulus of the many-body wave function. Then, one can compare the probability distribution function of the last particle $P(x_N) \propto |\psi_{\mathrm{con}}^{\bar{x}_1,\bar{x}_2,\ldots,\bar{x}_{N-1}}(x_N)|^2$ and the phase of the conditional wave-function with the corresponding quantities of the black soliton from the GPE fully determined by ψ_{GPE}. As there is no quantitative and qualitative difference between the numerical results for both cases considered in this section in Fig. 4.1 we show an example of the probability distribution of the last particle for the contact interactions only and we compare it with the solutions of the non-linear Schrödinger equation (2.39), which were found with the help of the paper [166] (see also [167, 168]). These solutions are given in terms of the elliptic Jacobi functions. We plot the mean field solutions with the average momentum $\frac{2\pi}{Li}\int \psi^*_{GPE}\frac{\partial}{\partial x}\psi_{GPE}\,\mathrm{d}x$ equal to the total momentum of the yrast state per particle K/N. In the Fig. 4.1 we only repeat the result of [124], the one for the weakest interaction.[2]

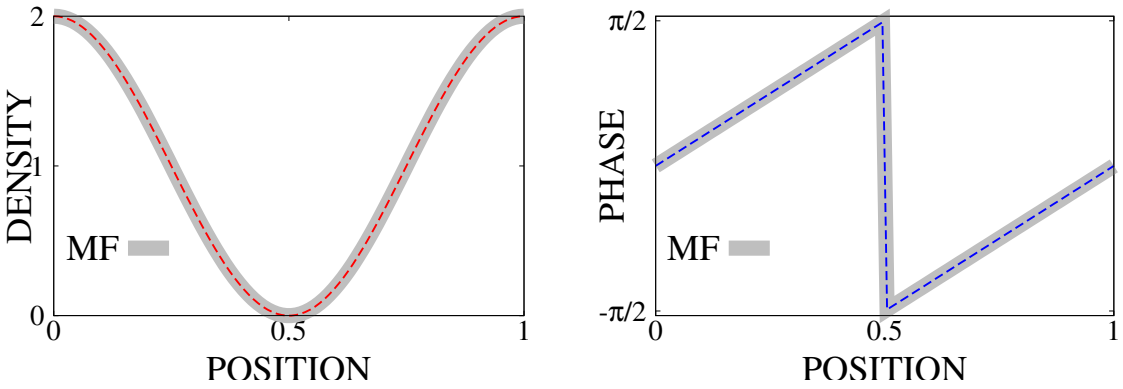

Figure 4.1: The probability density (left) and the phase (right) of the single-particle conditional wave-function obtained from the many-body yrast state with the total momentum $K = N/2$ by drawing $N-1$ positions, as described in the main text. The corresponding properties of the mean-field solutions are presented with the gray thick line. Total number of atoms $N = 8$, the interaction strength $g = 0.08$. Position is in units of the box length L.

The role of the single Fock state for weakly interacting contact gas was also discussed in [122]. As we see, it is also true for weakly interacting repulsive dipolar gas. We recall (see also Chapter 2.3.2) that for the noninteracting limit of the Lieb-Liniger model an yrast state (type-II excitation) with momentum K is a state with K atoms occupying the plane wave with momentum $k = 1$, namely the orbital $\frac{1}{\sqrt{L}}\,e^{i2\pi x/L}$, and the rest of them remain in the state $\frac{1}{\sqrt{L}}$ corresponding to $k = 0$:

$$|N,\,K,\,0\rangle := |n_0 = N-K, n_1 = K\rangle. \tag{4.4}$$

with an energy $E = \frac{2\pi^2}{L^2}K$.

[2] In fact, because of the dominant role of a single Fock state, results from the discretized imaginary time evolution in Fig 4.1 were obtained for the ideal gas as it would not be different to weakly interacting gas with $gN = 0.64$

The perturbation theory teaches us that at least for weak interactions (short- and long-range) the yrast states should be dominated by the eigenstates identified already in the non-interacting case, given in Eq. (4.4), as shown in this section. At the same time, we try to convince the Reader, that the many-body yrast states have solitons built-in. On the other hand, we see that dominant role is played by the solutions of the non-interacting case, where there is no source for the nonlinearity in a corresponding GPE and henceforth no orthodox soliton can appear. What is the reason that the solutions with nice solitonic properties, like density notches and phase jumps, emerge in this regime? Are the additional Fock states forming the yrast states, with residual weights not exceeding 0.5%, sufficient to build up the solitonic properties?

To answer these questions we analyze below the conditional wave function of the yrast states in the case without interaction. We start with the statistical properties of the system in relation to a measurement.

4.3 Revisiting the noninteracting limit

4.3.1 Multiparticle wave function versus measurement

In this subsection we reconstruct the experimental-like measurement by drawing N positions from an yrast state using its probability density $|\Psi^0_{NK}(\vec{x})|^2 = |\langle \vec{x}|N,\, K,\, 0\rangle|^2$, where $\vec{x} = (x_1, ..., x_N)$, as the N-body distribution. To perform such drawing we use the algorithm of Metropolis. We repeat this procedure many times, collecting configurations $\{\vec{x}\}_i = \left\{\vec{x}^i_1, ..., \vec{x}^i_N\right\}$ from each (i-th) shot, as experimentalists have on CCD cameras. We align the samples by rotating them such that their center of mass point in the same direction (see Chapter 2). After the alignment procedure we make a histogram of particles positions.

The results are presented in Fig. 4.2 for yrast states of the ideal gas (4.4) in two cases: the total momentum $K = N/2$ (left column with green histograms) and the total momentum $K = N/4$ (right column with red histograms). As N grows the positions' histograms approach the mean-field densities (in a rotated frame). Hence, we show that even in the case of the ideal gas, one can extract from the many-body eigenstate a distribution with density notch, the same which appears in the time dependent mean-field analysis. Moreover the Fig. 4.2 demonstrates that such distribution can be extracted from the measurements. In the next subsection we study the black soliton-like states analytically.

4.3.2 Black soliton-like States

As observed in the Sec. 4.2 the many-body eigenstate minimizing the energy in the subspace with the total momentum $K = N/2$ is dominated just by the single Fock state. Here we focus on the conditional wave-function of this state to show how it leads to the density notches and jump in the phase. In the spatial representation this state reads:

$$\psi\left(\vec{x}\right) := \langle \vec{x}|N,\, K = N/2,\, 0\rangle = \frac{1}{\sqrt{L^N \binom{N}{N/2}}} \sum_{\sigma} e^{i2\pi\left(x_{\sigma(1)} + x_{\sigma(2)} + ... + x_{\sigma(N/2)}\right)/L}, \tag{4.5}$$

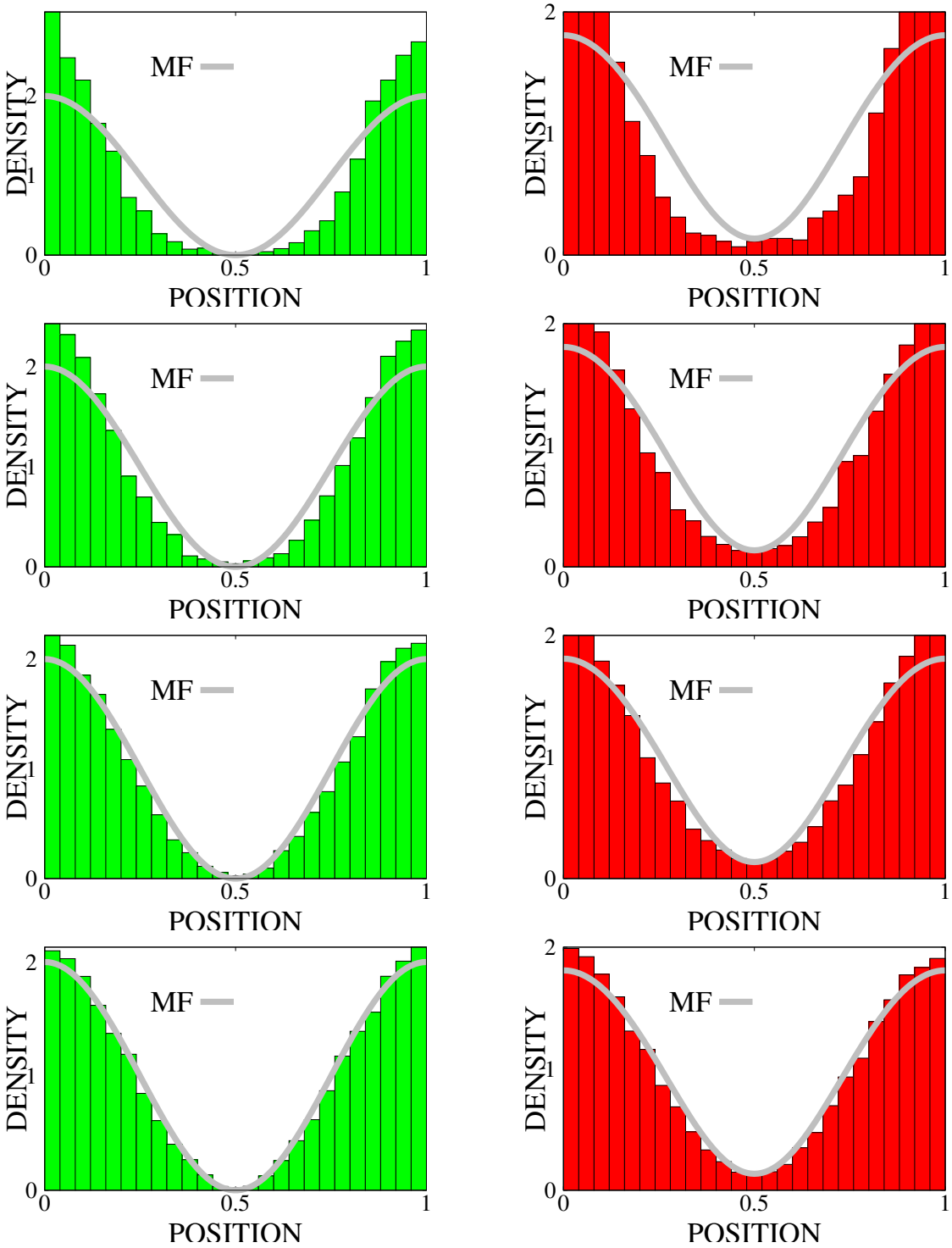

Figure 4.2: Histograms of positions drawn from the many-body yrast state of the ideal gas. The left column is for states with momentum $K = (N/2)$ corresponding to dark solitons. The right column is for the yrast state with fixed total momentum $K = N/4$. The number of atoms, from top to bottom, is $N = 4$, $N = 8$, $N = 16$ and $N = 32$. The solid gray line is the mean-field black soliton for $g = 0$. In all panels the number of samples was 1000. The histograms were computed after shifting particles such that their centers of mass point in he same direction (see Chapter 2). All samples drawn from N-particle distribution. Position is in units of the box length L.

where the sum is over all possible subsets of $N/2$ atoms out of N. We look at the many body wave-function conditioned to "measured" positions of $N-1$ atoms, i.e. we treat the first $N-1$ positions as parameters. The resulting conditional wave-function of N-th particle is:

$$\psi_{\mathrm{con}}^{x_1,\ldots,x_{N-1}}(x_N) \propto S\, e^{2i\pi x_N/L} + M, \tag{4.6}$$

where S is the sum of $\binom{N-1}{N/2-1}$ terms consisting of products of $N/2-1$ plane waves. Similarly the number M is the sum of $\binom{N-1}{N/2}$ terms consisting of products of $N/2$ plane waves. Their explicit forms, denoting the phase factors with $a_i := e^{2i\pi x_i/L}$, are given by

$$\begin{aligned} S &= \sum_{\sigma\in A_{N/2-1}} a_{\sigma(1)}\, a_{\sigma(2)} \ldots\, a_{\sigma(N/2-1)}, \\ M &= \sum_{\sigma\in A_{N/2}} a_{\sigma(1)}\, a_{\sigma(2)} \ldots\, a_{\sigma(N/2)}, \end{aligned} \tag{4.7}$$

where the sums are over all possible subsets of $N/2-1$ and $N/2$ positions from the set $\{x_1,\, x_2,\, \ldots, x_{N-1}\}$. Note that we perform analysis for any positions of the first $N-1$ atoms, not for the ones drawn from the many-body distribution, as it was done in the previous section. Both stochastic functions, S and M have the same number of terms, $\binom{N-1}{N/2} = \binom{N-1}{N/2-1}$. Each term from the sum in S has a counterpart in M due to the identity: $\left(\prod_{i=1}^{N-1} a_i\right)\left(\prod_{j=1}^{N/2-1} a_j\right)^* = \prod_{j=N/2}^{N-1} a_j$. This leads to a conclusion that the complex number S is nothing else, but the complex number M reflected and rotated on the complex plane, i.e. $\left(\prod_{i=1}^{N-1} a_i\right) S^* = M$. With this observation we can write the conditional wave-function (4.6) in a simpler form

$$\psi_{\mathrm{con}}^{x_1,\ldots,x_{N-1}}(x_N) \propto 1 + e^{2i\pi(x_N+X)/L}, \tag{4.8}$$

where $X = \sum_{i=1}^{N-1} x_i - \frac{L}{\pi}\mathrm{A}rg\,(M)$. In other words we find that irrespectively of the positions of $N-1$ atoms, the yrast state (4.5) treated as a function of the Nth atom has the form $1+e^{2i\pi x_N/L}$ up to a shift of x_N by a distance X depending on all other particles. The conditional wave-function (4.8) has a density profile $1+\cos\left(2\pi\ \left(x_N - X\right)/L\right)$ mimicking the density notch known for soliton. In the position of density minimum at X, the phase jumps by π– again as in the black soliton known from the non-linear Schrödinger equation. These density and phase profiles coincides with the results for black soliton-like states, presented in Fig. 4.1. As no source of non-linearity is present these are no real solitons; we cannot speak about healing length or compensation between the dispersion and inter-atomic repulsion. Still we can draw an interesting conclusion: the typical properties of the soliton, density notch and the appropriate phase jump, appear already in the ideal gas case. We also see a good agreement between the profiles of the conditional states and the 'solitons' found in the corresponding Schrödinger equation. This agreement may seem accidental: in the naive derivation of the non-linear Schrödinger equation one assumes that the many-body wave function is a product state with all atoms occupying the same orbital. In the case of the ideal gas the conditional wave-function has indeed a form independent of all other $N-1$ positions, but up to a shift X. The solitonic-properties result from the Fock state $|\frac{N}{2}, \frac{N}{2}\rangle$. Due to the bosonic symmetrization this state, written in the position representation in Eq. (4.5), is highly correlated and far from a product state. We reach a paradox: we find the mean-field solutions in the many-body

state which is very far from the assumptions on which the mean-field model relies. This paradox strongly reminds the famous debate about the interference of the Fock states [139, 169]. The average density computed in the Fock state is uniform. On the other hand, in each experimental realizations there was appearing a clear interference pattern [170], although at a random position. It has been explained that the interference pattern arises in the course of measurements [139, 171]– the wave-function under the condition that a few particles were measured at certain positions exhibits indeed a clear interference fringes. The appearance of the black 'solitons', as well as the appearance of the interference fringes, can be understood within the following form of the many-body wave-function [172]:

$$\psi(\vec{x}) = \int_0^L \mathrm{d}X\, e^{-i\pi(2\hat{K}-N)X/L} \prod_{i=1}^{N} \psi_{GPE}(x_i) \\ \propto \int_0^L \mathrm{d}X\, e^{-2i\pi\hat{K}X/L} \left(e^{i\pi NX/L}\right) \prod_{i=1}^{N} \left(1 + e^{2i\pi x_i/L}\right). \quad (4.9)$$

In other words, the state is a superposition of the same product states, but with all possible positions preserving the translational symmetry. "Measuring" a few positions would break the translational symmetry and cause collapse of the wavepacket onto one of the superposed states $\prod_{i=1}^{N} \psi_{GPE}(x_i + X)$, namely to the state (4.8). Hence, the density notch appears at a random place, determined by the first few detected particles as discussed in [125, 139, 172].

As a side note, we would like to mention that the Fock states we investigate are broadly discussed by the Quantum Information community. The state $|\frac{N}{2}, \frac{N}{2}\rangle$ is called there the twin Fock state. The experiments [173, 174] demonstrated that the twin Fock state is useful in the interferometry, reducing the uncertaintities strongly below the "classical" shot noise limits.

4.3.3 Gray soliton-like states

The conditional wave-function of the Fock state $|n_0 = N - K,\, n_1 = K\rangle$, i.e. a Dicke state [175], is still of the form:

$$\psi_{\mathrm{con}}^{x_1,\ldots,x_{N-1}}(x_N) \propto S_K\, e^{2\pi i x_N/L} + M_K. \quad (4.10)$$

The formulas corresponding to Eq. (4.7) read

$$S_K = \sum_{\sigma\in A_{K-1}} a_{\sigma(1)}\, a_{\sigma(2)} \cdots a_{\sigma(K-1)}, \\ M_K = \sum_{\sigma\in A_K} a_{\sigma(1)}\, a_{\sigma(2)} \cdots a_{\sigma(K)}, \quad (4.11)$$

where A_K are all subsets of K positions from the $N-1$ "measured" particles. The probability density is given by

$$|\psi_{\mathrm{con}}^{x_1,\ldots,x_{N-1}}(x_N)|^2 = |S_K|^2 + |M_K|^2 + 2|S_K\, M_K|\, \cos(\phi(x_N)) \quad (4.12)$$

where $\phi(x_N) = 2\pi\, x_N/L + \mathrm{Arg}\,\{S_K - M_K\}$. Clearly this density has to be larger than $(|S_K| - |M_K|)^2$; namely, the more the absolute values $|S_K|$ and $|M_K|$ differ, the shallower is the dip

in the density. We illustrate grey "solitons" in Fig. 4.2 (red panels) by histograms obtained for $K = N/4$, and compare them with the mean-field solution in the non-interacting limit with the average momentum $\langle \hat{k} \rangle = 1/4$. The wave-function of the mean field gray soliton converges to $\sqrt{\frac{N-K}{K}} + \sqrt{\frac{K}{N}}\, e^{2\pi i x/L}$.

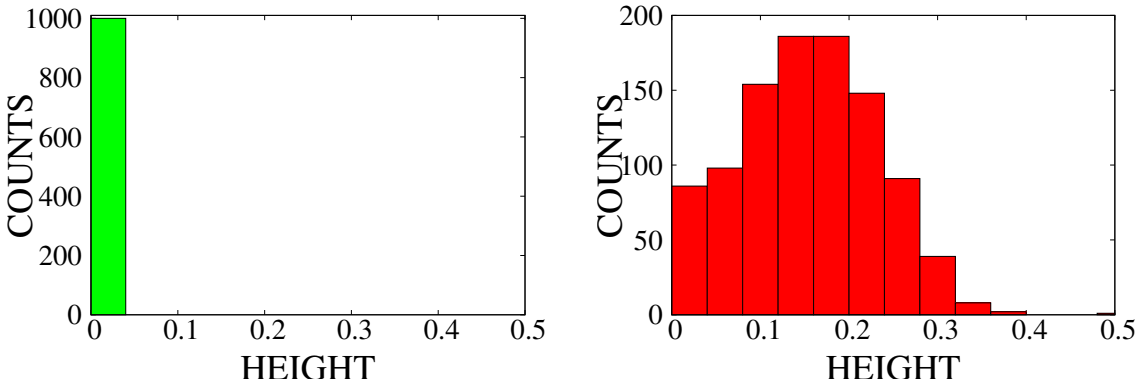

Figure 4.3: Histograms of heights of square of normalized conditional wave function at its minimum drawn from the many-body yrast state of the ideal gas for $N = 32$ atoms. The left panel: $K = N/2$ (corresponding to black soliton), the right panel $K = N/4$. In both cases the number of samples was 1000.

Contrary to the black "soliton" case the form of the conditional wave-function of the gray "soliton" Eq. (4.12) is not universal. We illustrate its diversity in the right panel of Fig. 4.3, showing the histogram of the heights of the conditional wave-function obtained from 1000 samples. The height equal to 0 corresponds to the black soliton. We note that the depth of grey solitons varies significantly from shot to shot.

4.3.4 Multiple soliton-like states

The superposition of two solutions of some non-linear equation usually is not the solution anymore. However, for the equations supporting solitons, one can perceive some sort of the superposition rule. We want to verify if there exists multiple solitons-like solutions in the ideal gas. In the limit of vanishing interaction the eigenstate with two black solitons built-in converges to the Fock state $|n_{-1} = N/2,\, n_1 = N/2\rangle$. One can perform the analysis similar to the one from the previous section to obtain the conditional wave-function

$$\psi_{\mathrm{con}}(x_N) \propto \cos(2\pi(x_N - X)/L), \tag{4.13}$$

where the shift X is the random variable which depends on the positions $x_1, \ldots, x_{N-1}$. The probability density is given by $\cos^2(2\pi(x_N - X)/L)$ with two local minima at positions $X + 1/4L$ and $X + 3/4L$. At each node the conditional wave function (4.13) changes sign; i.e,. it has a π-jump in the phase, similarly to the black solitons. It is easy to find the solutions with M black "solitons": the many-body eigenstate with M black "solitons" is $|n_{-M/2} = N/2;\, n_{M/2} = N/2\rangle$.

4.3.5 Dynamics of solitons

Can "solitons" move? Within the many-body picture such movement is impossible: the states we discuss are the eigenstates of the Hamiltonian, which would gain in the evolution only a global factor e^{-iEt} without any physical significance. On the other hand, after breaking the symmetry by fixing the first $N-1$ positions, we obtained a conditional wave-function which is not a stationary solution of the mean field model. The equivalent of a single black soliton is $\psi_{\mathrm{con}}(x_N) \propto 1 + e^{i2\pi(x_N - X)/L}$, namely it is a superposition of two plane waves with the energies $E_0 = 0$ and $E_1 = \frac{2\pi^2}{L^2}$. Hence, the state evolves in time,

$$\psi_{\mathrm{con}}(x_N, t) \propto 1 + e^{i2\pi(x_N - X)/L - iE_1 t} = 1 + e^{i2\pi(x_N - vt - X)/L}, \tag{4.14}$$

with the velocity $v = \pi/L$, as the black soliton in the case of periodic boundary conditions should move. A similar analysis for two black solitons shows that they are not moving at all, again exactly like in the mean field picture.

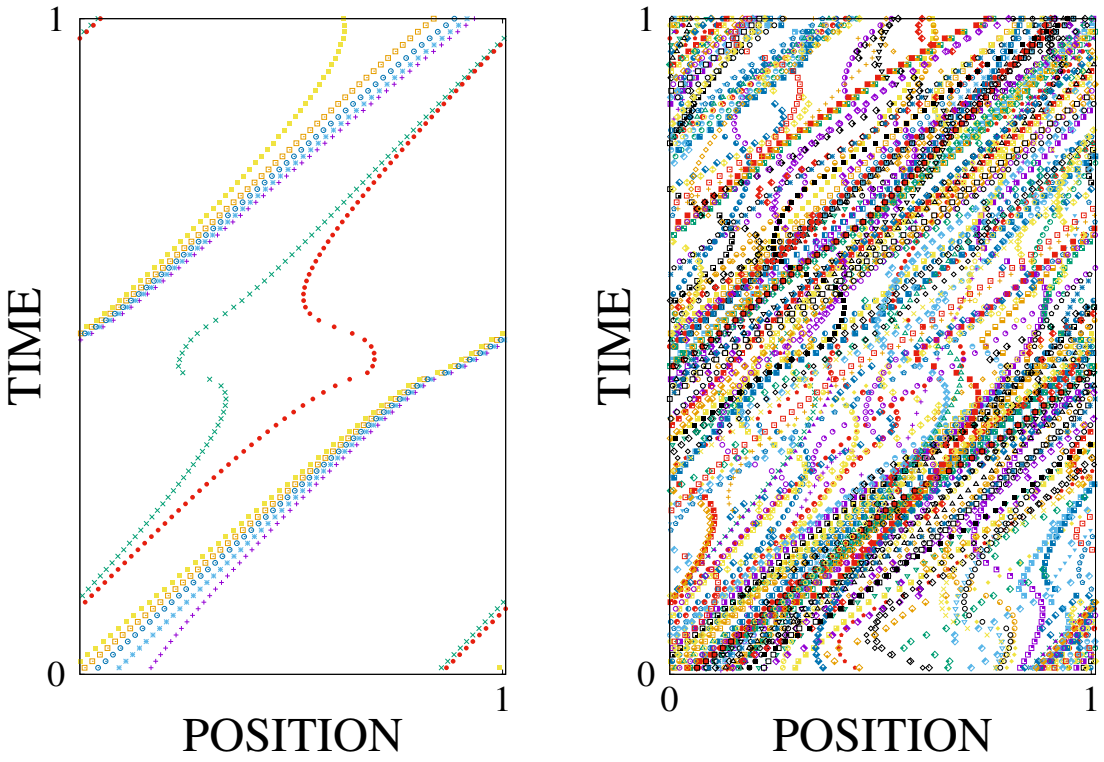

Figure 4.4: Bohmian trajectories. Left: Trajectories of all $N = 8$ Bohmian particles from a single sample. Right: 80 trajectories obtained from 10 samples. The initial positions were shifted to match the density notches, as in Fig. 4.2. Position is in the unit of the box length L. Time is dimensionless.

Naively, to obtain a motion of solitons one would just evolve in time the corresponding conditional wave-functions. This, however, fails completely in the case of the gray 'solitons', which within such procedure would move with speed π/L, as the black solitons. To see the solitonic motion we use more sophisticated method: the Bohmian interpretation of the Quantum Mechanics [176–178]. In the Bohmian picture one represents the state as a collection of N point-like masses

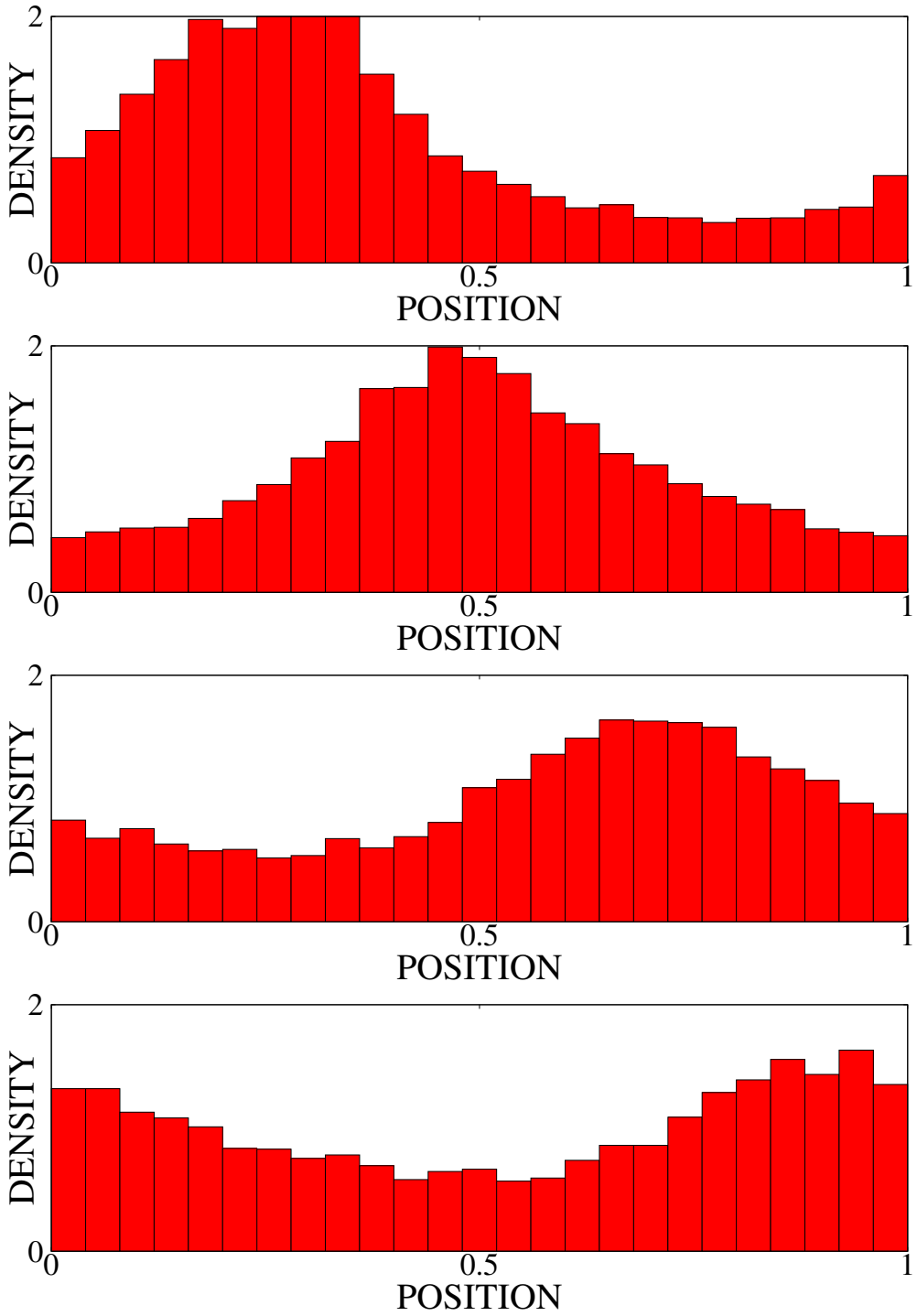

Figure 4.5: Histograms of particles positions at a few instants of time. The histograms were obtained from positions of the Bohmian particles obtained in 1000 realizations at times, from top to bottom $T = 0.1,\ 0.2,\ 0.3,\ 0.4$. Position is in units of the box length L. Time is dimensionless.

moving with the time dependent velocities. Their initial positions should be drawn from the N-body probability distribution $|\psi(\vec{(x)})|^2$. They move similarly to the Newtonian particles, but with the velocities depending on all other particles. The velocity of the lth particle is given by

$$v_l = \mathrm{I}m \left\{ \frac{\partial_l \psi(\vec{x})}{\psi(\vec{x})} \right\}, \tag{4.15}$$

where $\partial_l := \frac{\partial}{\partial x_l}$ is the partial derivative with respect to the l-th particle.

In the case of the gray soliton-like state (4.6), the velocity of the N-th particle reads:

$$v_N = -\frac{\pi}{L} + \frac{\pi}{L} \frac{|M_K|^2 - |S_K|^2}{|\psi_{\mathrm{con}}^{x_1,\ldots,x_{N-1}}(x_N)|^2}, \tag{4.16}$$

where the probability density appearing in the denominator is given in Eq. (4.12). The bohmian particle moves then with the velocity depending on the local density (accelerating under the density-notch) and the total solitonic depth encoded in the parameters S_K and M_K.

The results are presented in Fig. 4.4 and 4.5 and in the case of $N = 8$ atoms and the initial state $|n_0 = 5, n_1 = 3\rangle$. We show there the examples of trajectories of all 8 particles, drawing it once (the left panel of Fig. 4.4) and then 10 times (the right panel of Fig. 4.4). At few chosen instants of time we reconstructed in Fig. 4.5 the histograms, using 1000 samples of the initial positions. We observe that the solitons are moving from left to right, but also the corresponding density notch in the histogram smears for longer evolution time. This can be understood already from Fig. 4.3 which shows that the states $|n_0 = 3N/4, n_1 = N/4\rangle$ are rather collections of states with different velocities, which cause a dispersion shown in Fig. 4.5.

4.3.6 Validity range

How long the non-interacting yrast states approximate well the eigenstates of the interacting system? We start our investigation with the analytical solution of H_{LL}. The many-body yrast states of the Lieb-Liniger model are constructed from the plane waves with N pairwise different quasi-momenta. These quasi momenta are solutions of the set of transcendental Bethe equations. On the other hand we know already that for the ideal gas the exact solution is the single Fock state, with $N - K$ atoms in momentum 0 and K atoms in momentum $k = 1$. Then one can ask the question what are the Lieb's quasi-momenta in the limit of vanishing interaction. We checked, in the case of the black soliton, that half of the quasi-momenta known from the Lieb solutions converge to 0 and the second half to 1. It means, regarding the previous sections, that the quasi-momenta become the true particle momenta. The quasi-momenta are not analytic functions of the interaction strength at $g = 0$; they converge with the rate $\sqrt{g}$. Since the number of equations for quasimomenta grows with N, the small parameter should be rather the inverse of the healing length $\sqrt{gN/L} = 1/\xi$.

We verify this predictions in Fig. 4.6, where we show the fidelity between the yrast state with momentum $K = N/2$ for both contact and dipolar interactions and the twin-Fock state $|N/2, N/2\rangle$. Both figures are practically indistinguishable from each other, especially for healing lenghts > 0.5. It shows, that for the small parameter $1/\xi$ all the solitonic properties lay in the bosonic nature

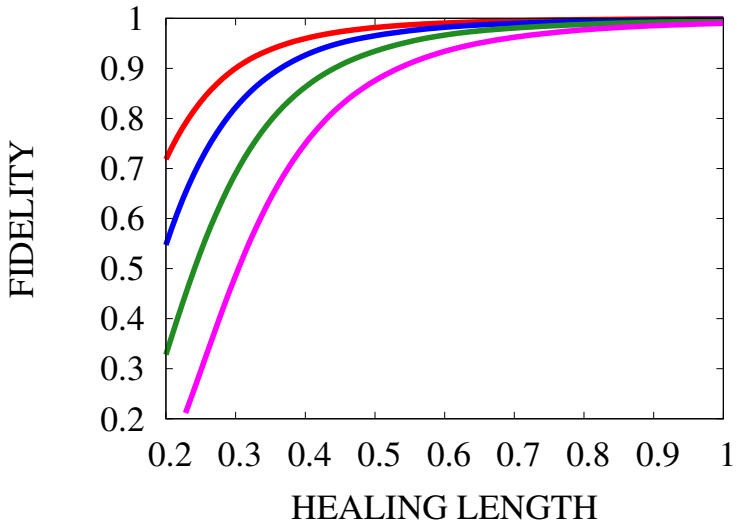

Figure 4.6: Fidelity between the yrast state with momentum $K = N/2$ obtained numerically from Eq. (4.1) and the twin-Fock state $|N/2, N/2\rangle$ as a function of the healing length $1/\sqrt{gN/L}$ or $1/\sqrt{g_{\rm dd}N/L}$. Note, that for both cases one cannot distinguish the results. Number of atoms, from top to bottom $N = 8,\ 16,\ 32,\ 64$. Position is in units of the box length L.

of the system, rather than in a specific form of interparticle interactions. Note that the ideal gas approximation is fairly accurate even for the healing length significantly shorter than the size of the box. This agrees with the analysis in [122]. However, as the number of atoms N increases, the fidelity drops faster, although the strength of interactions is smaller for a higher number of atoms. Indeed, for a bigger system also the number of possible Fock states grows. There are many Fock states which are energetically very close to the twin-Fock state $|N/2, N/2\rangle$ and even a small perturbation enhances their population in an actual yrast state obtained numerically in the plane wave basis.

We stress that there may be still a correspondence between the conditional wave-functions and the mean-field solitons even for the healing lengths much shorter than L [124, 125, 179]. Only the solitonic features can not be explained within the ideal gas picture used in the previous section. For the ideal gas, the width of the solitonic notch is fully determined by $k = 1$ single particle momentum appearance. Analysis of the plane wave basis shows us immediately that narrower dips in the density need Fock states with $n_k \neq 0$ for $k > 1$.

4.4 Conclusions

Since the seminal work of E. Lieb [113, 114] there are numerous studies of the relation between the two descriptions of N interacting bosons on a ring: the nonlinear mean-field model and the more fundamental linear many-body description.

We investigate the type II Lieb's elementary excitations in the limit of vanishing interaction strength for the contact and dipolar interaactions. These excitations converge simply – regardless of the type of interactions – to the Fock states in the plane-wave basis, in particular the many-body

black soliton becomes the twin Fock state. Particles in the twin Fock states are in fact strongly correlated due to the bosonic statistics. As in the paper [124, 125, 179], we start with the N-body eigenstates, from which we obtain a single-body wave-functions conditioned to the first $N-1$ particles measured. We find that the conditional wave-function has the typical solitonic properties - the density notches with appropriate phase jumps. Of course the soliton-like states are not the true solitons - there is no nonlinearity which would dictate the width of the objects. Adding interaction such that the healing length decreases significantly below the size of the box would just shrink the density notches. Note, that in the Lieb-Liniger model and its hard wall box analog the small number of particles does not allow to fulfill the mean-field conditions $\xi \ll L$ and $\gamma = gL/N \ll 1$ at the same time [124, 125, 179]. The same applies to the system with dipolar interactions. Accordingly, one cannot predict whether a new type solitonlike states in GPE with purely dipolar repulsive interactions [54] corresponds to the eigenstates of the underlying many-body problem. For a small system, it requires too strong interactions. On the other hand, due to the numerical complexity, adding atoms to the system limits the applicability of the method based on the conditional wave function. A different approach has to be invented.

Our findings for the ideal gas open at least three other avenues to study. As the twin-Fock states are already produced experimentally, one can ask if it is possible to transform them into soliton-like states. The interesting problem is the correspondence between the states created via phase imprinting on the Bose-Einstein condensate and the real many-body solitons. At least for ideal gas it is clear that such experimental procedure does not lead to the yrast states – the phase imprinting would keep the multiparticle wave-function in the product state, whereas the yrast state is the highly entangled twin-Fock state. Finally, according to Eq. 4.9 for the ideal gas an interesting hypothesis arises. Namely, that the superposition of GPE solutions for the interacting gas reproduce all the properties of the yrast state. If that is true it would also complement an observation that some superposition of yrast state, gives a corresponding GPE soliton[123, 126, 127, 180].

Chapter 5

Roton in a few-body dipolar system

The roton-maxon spectrum was predicted in a dipolar gas of polarized ultracold atoms almost 20 years ago [75, 76]. This happens for relatively weak interactions, for which the system is in the Bose-Einstein condensate state. Therefore, one can use the mean-field or Bogoliubov description and find the roton state as a Bogoliubov quasi particle (see Chapter 1.3 for references). Usually the dipolar system is studied within the Bogoliubov approximation (see Chapter 2.5.2), so that there is no access to the detailed structure of the low lying excitations. Only a few many-body investigations were performed for the roton state using different techniques [181–184]. A good attempt can be made by a numerically exact solution to a many-body problem with a rotonic characteristic. Even if found for a relatively small number of particles, modern experiments with a precise control over only a few atoms in optical lattices or single traps (see for instance [32, 116, 143, 146, 185]) allow testing its physical predictions.

In this Chapter we present numerically exact results for a quasi-1D model, which admits the roton excitation in a dipolar analogue of the Lieb-Liniger model. When the interatomic forces are of the attractive character on the short-scale, whereas the long-range part of potential is repulsive, the interplay of these two interactions may lower the energy of the roton mode even to the ground state level. It opens a significant question: is it possible in a dipolar analog of the Lieb-Liniger model that the two branches cross, such that it is a type-I Bogoliubov excitation, in particular the roton, which would appear in the lower branch?

It is a purpose of this Chapter to show that by tuning short-range interactions and adjusting a ring geometry one can continuously change [186] the character of the lowest energy state for a given total momentum of the system from a type-II excitation to the roton mode. We also analyze a numerically exact roton's wave function in the weakly interacting regime and its position and momentum properties.

5.1 Model

We consider N dipolar bosons confined in both transverse directions $\hat{y}$ and $\hat{z}$ with a tight harmonic trap of a frequency $\omega_\perp$. All atoms are polarized along the $\hat{z}$ axis. As it was introduced in

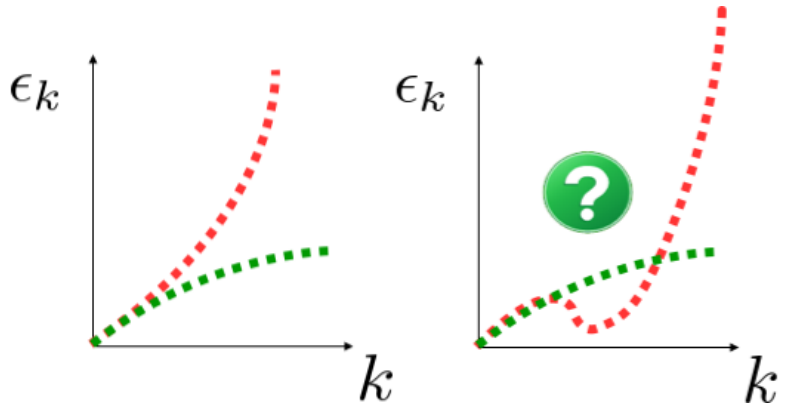

Figure 5.1: Schematic representation of the problem. Excitation spectrum in the Lieb-Liniger model with point-like interactions (left panel) consists of two important families of excitations: type-I excitations (red points) and type-II excitations (green points). Is it possible that in the dipolar analog of this model with long-range repulsion and short-range attraction a type-II excitation would appear in the lower branch?

Chapter 2 our quasi-1D system Hamiltonian reads:

$$\hat{H} = \sum_k \frac{\hbar^2 k^2}{2m} \hat{a}_k^\dagger \hat{a}_k + \frac{1}{2L} \sum_{k_1,k_2,k} \hat{a}_{k_1+k}^\dagger \hat{a}_{k_2-k}^\dagger V_{\text{eff}}(k) \hat{a}_{k_1} \hat{a}_{k_2}, \tag{5.1}$$

with $\hat{a}_k$ ($\hat{a}_k^\dagger$) anihilating (creating) a boson with momentum k and $V_{\text{eff}}(k) = V_{\text{SR}}(k) + V_{\text{dd}}(k)$.

We remind that the quasi-1D dipolar potential is expressed as $V_{\text{dd}}(k) = \frac{3\hbar^2 a_{\text{dd}}}{m l_\perp^2} \left(1 + f\left((l_\perp k)^2/2\right)\right)$ with $l_\perp = \sqrt{\hbar/m\omega_\perp}$. In this chapter we consider repulsive dipolar interaction with $a_{\text{dd}} > 0$. The function f which appears in Eq. 4.1 is equal to $f(u) = u\, e^u \text{Ei}(u)$, where Ei is the exponential integral [156].

Stability of our calculations requires smoothing of a usual short range interaction model used in the ultracold physics, the delta function. We choose a Gaussian model [187–195], namely

$$V_{\text{SR}}(k) = V_0 e^{-\frac{1}{2}k^2 r^2} \tag{5.2}$$

with r standing for the potential range and $|V_0|$ for its depth ($V_0 \leq 0$ later in this work). This step makes our model more realistic, imitating the attractive van der Waals interaction. Note, that our short-range potential interaction produces zero force at x=0, thus the growing kinetic energy of the narrowing wave packet prevents the system from the collapse. This indicates that our Hamiltonian is bounded from below. For convenience we set

$$V_0 = \frac{\hbar^2 a}{m l_\perp^2} \tag{5.3}$$

with $a \leq 0$ mimicking an usual scattering length, which can by tuned in experiments by Feschbach resonances. The relation between Gaussian model parameters a, r and the real scattering length can be found in [196] and references therein. Below we use box units where $L/2\pi$, $2\pi\hbar/L$ and $4\pi^2\hbar^2/mL^2$ are the units of length, momentum and energy respectively.

As we mentioned in Chapter 2.2.3, the expression for the effective potential $V_{\text{eff}}(k)$ corresponds to calculating the interactions along the circumference of a ring rather than along the chord. In

Appendix 5.A we show, using a typical example, that both approaches do not differ significantly. This holds for all the findings in this thesis.

We access the many-body eigenstates of Hamiltonian (4.1) by exact diagonalization using the Lanczos algorithm [137]. Our calculations are performed in the Fock space spanned by the plane-wave basis with a maximum total kinetic energy of the system $E_{\max} = k_{\max}^2/2$ – with single-particle momentum $k_{\max} \gg 1/r$ – sufficiently high to assure convergence. Here we employ the fact that the total momentum of the system $\hat{K} = \sum_k k\, \hat{a}_k^\dagger \hat{a}_k$ is conserved, $\left[\hat{H}, \hat{K}\right] = 0$, so its eigenvalues K are good quantum numbers, used here together with the total number of atoms N to label different eigenstates $|N,\, K,\, i\rangle$ enumerated by i with $i = 0$ corresponding to an yrast state (see Chapter 2.3).

5.2 Results

In the following paragraphs of this Chapter we consider two different situations, namely with weak interactions where the depletion (given by $P(K = 0)$ in Fig. 5.2d and 5.3d) of a ground state is less than 5% and stronger interactions where its value is around 20%. The results for the weak interactions will serve us as a well tested guide through the beyond mean-field analysis.

5.2.1 Weak interactions

We start our analysis of yrast states for the weak interactions. We consider $N = 16$ dysprosium atoms with $a_{\rm dd} = 132\ a_0$ and the potential range $r = 182\ a_0$, where a_0 is the Bohr radius. The value of r, in this case, equals the characteristic length of the attractive part of van der Waals interactions for dysprosium atoms [197]. We initially set a and $\omega_\perp$ corresponding to the usual situation where the yrast states rather resemble the lowest excitation branch from the Lieb-Liniger model (see black squares in the top panel of Fig. 5.2 and Chapter 2.3.1). We compare it with the Bogoliubov spectrum (black dashed line) given by (see Chapter 2.5.2)

$$\epsilon_k = \sqrt{\frac{k^2}{2}\left(\frac{k^2}{2} + 2NV_{\rm eff}(k)\right)} \tag{5.4}$$

Then we continuously change a and $\omega_\perp$ (a simillar effect would be observed if one changes the length of the box) keeping $V_{\rm eff}(0) = \text{const.}$[1] We finally end with the profoundly different spectrum (red points in Fig. 5.2) with the characteristic inflection point for $K = 2$. Moreover, in this case, the spectrum resembles more the one given by Eq. (5.4).

In the bottom panel of Fig. 5.2 we turn our focus to the shape of $NV_{\rm eff}(k)$ for small k where the Bogoliubov spectrum from Eq. (5.4) is not dominated by the large kinetic energy (free particles behaviour). From the analysis of Eq. (5.4) we see that the first derivative of $2NV_{\rm eff}(k)$ has to be negative enough to bend the Bogoliubov spectrum and make the inflection (minimum), i.e. the effective interaction potential has to drop fast enough. This is reflected by the difference of the tilt of $V_{\rm eff}(k)$ between both cases from the bottom panel of Fig. 5.2 for small k. We remind the Reader

[1] $V_{\rm eff}(0) = \int dx\, U_{\rm eff}(x)$ determines the general repulsive or attractive character of interaction

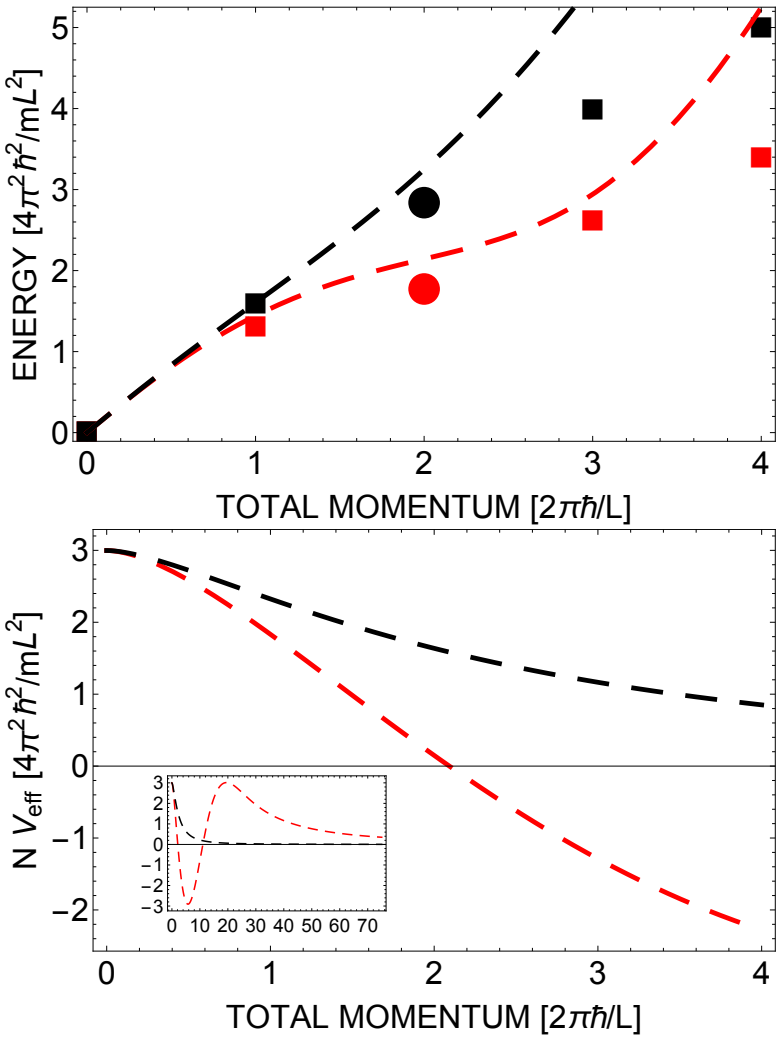

Figure 5.2: Results for weak interactions. Top: Energy of the yrast states for $a = 0$ and $\omega_\perp \approx 2\pi \times 41$ kHz (black squares) and $a \approx -378\, a_0$ and $\omega_\perp \approx 2\pi \times 365$ kHz (red squares) for $N = 16$ dysprosium atoms ($a_{\mathrm{dd}} = 132\, a_0$ and $r = 182\, a_0$) as a function of the total momentum compared with the corresponding Bogoliubov excitation spectrum (dashed lines). Bottom: Shape of the interaction potential in the momentum space $NV_{\mathrm{eff}}(k)$ for small k. In the inset, the whole course of $NV_{\mathrm{eff}}(k)$ is presented.

that even a slight change of a would change the spectrum from Eq. (5.4) dramatically; decreasing a in this case by more than 2.5% would result in the imaginary value of energy. In the inset we plot $NV_{\mathrm{eff}}(k)$ for larger k also. In that regime, a specific course of the effective potential has no significant impact on the Bogoliubov spectrum as it is dominated by the kinetic energy contribution from Eq. (5.4).

We test our hypothesis about the change of the character of the yrast state for $K = 2$ we compare it and the first excited state with the number conserving Bogoliubov approximation (see Chapter 2.5.2) in the following way. We trace a continuous transformation of the yrast state from type-II to type-I excitation we evaluate the fidelities $|\langle N, K, i|N, K\rangle_B|^2$, which is depicted in Fig. 5.3 (top panel). We remind the Reader that $|N, K\rangle_B \propto \left(u_K \hat{a}_0 \hat{a}_K^\dagger + v_K \hat{a}_0^\dagger \hat{a}_{-K}\right) |N, 0\rangle_B$ (see

Chapter 2.5.2). For the initial values of the parameters a and $\omega_\perp$ the first excited state is close to a Bogoliubov excitation. Then we observe a gradual exchange of the states' character as we modify the effective potential ending with a complete role reversal of the two first states. Note, that the sum of the fidelities (black dotted line in Fig. 5.3 is almost equal to 1 at any stage of the transition. It means that Bogoliubov excitation $|N, K = 2\rangle_B$, to a good approximation, remains in a plane spanned by the two lowest eigenstates.

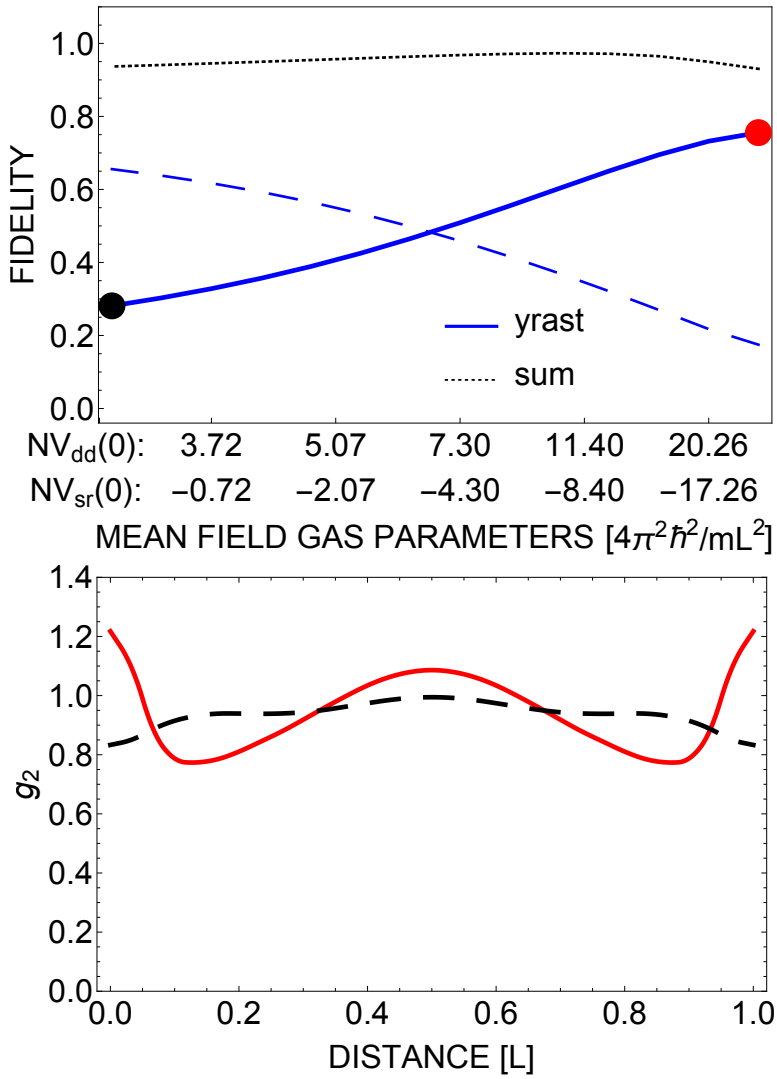

Figure 5.3: Results for weak interactions. Top: Fidelities between the first two eigenstates and Bogoliubov excitation for $K = 2$ as a function of a and $\omega_\perp$ (N and a_{dd} are constant and as in Fig. 5.2). Bottom: The normalized second order correlation function $g_2(x)$ as a function of a distance for two states from the top panel marked by color filled circles.

What are the physical implications of the above fidelity analysis? To show the qualitative change of the yrast state for $K = 2$ we calculate the normalized normally ordered second-order correlation function (widely used in the quantum optics)

$$g_2(x) := \langle \Psi^\dagger(x)\Psi^\dagger(0)\Psi(0)\Psi(x)\rangle / \langle \Psi^\dagger(x)\Psi(x)\rangle \langle \Psi^\dagger(0)\Psi(0)\rangle$$

(bottom panel of Fig. 5.3), which can be measured in experiments with ultracold atoms, see for instance [198–201]. We observe a dramatic difference between two yrast states for border cases from Fig. 5.2 (marked as black and red points). Namely that almost flat distribution typical for type-II excitation in weakly interacting regime is replaced by a function exhibiting an enhanced regular modulation with the number of maxima given by K_{rot}, which is the roton momentum. We have the following interpretation of this behaviour. The function $g_2(x)$ is related to the probability of finding a particle at position x provided that the first one was measured at $x = 0$. We expect that the second order correlation function should have modulation with periodicity depending on the typical non-zero single particle momenta in the system. The value of a single particle momenta is a random variable given by distribution, which is often not peaked at the total momentum of the system (as discussed in details below). Therefore the modulation in g_2 function, if there is any, does not have to correspond to the total momentum K. In this respect the Bogoliubov excitations, ie. states $\hat{b}^{\dagger}_{k=K}|\mathrm{vac}\rangle$, are special, because a typical non-zero single-particle momentum is equal to the total momentum of the system. The fact that the g_2 function of the yrast state with $K = 2$ has also modulation with period $1/K$ ensure us that we deal with a Bogoliubov excitation in the yrast states' branch.

Note, that for a small number of particles we are able to find stable solutions corresponding to realistic mean field gas parameters ($NV_{\mathrm{sr}}(0) = -23.98$, $NV_{\mathrm{dd}}(0) = 26.98$) only for the Bogoliubov spectrum with the inflection, not to the one with the characteristic local minimum. Using the mean field gas parameters ($NV_{\mathrm{sr}}(0)$, $NV_{\mathrm{dd}}(0)$) for which the Bogoliubov spectrum has the local minimum implies much stronger interactions for our few-body system. Our result would approach Bogoliubov's predictions in the limit of $N \to \infty$ (see Appendix 5.B).

5.2.2 Strong interactions

Here, we turn to the strong interactions scenario with $N = 10$, which is beyond the Bogoliubov approximation. In Fig. 5.4 we summarize our findings, where the characteristic local minimum for $K = 3$ is present. In this case the spectrum is calculated with an accuracy of several percent only. Our previous conclusions hold also for this situation. As in the previous case, the second order correlation function of our candidate for roton exhibits the enhanced regular modulation with periodicity corresponding to $1/K_{\mathrm{rot}}$, where $K_{\mathrm{rot}} = 3$ is the position of the minimum in the spectrum (bottom panel of Fig. 5.5) and the total momentum of the yrast state. In the inset of Fig. 5.5 (bottom panel) we show the second order correlations functions of the yrast states with $K = 2$ or $K = 4$, which also have traces of the modulations with a period $1/K_{\mathrm{rot}}$.

The spectrum and modulation of the second order correlation function indicate that we still have a roton-like state, even though this regime is beyond the Bogoliubov approximation validity range.

Remark Note that the presence, position, and depth of the roton minimum for both cases considered in this work are tunable by varying the number of atoms N, trapping frequency $\omega_{\perp}$ and the short-range coupling strength as it was predicted for the roton state in the meanfield studies

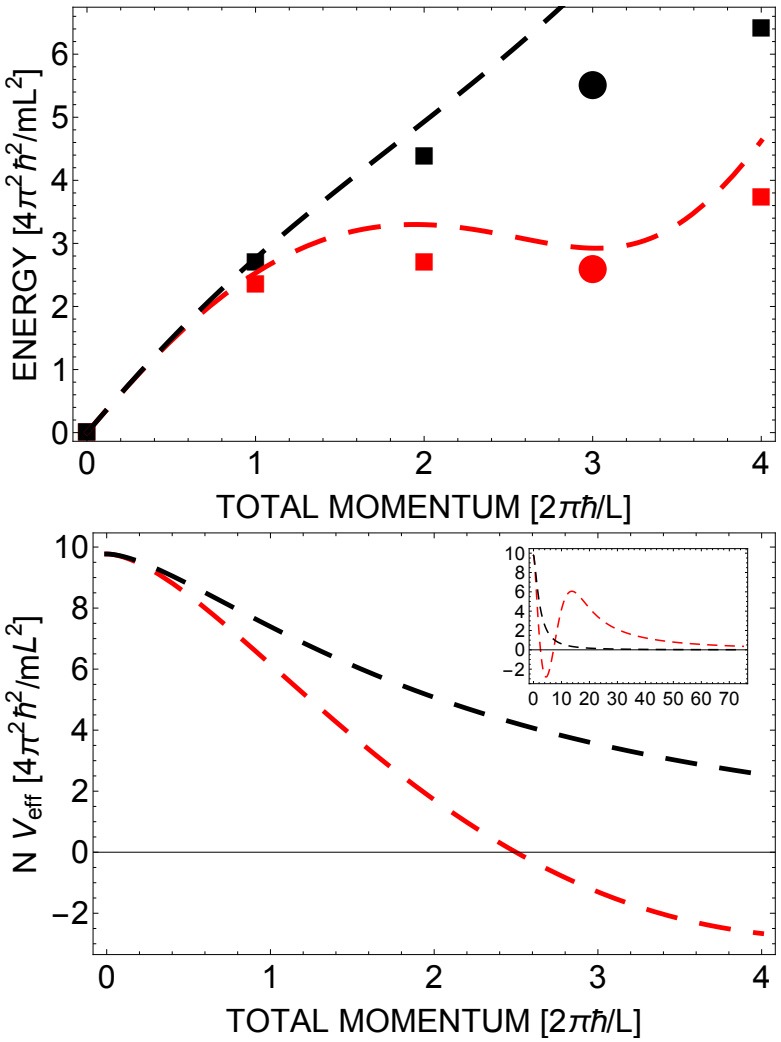

Figure 5.4: Results for stronger interactions. Top: Energy of the yrast states for $a = 0$ and $\omega_\perp \approx 2\pi \times 35$ kHz (black squares) and $a \approx -2080\, a_0$ and $\omega_\perp \approx 2\pi \times 190$ kHz (red squares) for $N = 10$ atoms ($a_{\rm dd} = 792\, a_0$ and $r = 272\, a_0$) as a function of the total momentum compared with the corresponding Bogoliubov excitation spectrum (dashed lines). Bottom: Shape of interaction potential in the momentum space $NV_{\rm eff}(k)$ for small k. In the inset, the whole course of $NV_{\rm eff}(k)$ is presented.

of ultracold dipolar gases [75]. We choose $K_{\rm rot}/N < 1/2$ to minimize the impact of the *umklapp* process [114], discussed earlier in Chapter 2.3.1.

5.2.3 Spatial imaging of roton excitation

How does the calculated g_2 function correspond to an experimental imaging of particles positions using a CCD camera? Having a many-body wave function of a given eigenstate, in particular the roton state, we can explore a multivariate probability distribution of particles positions as it was shown earlier in Chapters 2.4.2 and 4.3.1. Using Metropolis algorithm we draw N positions from the multi particle probability distribution $|\Psi^0_{NK}(\vec{x})|^2$ where $\vec{x} = (x_1, ..., x_N)$ is a position vector of N particles and $\Psi^0_{NK}(\vec{x})$ is the many-body eigenstate in a position representation.

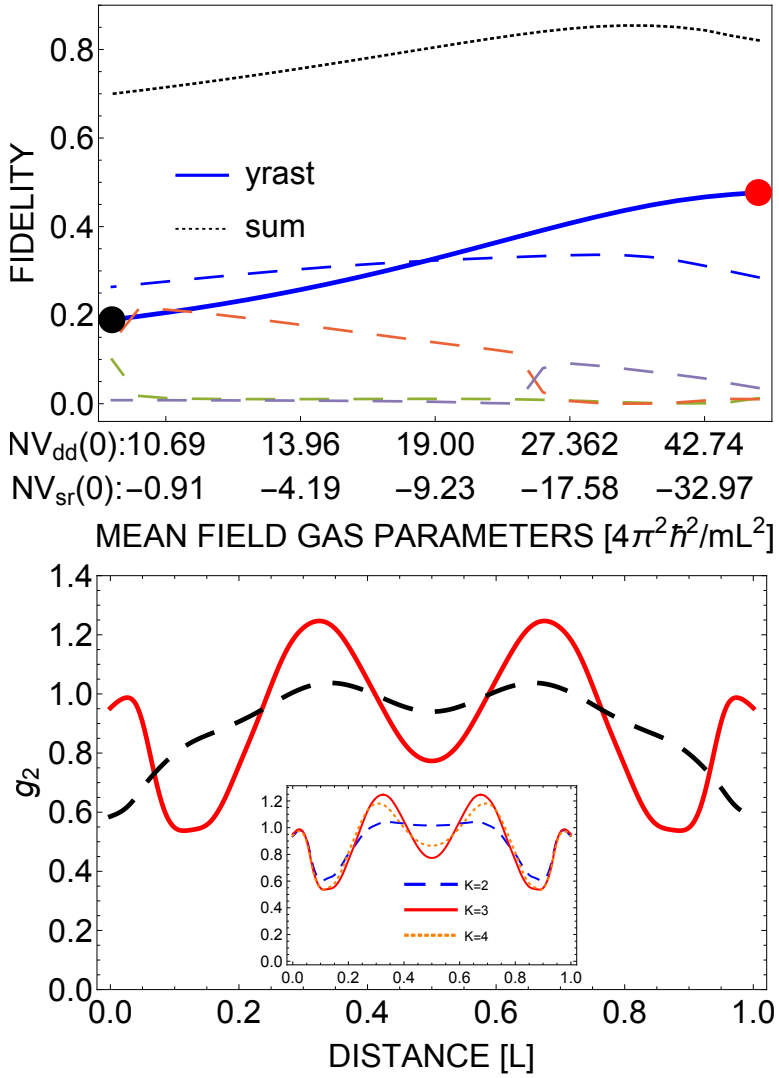

Figure 5.5: Results for stronger interactions. Top: Fidelities between the first five eigenstates and Bogoliubov excitation for $K = 3$ as a function of a and $\omega_\perp$ (N and $a_{\rm dd}$ are constant and as in Fig. 5.4. Bottom: The normalized second order correlation function as a function of a distance for two states from the top panel marked by color filled circles. Inset: comparison between yrast states $K = 2$ (dashed blue line), $K = 3$ (orange dotted line) and $K = 4$ (red line) for the spectrum with the local minimum.

We repeat this procedure many times, collecting configurations $\{\vec{x}\}_i = \{\vec{x}_1^i, ..., \vec{x}_N^i\}$ from each (i-th) shot. A particles' positions histogram obtained from all configurations would be uniform as the center of mass for each $\{\vec{x}\}_i$ is randomly placed in accordance with a rotationally uniform distribution (see also Chapter 2.4.2).[2] On the other hand, the distances between particles in each configuration are translationally invariant and may reveal any potentially hidden pair correlations for a given eigenstate. Indeed, the probability distribution of the inter particle distances is directly related to the $g_2(x)$ function. How many samples one needs to estimate it? In Fig. 5.6 we compare probability distribution function histograms of distances between particles in each configuration

[2]For the ideal gas from the previous Chapter, this also holds true, but fluctuations are much smaller than in this case.

$\{\vec{x}\}_i$ 'measured' numerically for different number of configurations involved in average calculated for the roton state with the mean field gas parameters identical to the ones from Fig. 5.4 ($K_{\mathrm{rot}} = 3$), but obtained for $N = 7$ particles due to the factorial growth of terms in the expression for the many-body wave function with N. The distance between i-th and j-th particle is defined as:

$$d_{ij} = \min\left(|x_i - x_j|, 1 - |x_i - x_j|\right) \tag{5.5}$$

with $0 \leq d_{ij} \leq 0.5$. As we can see the results converge rather fast as we increase number of configurations involved. The inset of Fig. 5.4 explains why we observe only the local maximum for $x = 1/3L$ in the histograms and not for $x = 2/3L$ also. It is simply because of our natural definition of distance between particles on a ring geometry.

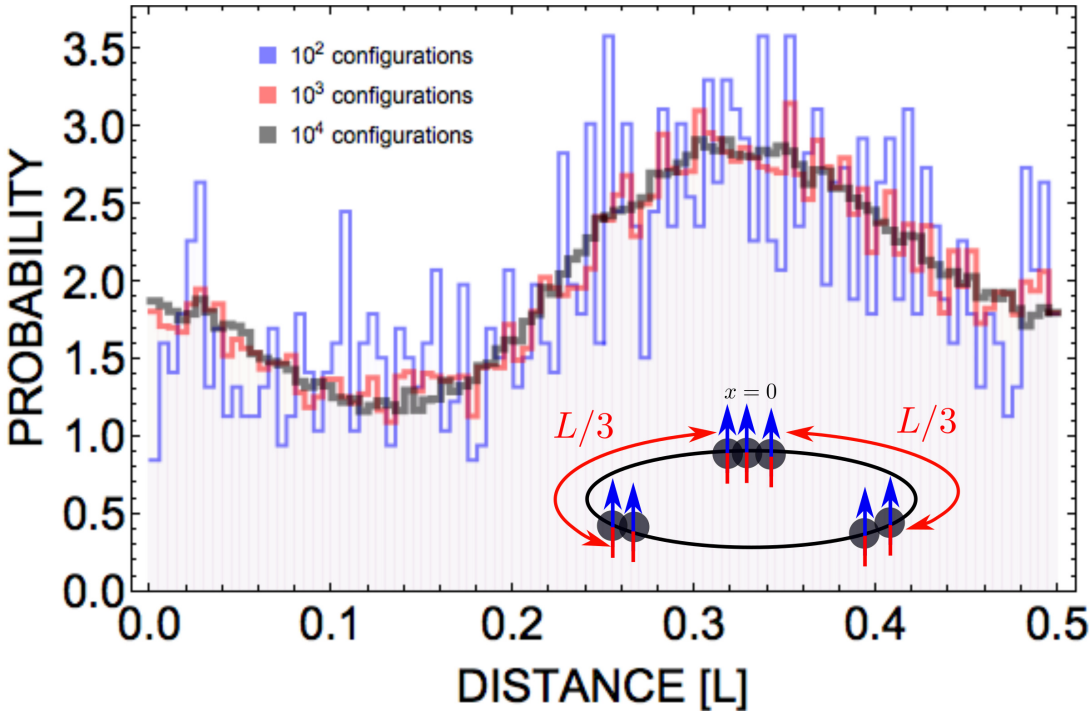

Figure 5.6: Probability density histograms of distances between particles for $N = 7$ atoms, $a_{\mathrm{dd}} = 1131\, a_0$, $r = 272\, a_0$, $a \approx -2971\, a_0$ and $\omega_\perp \approx 2\pi \times 190$ kHz calculated for 10^2 (blue line), 10^3 (red line) and 10^4 (black line) configurations. The mean field gas parameters are the same as for the roton state in Fig. 5.3c. The distance between maxima in the roton state (red histogram) equals $1/K_{\mathrm{rot}}$ ($K_{\mathrm{rot}} = 3$ in this case). The particles' positions were drawn with the Metropolis algorithm. Inset: Graphical interpretation of the histograms for the roton state.

5.2.4 Single particle momentum analysis

To fully comprehend the difference between the two types of low-energy excitations we study the probability $P(k) = \frac{1}{N}\langle \hat{a}_k^\dagger \hat{a}_k \rangle$ of finding a single-particle moving with momentum k for yrast states with various K. For both weak (top panel) and strong (bottom panel) interactions the yrast states with $a = 0$ (black markers in Fig. 5.7) $P(k = 1)$ increases as we increase K. This corresponds to a dominant role of one of the Dicke states (exactly K atoms with $k = 1$ and $N - K$

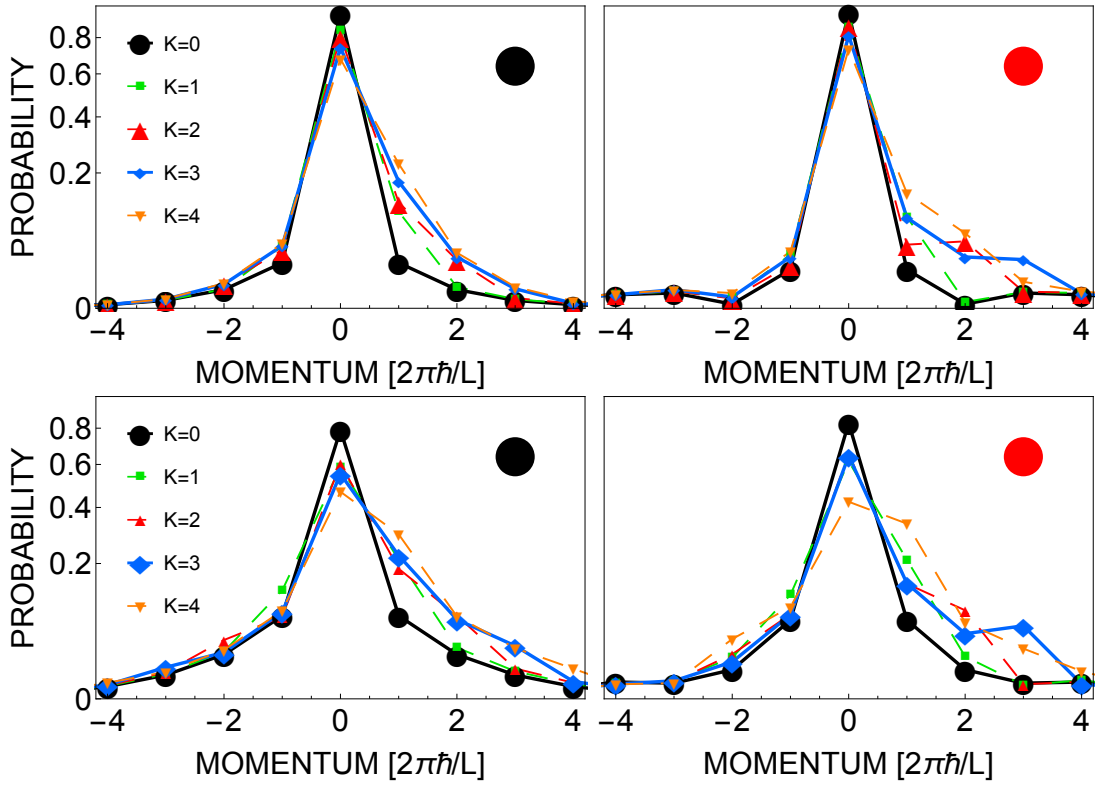

Figure 5.7: Single-particle momentum probability $P(k)$ for all states (five for each spectrum) from top panels of Fig. 5.2 and 5.4. Top: Weak interactions. Bottom: Strong interactions.

with $k = 0$) in their many-body wave function (see Chapter 4), especially for weak interactions. On the other hand, in the rotonic cases (red markers in Fig. 5.7) we observe a local maximum of $P(k)$ for $k = K_{\mathrm{rot}}$ for the yrast states with K_{rot}, which clearly resembles recently published result by F. Ferlaino's group [35]. It means that the yrast state for K_{rot} has a single particle excitation character rather than a collective one. Therefore, one can completely change the character of the low-energy excitations within our experimentally achievable procedure.

5.3 Discussion

We find with our numerically exact treatment that all the properties of the roton state discussed earlier can be understood by analysing contributions of different Fock states to its wave function. In both cases of interactions studied in this work, we find that the dominant contribution to the roton states comes from the so called W state

$$|W\rangle = |0_{-k_{\mathrm{max}}}, ...(N-1)_0, 0_1, 1_2, ..., 0_{k_{\mathrm{max}}}\rangle,$$

as one would expect for the Bogoliubov excitations (see Chapter 2.5.2). The latter state is important from the fundamental point of view, as representative of an entanglement class [202], and applied side - it can be used to beat the standard quantum limit for the metrological tasks [203]. The state was recently produced via non-demolition measurement [204]. According to our earlier findings in Chapter 4, the low-lying excitations of weakly interacting bosons are highly-entangled states

dominated by the Dicke state, a result of the bosonic statistics mainly. However, the interplay between the short-range and long-range interactions of the opposite sign can promote the excitation with the dominant W state as a low-lying excitation for $K > 1$ in the system.

As we can see in the Appendix 5.B the features of the many-body problem solution depends on the value of the mean field gas parameters rather than the number of atoms itself as long as the depletion of the system is not big (it is getting smaller and smaller as we increase the number of atoms decreasing the strength of the interactions at the same time). This makes our results for relatively small number of particles, stronger interactions and tight trapping frequencies easier to verify experimentally. For example if one wants to confirm our predictions for spectrum for the roton with the mean field parameters as in Fig. 5.4, $K_{\mathrm{rot}} = 3$, $N = 600$ and a ring of $5\mu\mathrm{m}$ length, it will require usage of dysprosium atoms with $a_{\mathrm{dd}} = 132\ a_0$ and $\omega_\perp \approx 2\pi \times 1.9$ kHz and tuning the short-range scattering length with Feshbach resonances.

5.4 Conclusion

To summarize, we showed that manipulating physical parameters in our model one can continuously alter the character of a given yrast state from type-II excitation to the roton mode. We emphasise the fact that the effect is already present in relatively small systems enabling use of the simplest exact diagonalization of the whole Hamiltonian. All interesting properties of the roton-like mode both in the momentum and the position representations come from the fact, that the W state plays the dominant role in the roton state in the plane wave basis. It is in the stark contrast to the weakly repulsive bosons, where the dominant role of the Dicke states is observed (see Chapter 4) We show that the normalized second order correlation function, accessible in experiments, displays characteristic enhanced regular modulation for the roton state. Within our many-body model we access stronger regimes between the weakly interacting one and the Helium-II scenario, finding the roton mode also in this case. Our results open new questions concerning quasi-1D systems with both long-range and short-range interactions. Is it possible to fully replace type-II branch with type-I branch as low-lying excitations? Would solitonic branch still exist in the spectrum? The thermodynamic properties of dipolar bosons were investigated only approximately, in the weakly interacting regime [205–207]. The results presented in this chapter can motivate further research in this direction, but using full many-body approach accounting for the lower branch and the transitions discussed here.

Appendix

5.A The effective potential. Realistic versus periodic

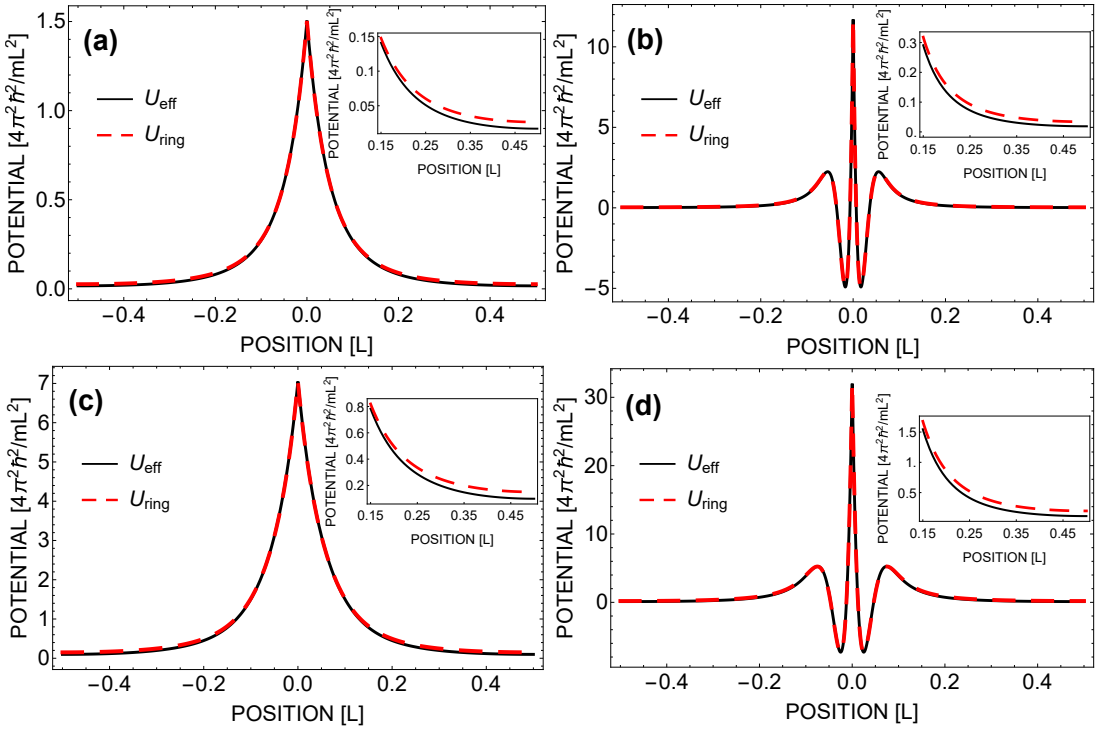

Figure 5.A.1: Comparison between the effective potential $U_{\text{eff}}(x)$ calculated with periodicity accounted for (black line) and $U_{\text{ring}}(x)$ with the distance over the chord (red dashed line). (a) Parameters as for the black squares from Fig. 5.2. (b) Parameters as for the red squares from Fig. 5.2. (c) Parameters as for the black squares from Fig. 5.4. (d) Parameters as for the black squares from Fig. 5.4. Insets: Magnification of the region, where the difference between two methods are the most significant.

As we mentioned in Chapter 2.2.3 in reality particles trapped in the ring-shaped potential would interact via interaction potential depending on the shortest distance between them, the length of a chord. As we replace the ring with a box with periodic boundary condition,the effective potential in the space representation $U_{\text{eff}}(x)$ is only approximate model of the physical interaction described

by $U_{\mathrm{ring}}(x)$ introduced earlier in Chapter 2.2.3.

How good is this approximation? In Fig. 5.A.1 we compare both approaches using examples from this Chapter.[3] As we see both curves are almost indistinguishable in the regions where the value of the effective potential is meaningful. A very small difference in all cases from Fig. 5.A.1 is observed only on the potential tail.

5.B Convergence towards $N \to \infty$ limit

In the Bogoliubov approximation one operates with the mean field gas parameters $NV_{\mathrm{sr}}(0)$, $NV_{\mathrm{d}d}(0)$ (in the box units defined in the main text) with the assumption of weak interactions and large number of atoms N. Obviously, in the many-body approach, where N is finite, the energy of the pairwise interactions is significantly higher. Then, one can ask how many atoms (how weak interactions) one needs to converge with the many-body solution towards $N \to \infty$ limit. To answer it, we study energies of a series of yrast states (left panel of Fig. 5.B.1) and their overlaps with the corresponding Bogoliubov excitations given by fidelities (right panel of Fig. 5.B.1) defined in the main text. We obtain both the spectrum and the fidelities for different number of atoms N ranging from 7 to 16. The parameters for different N are chosen to always produce the same Bogoliubov excitation spectrum with the inflection point as for red dashed line in Fig. 5.2a in the main text. We see that even for small number of atoms $N = 16$ we obtain very good overlap with the Bogoliubov approximation, especially for $K \leq 2$. However, our numerically exact solution includes all the possible correlations between atoms, hence it cannot be fully reproduced by single Bogoliubov excitation.

[3] In other cases with atoms moving on rings considered in this thesis comparisons hold the same conclusions.

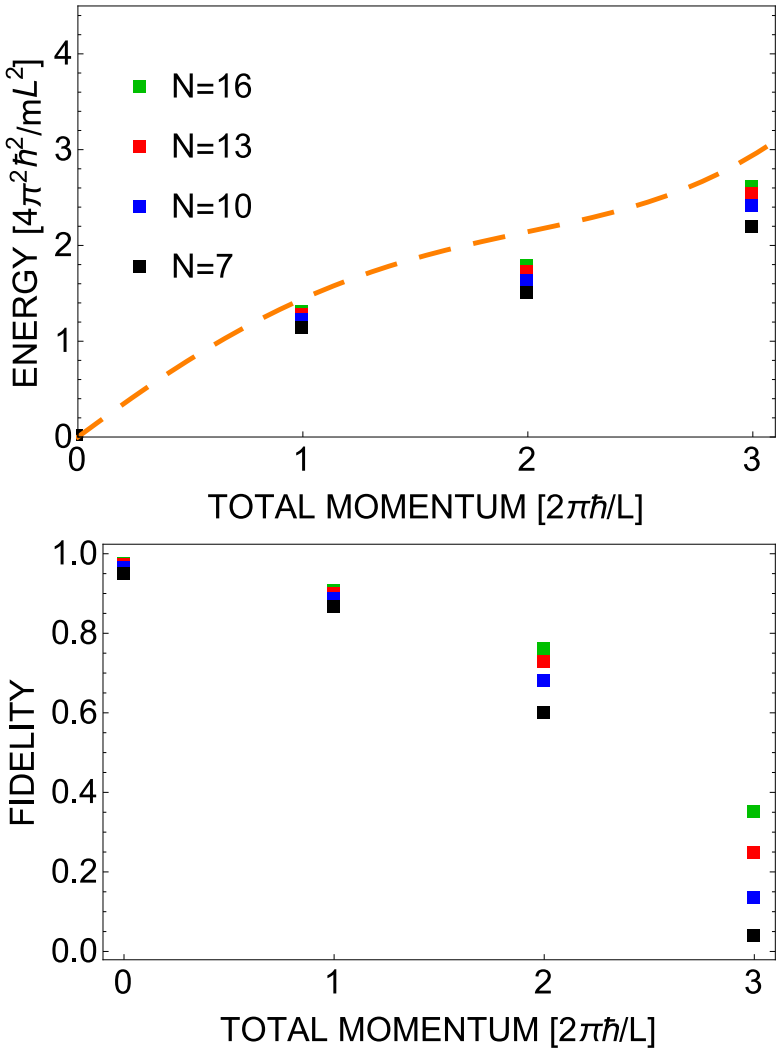

Figure 5.B.1: Upper panel: Energy of the yrast states as a function of the total momentum compared with the corresponding Bogoliubov excitation spectrum (orange dashed line) for different number of atoms, from top to bottom N = 16 (green), 13 (red), 10 (blue), 7 (black). Mean field gas parameters for all the results are the following (in the box units defined in the main text): $NV_{sr}(0) = -23.98$, $NV_{dd}(0) = 26.98$. For $N = 16$ it corresponds to parameters from Fig. 5.2 (red squares spectrum). Bottom panel: Fidelities between the yrast states and Bogoliubov excitations for the yrast states from the upper panel. Color coding and parameters as in the upper panel (from top to bottom: N = 16, 13, 10, 7).

Chapter 6

Droplet-soliton transition in quasi-1D dipolar Bose gas

As we learned from Chapter 1, solitons depending on local nonlinearity appear in a plethora of physical systems. In preceding years a lot of focus has been devoted to bright solitons originating from non-local interactions also, in particular from dipolar forces, for instance, see [208] and references therein. Recently, a different self-bound state was generated in samples interacting via anisotropic dipolar interactions in 3D [33, 34, 97, 209]. Liquid droplets result from the quantum fluctuations known as Lee-Huang-Yang (LHY) correction.[1] In quasi-1D geometry, the counterpart of LHY gives droplet solutions also [107, 212]. In this case, the authors of [107] studied a transition between droplet states and dipolar bright solitons.

In this Chapter, we consider a many-body system with repulsive short-range interactions and attractive dipolar potential. We study its ground state for net attractive and repulsive interactions for a small number of atoms. While for the former case it always has negative energy, for the latter one the interactions have to be strong enough to observe a bound state. We show that crossing the border between net attractive and repulsive interactions entails a distinct change in the ground state properties. We identify a new droplet state present even for very small systems and also a dipolar bright soliton state. In the second part of this Chapter, we move to larger systems. We propose a new version of the GPE and analyze it. We obtain an excellent agreement between the GPE and the exact diagonalization for small systems. We show a diagram depicting transition between droplets and bright solitons for large systems. We emphasize the fact that we do not include the LHY term.

6.1 Model

In this chapter we consider almost the same system as in Chapters 4-5. We only take a different polarization angle $\theta = 0$ making our non-local interactions attractive. Namely, our quasi-1D system

[1] Quantum droplets are also studied in the context of Bose-Bose mixtures, see for instance [95, 105, 210, 211] and references therein.

is governed by Hamiltonian:

$$\hat{H} = -\frac{\hbar^2}{2m}\int dx\hat{\psi}^\dagger(x)\nabla^2\hat{\psi}(x) + \frac{1}{2}\int dxdx'\,\hat{\psi}^\dagger(x)\hat{\psi}^\dagger(x')V_{\text{eff}}(x-x')\hat{\psi}(x)\hat{\psi}(x') \tag{6.1}$$

with $\hat{\psi}(x)$ being a standard bosonic field operator. The effective potential consists of the long-range dipolar part and the short-range part, namely $U_{\text{eff}}(x) = U_{\text{dd}}(x) + U_{\text{SR}}(x)$.

The quasi-1D dipolar potential reads

$$U_{\text{dd}}(x) = -\frac{C_{\text{dd}}}{2\pi l_\perp^2}\frac{v_{\text{dd}}\left(x/l_\perp\right)}{l_\perp}, \tag{6.2}$$

where $v_{\text{dd}}(u) = -\frac{1}{4}u_{\text{dd}}(u)$ (see also Eq.(2.18)). This effective quasi-1D potential comes from integration of the full $3D$ dipolar interaction over both transverse variables (see 2.2.2). The singular part coming from this integration [134] is incorporated within the short range interaction.

As for the purpose of this Chapter, the atoms repulse each other on the short distance. Thus, we use the usual model of short-range interactions, the delta function [2]

$$U_{\text{sr}}(x) = \frac{\hbar^2 a}{m l_\perp^2}\delta(x) \tag{6.3}$$

with $a \geq 0$ mimicking a scattering length, which can by tuned in experiments by Feschbach resonances. Below we use box units where L, $\hbar/L$ and $\hbar^2/mL^2$ are the units of length, momentum and energy respectively. In addition to the new units, we also define coefficients $g = \frac{\hbar^2 a}{m l_\perp^2}$, $g_{\text{dd}} = \frac{C_{\text{dd}}}{2\pi l_\perp^2}$, an aspect ratio $\sigma = l_\perp/L$ and rescaled function $v_{\text{dd}}^\sigma(x) := \frac{1}{\sigma}v_{\text{dd}}(x/\sigma)$, so that finally effective potential takes a compact form

$$U_{\text{eff}}(x) = -g_{\text{dd}}v_{\text{dd}}^\sigma(x) + g\delta(x). \tag{6.4}$$

6.2 Ground state of a few-body system

We are interested in properties of the ground state of the systems. In particular, how do they depend on interactions strength? We focus on manipulating two of the interactions parameters: ratio between dipolar and contact interactions $f_{\text{dd}} = g_{\text{dd}}/g$ and g_{dd} itself. We expect that for $f_{\text{dd}} > 1$ the ground state has negative energy and atoms form a self-bound state similar to the bright solitons studied very thoroughly in the context of ultracold gases [208]. On the other hand, the ground state with negative energy for $f_{\text{dd}} < 1$ (dominant repulsion) was also presented in quasi-1D systems within the modified mean-field analysis in the extreme case of $f_{\text{dd}} = 0$ (with $g_{\text{dd}} > 0$) [108, 213]. With the model presented in this Letter, we can investigate features of the system in a fully many-body manner across the whole range of parameters values. Chiefly, we are interested in the ground state change while crossing $f_{\text{dd}} \sim 1$. Does any kind of a transition occur there?

[2] In the previous chapter, we have used a Gaussian potential as the attractive short-range interactions model to ensure the stability of numerical calculation. However, in the repulsive case, the usual point-like potential does not introduce any numerical complication and is suitable for analysis. We emphasize that our selection of a short-range potential has a purely technical character.

We attempt to find a few-body ground state for $f_{\rm dd} < 1$ and $f_{\rm dd} > 1$ with negative energy and characteristic width smaller than L, so that we can study the spatial properties of such a bound-state. We access the many-body eigenstates of Hamiltonian by exact diagonalization using the Lanczos algorithm (2.4).

6.2.1 Weak interactions

We try to answer some of these questions by considering different values of dipolar and short-range couplings while keeping $f_{\rm dd} < 1$ constant. Strictly put, we introduce a scale factor λ that changes the effective potential in a following way:

$$U^{\lambda}_{\rm eff}(x) = \lambda U_{\rm eff}(x). \tag{6.5}$$

In Fig. 6.1 we present the outcomes of our analysis. In the top panel we plot the ground state energy in the system as a function of λ. The spectrum is parabolic and can be entirely understood within the second order perturbation theory. Moreover, we observe that for $\lambda \sim 5.5$ the eigenenergy becomes negative.

In the bottom left of Fig. 6.1 we study the second order correlation function $G_2(x,0)/N(N-1)$ (see Chapter 2.1.2) as a function of a distance. We see that increasing the strength of interactions leads to the appearance of a local minimum for $x = 0$ and a local maximum for $x = 0.5$. Moreover, as the strength of the interactions increases, the value of the minimum decreases. At some point, this leads to a ground state with negative energy. We propose the following interpretation of this result. As the short-range interactions are getting stronger, the atoms become more and more impenetrable, but at the same time, the attraction tries to cluster atoms as it dominates on longer distances. Only if the repulsion between atoms move them apart enough to sense mainly the attraction a bound state may appear. It seems that the existence of local minimum and local maximum may be the necessary conditions to create an eigenstate with negative energy for $f_{dd} < 1$. Still, our interactions are very weak and our system almost ideal with atoms practically occupying only one single-particle state with $k = 0$ (bottom right in Fig. 6.1).

In summary, it is possible that the ground state of the few-body system described by the Eq. 6.1 has negative energy for strong enough interparticle interactions, even if the repulsion between the atoms dominates in the system. In fact, it is a simple observation from the second order perturbation theory. However, the weak interactions considered in this subsection do not allow for a more complex spatial analysis (in the style of chapters 3 and 4) of the ground state, because of the almost uniform distribution of the atoms on the ring; $\frac{G_2(x,0)}{N(N-1)}$ is still almost flat. For this, we move to the stronger interactions scenario.

6.2.2 Strong Interactions

We showed in the previous subsection that the ground state of our system may admit negative energy for the net repulsive interactions ($f_{\rm dd} < 1$) if they are strong enough. Now, we move to much stronger interactions than in the previous subsection. As an example, in Fig. 6.2, we present probability density histograms for two cases with the net repulsive interactions (top panel,

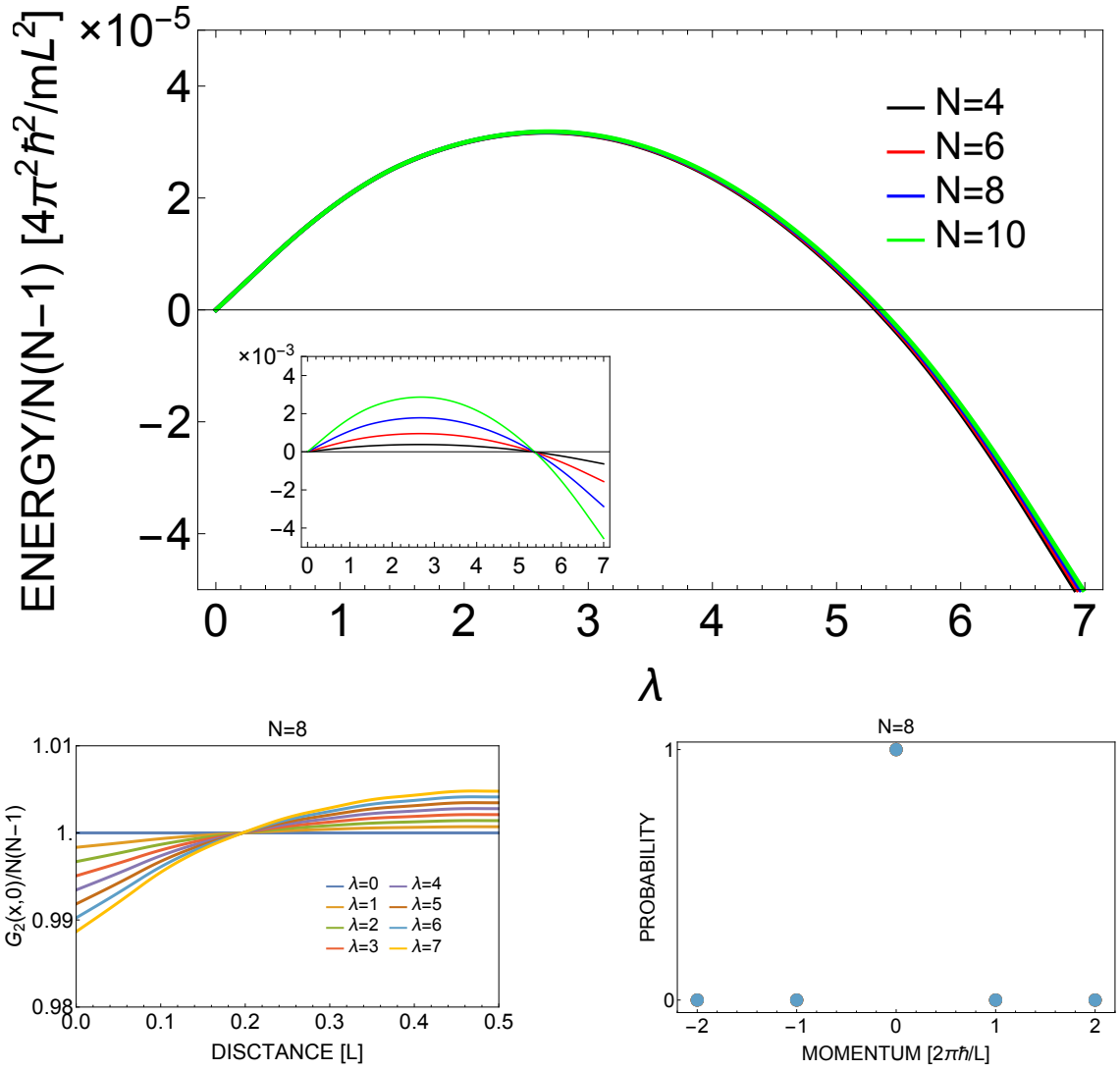

Figure 6.1: Top: Energy of the ground states as a function of a real number λ corresponding to different strength of the interparticle interactions with $f_{\mathrm{dd}} = 0.997$ for $N = 4$, 6, 8, 10 atoms. In the inset the same plot, but the energy value is not divided by $N(N-1)$ factor. In all calculations here we take $\sigma = 0.25$. Bottom left: The second order correlation function as a function of a distance for $N = 8$ atoms and different λ for the ground states from the top figure. Bottom right: Single-particle momentum probability $P(k)$ for $N = 8$ and all λ from the bottom left panel.

$f_{\mathrm{dd}} = 0.9$) and the net attractive interactions (bottom panel, $f_{\mathrm{dd}} = 20$). We select the interaction parameters so that the histograms have a similar width for attractive and repulsive scenarios. Both histograms are obtained by drawing particles' positions from the many-body probability distribution with the Metropolis algorithm and aligned by rotating them such that their center of mass point in the same direction (see Chapter 2.4.2). We observe two spatially localized bound-states with completely different properties. First of all, for $f_{\mathrm{dd}} = 0.9$, the variance increases as the number of atoms grows, which is the opposite for $f_{\mathrm{dd}} = 20$. Additionally, in the first case we observe local peaks whose number agrees with the number of particles, whereas in the latter only central peak is observed. Although these are very small systems, we see the first signs of bulking for

$f_{\rm dd} = 0.9$ case and shrinking-peaking for $f_{\rm dd} = 20$. It resembles strongly the quantum droplets and bright solitons differences discussed in the recent papers about dipolar systems and Bose-Bose mixture [107, 212]. Therefore, we name the first case as a droplet-like and the second one as a soliton-like solution. We remind that the average energy of any state of the system described by Eq. (6.1) is expressed by (see 2.7):

$$\left\langle \hat{H} \right\rangle = -\frac{1}{2}\int dx \langle \hat{\psi}^\dagger(x)\nabla^2\hat{\psi}(x)\rangle + \frac{1}{2}\int dx dx'\, G_2(x,x')U_{\rm eff}(x-x') \tag{6.6}$$

with a normally ordered second order correlation function $G_2(x,x') := \langle \Psi^\dagger(x)\Psi^\dagger(x')\Psi(x')\Psi(x)\rangle$. In particular, we see that in order to develop a bound-state for $f_{\rm dd} < 1$ it requires the existence of a local minimum of $G_2(x,0)$ for $x = 0$ and a finite range of correlations.

With our exact diagonalization technique, we have immediate access to the function $\frac{G_2(x,0)}{N(N-1)}$. We compute it and analyze in Fig. 6.3 to better understand the internal structure of the states. A dramatic difference between both situations from Fig. 6.2 can be found. Most of all, for droplet-like states (top left panel), we observe a local minimum for $G_2(0,0)/N(N-1)$ which changes only slightly with the atoms number. Then, $G_2(x,0)/N(N-1)$ increases and reaches its maximum with a smaller value as N grows. At the same time, $G_2(x,0)/N(N-1)$ widens. For soliton-like states complete opposite holds; $G_2(x,0)/N(N-1)$ has a maximum for $x = 0$ that increases and its width shrinks with N. The total course of the G_2 functions agrees with the histograms in Fig. 6.2. Additionally, the single-particle momentum distribution (bottom panel of Fig. 6.3) features for both cases are consistent with the rest of our analysis. As a simple observation serves the fact, that in order to create a state shorter than L higher single-particle momenta are needed.

Summary In this section, we have shown that for few-body systems described by Eq. (6.1) the ground state may have negative energy even if the net interactions are repulsive. It only requires strong enough interactions, both local and non-local. Then, we analyze the differences between the bound-states for $f_{\rm dd} < 1$ and $f_{\rm dd} > 1$. In the first scenario, they are very similar in behavior to droplets, i.e. [107], and in the latter to bright solitons discussed in [208]. Latter in this work we confirm the correspondence between our soliton-like states from our few-body approach and the GPE from Eq. (2.39). The open question remains if our results for droplet-like states hold for bigger systems. We are unable to answer it within the exact diagonalization technique, therefore we turn our attention to a different description.

6.3 Local Density Approximation

As we realized in the previous sections of this Chapter, droplet-like solutions require the existence of a local minimum of $G_2(x,0)$ for $x = 0$. The GPE in quasi-1D (GPE) that supports bright solitons for dominantly attractive systems [208] would fail in reproducing our previous findings. On the other hand, in the opposite limit of an infinitely strong repulsion with $f_{\rm dd}$=0 (but $g_{\rm dd} \neq 0$) and $G_2(0,0) = 0$ adding a nonlocal term for the DD interactions (or instead introducing a harmonic potential) the authors [108, 213] proposed a different dipolar GPE (TGGPE) [3]. In fact,

[3] We call it Tonks-Girardeau Gross-Pitaevski equation

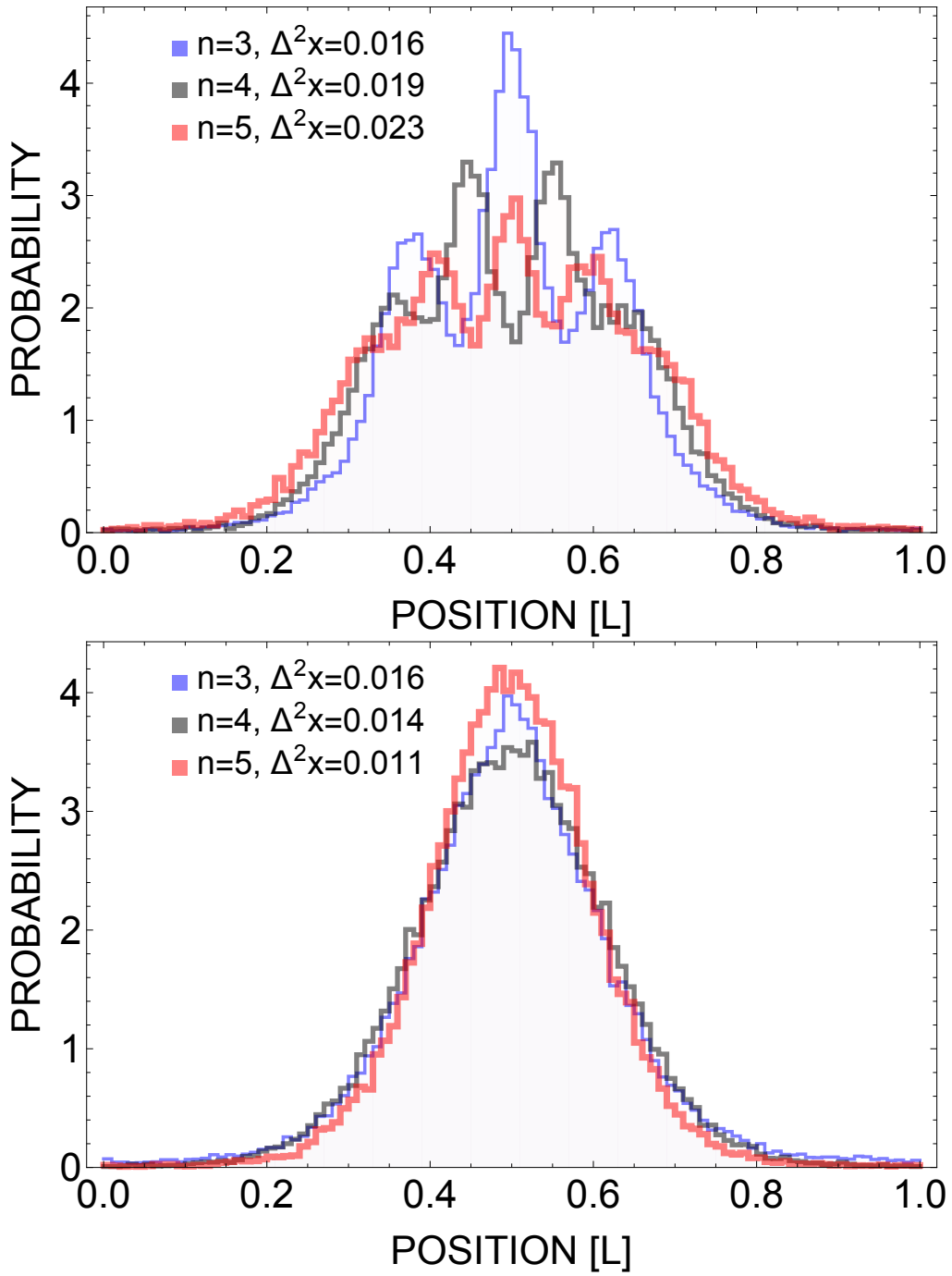

Figure 6.2: Probability density histograms of particles' positions for the ground state for $N = 3$ (blue solid), 4 (black solid) and 5 (red solid) atoms with $f_{\mathrm{dd}} = 0.9$, $a = 6$ and $\sigma = 0.2$ (top) and for $f_{\mathrm{dd}} = 20$, $a = 0.03$ and $\sigma = 0.2$ (bottom). The particles' positions were drawn with the Metropolis algorithm and aligned by rotating them such that their center of mass point in the same direction (see Chapter 2.4.2). Note that for very small systems the peak density value is biased by our alignment method, especially for the net attractive interactions.

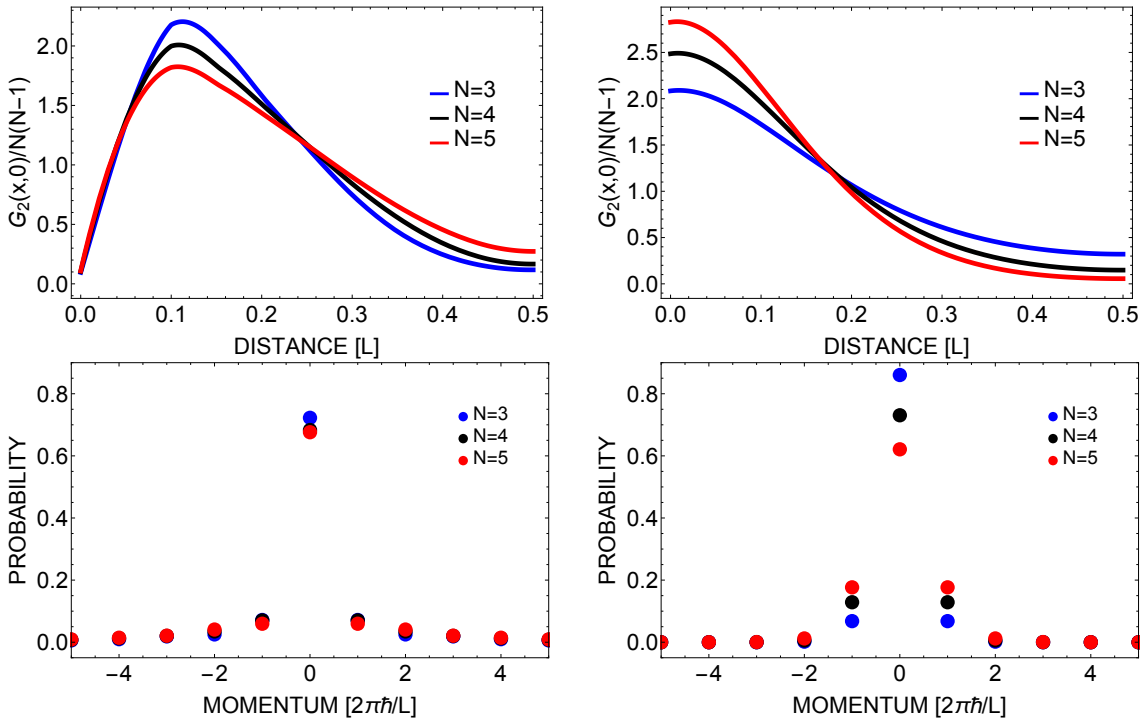

Figure 6.3: Top: Normalized second order correlation function as a function of a distance for the ground state for $N = 3$ (blue solid), 4 (black solid) and 5 (red solid) atoms with $f_{\mathrm{dd}} = 0.9$, $a = 6$ and $\sigma = 0.2$ (left) and for $f_{\mathrm{dd}} = 20$, $a = 0.03$ and $\sigma = 0.2$ (right) Bottom: Single-particle momentum probability $P(k)$ for the above states.

the authors of the above use the local density approximation (LDA) treating the nonlocal interaction in total analogy with a trapping potential in a standard LDA for confined ultracold gases.

6.3.1 Model

To study larger systems around $f_{\mathrm{dd}} \sim 1$ we propose a new extended GPE. We treat dipolar interactions classically assuming they change slower than a range of the second order correlation function, namely that $N\sigma \gg d \gg \sigma$ where d is a width (FWHM) of a ground state density, like in [108]. We also assume, that locally the atoms obey the ground state from the Lieb-Liniger model. We approximate its energy as a density function in a very simplified way, namely as

$$e_{\mathrm{LL}} = \frac{gN(N-1)}{2} \frac{|\psi|^6}{|\psi|^2 + \frac{3g}{N\pi^2}}. \tag{6.7}$$

With that, the energy functional for our system reads [4]:

$$\begin{aligned} E = \int dx \left[\frac{N}{2} |\nabla\psi|^2 + \frac{gN(N-1)}{2} \frac{|\psi|^6}{|\psi|^2 + \frac{3g}{N\pi^2}} \right] \\ - \frac{g_{\mathrm{dd}} N(N-1)}{2} \int dx dx' \, |\psi(x)|^2 \, v^{\sigma}_{\mathrm{dd}}(x - x') \, |\psi(x')|^2 \end{aligned} \tag{6.8}$$

[4] For full derivation see Appendix 6.A

where we normalize the wave function in the following way $\int dx\,|\psi(x)|^2 = 1$. Then, we finally arrive with a new version of GPE for which we coin a phrase Lieb-Liniger GPE (LLGPE). It can be written as:

$$\begin{aligned} iN\frac{\partial\psi(x)}{\partial t} = &-\frac{N}{2}\frac{\partial^2}{\partial x^2}\psi(x) + f_{\mathrm{LL}}\big[\psi(x)\big] \\ &- g_{\mathrm{dd}}N(N-1)\int dx' v^{\sigma}_{\mathrm{dd}}(x-x')\left|\psi(x')\right|^2\psi(x), \end{aligned} \tag{6.9}$$

where $f_{\mathrm{LL}}\big[\psi(x)\big] = \frac{\delta e_{\mathrm{LL}}}{\delta\psi^*}$.

Note that the above LLGPE equation can be seen as a generalization of the two others previously mentioned. In the limit of a very weak contact interactions $g \to 0$ we retrieve the GPE, while for $g \to \infty$ we restore the TGGPE. It should be emphasized that we use a very simplified energy density functional, which is a rough approximation of the full Lieb-Liniger expression, for instance see [214, 215] and references therein.

6.3.2 Comparison with the exact diagonalization results

We aim to solve the Eq. 6.9 for the exactly the same parameters as for the few-body case. For this, we use ITE technique (see Chapter 2.5), which is a very suitable method to find the ground state. We compare outcomes from ITE with the results from the exact diagonalization. In Fig. 6.4 we compare probability density histogram analyzed earlier and $\rho = N\,|\psi|^2$ from ITE. Keeping in mind that the equation should work rather for a large number of atoms, we observe a satisfactory agreement between both approaches. Most importantly, LLGPE captures the same N dependence as the exact solution. Moreover, we see that especially for $N = 5$ both approaches correspond to each other in a good way, both for soliton-like states and droplet-like states. In the first case, we also confirm sech-shape of the solution, so we will call it hereafter a bright dipolar soliton. The only source of discrepancy between LLGPE and the exact solution for $N = 3$ and $N = 4$ solitons is due to the alignment method of positions drawn from different MC runs.

Our comparison provides good reasons to focus on the features of LLGPE solutions itself. We move from a very small N towards bigger in hope of better understanding of droplet-like states.

6.3.3 Transition diagram and further analysis

As we have learned from the small system analysis, droplet-like states get wider as N grows, but bright solitons shrink. Then, it would be instructive to consider the first derivative of a width d of the solution of Eq. (6.9) over N as a function of the parameters f_{dd} and g_{dd}. In Fig. 6.5 (top panel) we present such an analysis. As we have expected, for $f_{\mathrm{dd}} < 1$ the derivative is positive. Then for $f_{\mathrm{dd}} > 1$ approaches 0. To check what happens at the border around $f_{\mathrm{dd}} \approx 1.05$, we calculate the density $\rho(x) = N\,|\psi(x)|^2$ using ITE and present it in the bottom left panel of Fig. 6.5. We immediately see that the exact solution of Eq. (6.9) confirms the change of the ground state nature. We also checked that increasing the N would result in a sharper transition.

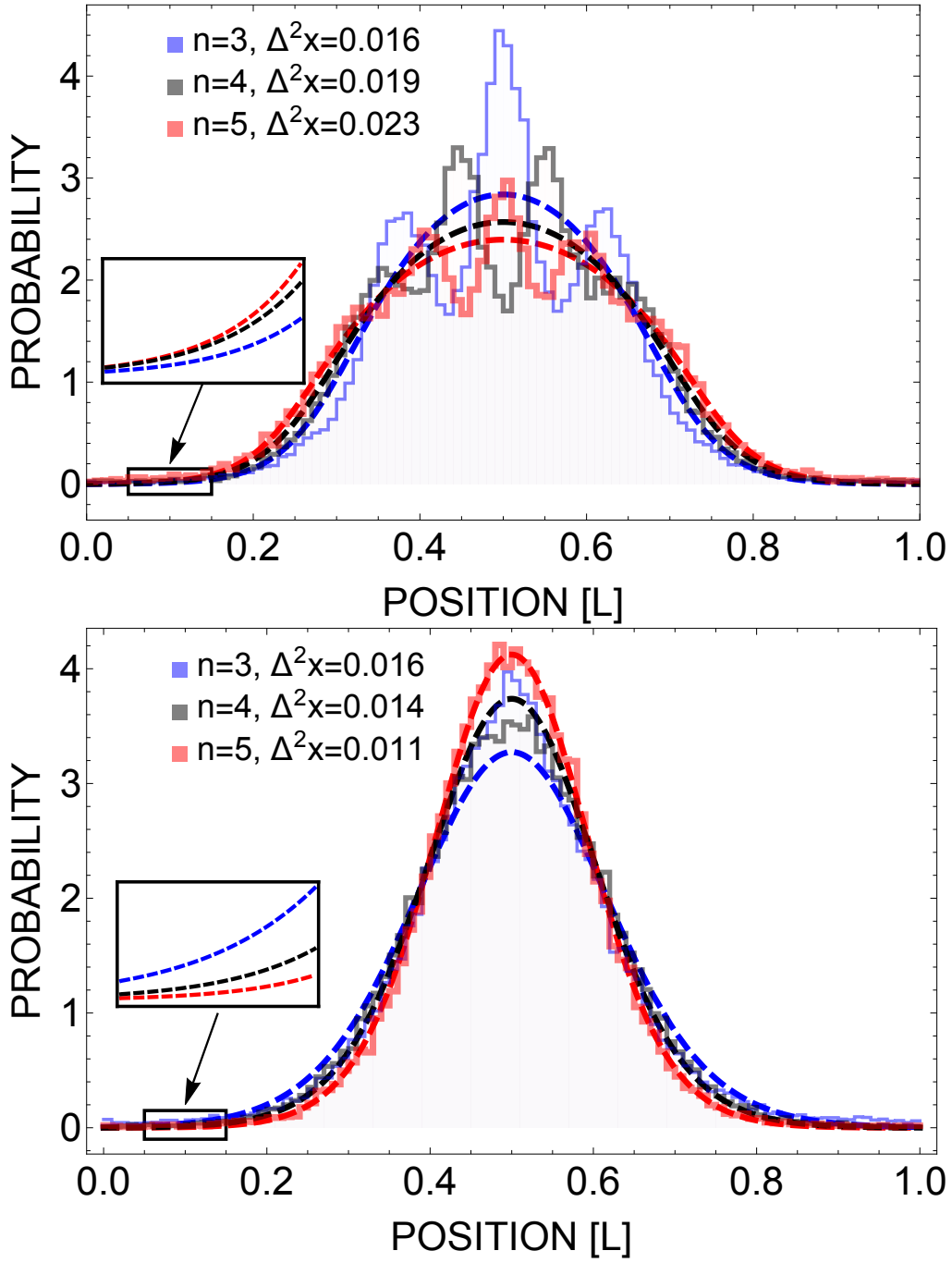

Figure 6.4: Probability density histograms of particles' positions for the ground state for $N = 3$ (blue solid), 4 (black solid) and 5 (red solid) atoms with $f_{\rm dd} = 0.9$, $a = 6$ and $\sigma = 0.2$ (top) and for $f_{\rm dd} = 20.$, $a = 0.03$ and $\sigma = 0.2$ (bottom) compared to solutions of Eq. (6.9). Note that for very small systems the peak density value is biased by our alignment method, especially for the net attractive interactions.

We take a closer look on the solutions dependence on the particle number N. In Fig. 6.5 (bottom right panel) we consider a spatial profile of droplet solutions $\rho(x)$ as a function of N obtained with ITE. For all cases and all N, the total energy of the system found with ITE is negative, entailing that the states are self-bound. For small N the shape of droplets change as N grows and it

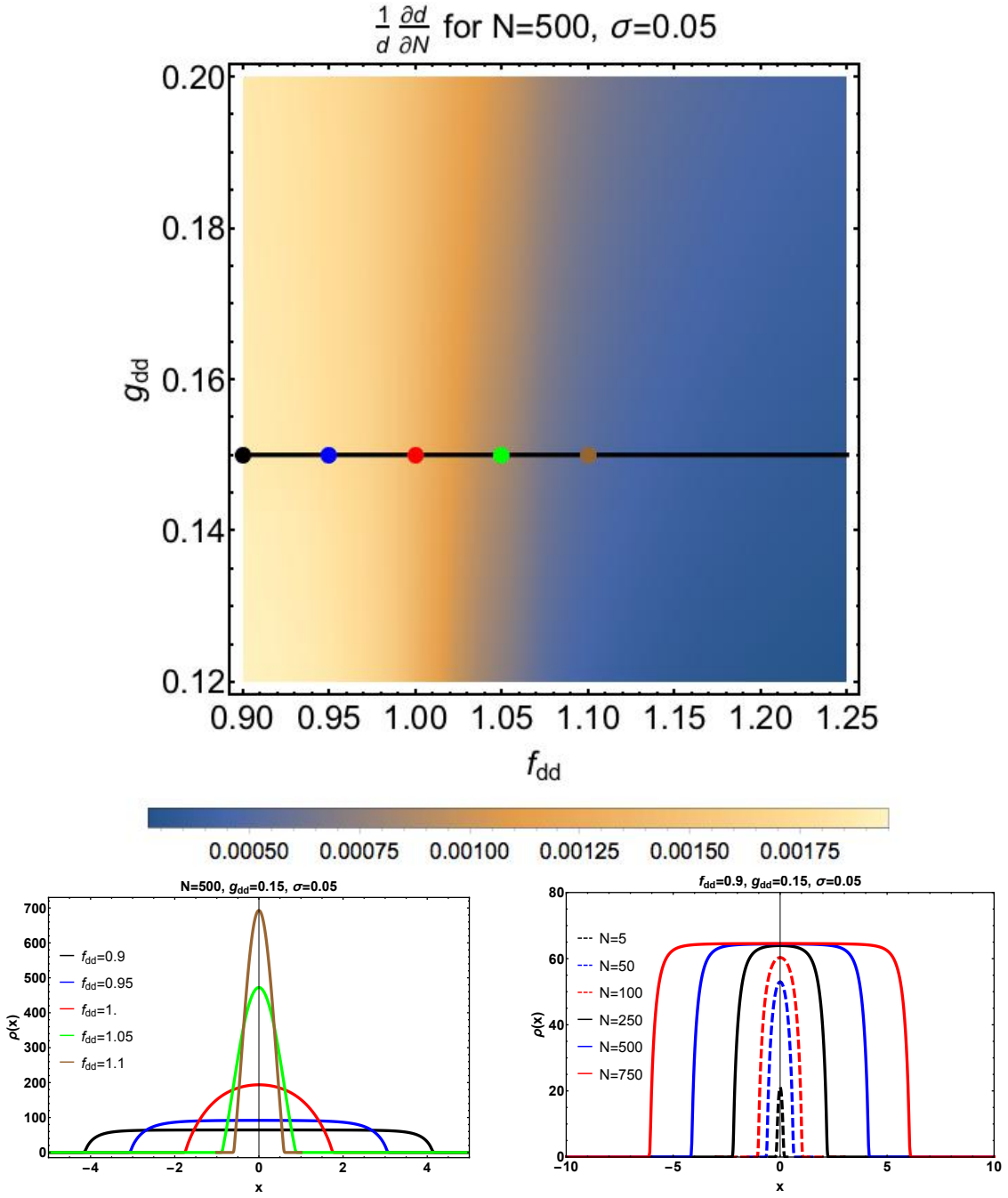

Figure 6.5: Top: First derivative of a width d of the solution of Eq. (6.9) over N as a function of the parameters f_{dd} and g_{dd}. Bottom left: Density for different f_{dd} with parameters as for the colour points from the top panel. Bottom right: Density plot for different N and parameters as for the black point from the top panel

is nonuniform with a non-negligible kinetic energy contribution. Still, in opposition to the solitonic solutions, it widens significantly with N. Then, as N is large enough, the droplet profile becomes flat-top reminding the behavior of classical liquid.

6.4 Conclusions

In conclusion, a novel droplet state and droplet-soliton transition was found at the crossing between net repulsive and attractive effective two-body interactions between the atoms. From the properties of Hamiltonian and our exact findings for the few-body dipolar system a necessary condition for the existence of the 1D droplet state is an occurrence of a local minimum of the normally ordered second-order correlation function $G_2(x, 0)$ for $x = 0$ and its finite size. This leads to a new version of a GPE (LLGPE) that includes this requirement by including a local term from the Lieb-Liniger model. Droplets found in this Chapter do not require a seminal LHY term widely discussed in the literature, thus they are of completely different origin. In opposition to the recent findings in [107] with LHY term we find a new self-bound state for any atoms number both in the few-body problem and in droplet solutions of LLGPE. In the future, a study of the chemical potential as a function of N for different f_{dd} and g_{dd} should be done. This would explain the actual nature of transition around $f_{\mathrm{dd}} \approx 1$.

Note, that our approach can be generalized for different non-local two-body (one-body) potentials with the same reasoning as in Appendix 6.A.

Appendix

6.A Derivation of the Lieb-Liniger GPE (LLGPE)

We consider N bosons interacting with short-range and dipolar forces, $U_{\text{eff}}(x) = U_{\text{dd}}(x) + U_{\text{SR}}(x)$ with $U_{\text{dd}}(x)$ and $U_{\text{SR}}(x)$ as in the main text. We remind that the system under investigation described by Eq. (6.1) in the main text is translationally invariant. Its Hamiltonian can be written in general as:

$$\hat{H} = \hat{T} + \hat{U}_{\text{SR}} + \hat{U}_{\text{dd}} \tag{6.10}$$

with $\hat{T}$ being kinetic energy. We assume that the ground state of the system is a bound-state with negative total energy. We want to describe the properties of it and to avoid a problem with the center of mass position uncertainty we break the translational symmetry as follows. Let subtract kinetic energy of the center of mass $\hat{T}_{\text{cm}}$ and add infinitesimal perturbation $-\hat{\epsilon}$ (localized in space) to Eq. (6.10). The localized perturbation serves here only as a mechanism of setting the center of mass position of the ground state. Once we set it, we neglect perturbation in Hamiltonian. Then, Hamiltonian of the system reads:

$$\hat{H} = \hat{T} + \hat{U}_{\text{SR}} + \hat{U}_{\text{dd}} - \hat{T}_{\text{cm}} - \hat{\epsilon} \tag{6.11}$$

We are interested in the expactation value (denoted here as $\langle\cdot|\cdot\rangle$) of the above Hamiltonian in the ground state. As we localized our bound state with the infinitesimal perturbation, we can now assume, for $|x-y| \gg \zeta$ where ζ is a typical range of correlations, that:

$$\forall_{|x-y|\gg\zeta}\langle\psi^\dagger(x)\psi^\dagger(y)\psi(x)\psi(y)\rangle \approx \langle\psi^\dagger(x)\psi(x)\rangle\langle\psi^\dagger(y)\psi(y)\rangle \tag{6.12}$$

Moreover, we additionally assume that the typical range of dipolar interactions is much larger than ζ:

$$\frac{1}{2}\int\langle\psi^\dagger(x)\psi^\dagger(y)V_{LR}(x-y)\psi(x)\psi(y)\rangle dxdy \approx \frac{1}{2}\int\langle\psi^\dagger(x)\psi(x)\rangle V_{LR}(x-y)\langle\psi^\dagger(y)\psi(y)\rangle dxdy \tag{6.13}$$

That is to say, we treat dipolar interactions classically. Next, we posit that there exists a length scale l, such that:

- $\forall_{x'\in[x,x+l]}U_{\text{dd}}(x') \approx U_{\text{dd}}(x)$

- $\forall_{x' \in [x, x+l]} \langle \psi^\dagger(x')\psi(x') \rangle \approx \langle \psi^\dagger(x)\psi(x) \rangle$
- $\int_x^{x+l} \langle \psi^\dagger(x')\psi(x') \rangle dx' \gg 1$

Subsequently, we discretize space into intervals of length l indexed by i. We can rewrite Hamiltonian as a sum of local term (short-range interactions and kinetic energy of atoms without kinetic energy of the center of mass) and non-local term (dipolar interactions):

$$\hat{H} = \sum_i \hat{H}^i = \sum_i \hat{H}^i_{\mathrm{loc}} + \sum_{ij} \hat{H}^{ij}_{\mathrm{dd}} \tag{6.14}$$

Note that Eq. (6.14) already does not contain the kinetic energy of the center of mass. Using our approximations we get:

$$\hat{H}^i \approx \hat{T}^i + \hat{U}^i_{\mathrm{SR}} + \sum_j U_{\mathrm{dd}}((i-j)l) \langle \psi^\dagger(j \cdot l)\psi(j \cdot l) \rangle l \tag{6.15}$$

where $\hat{T}^i$ denotes the kinetic energy operator and $\hat{U}^i_{\mathrm{SR}}$ the short-range potential operator. The last term of the above equations is constant within i-th interval, because we assumed earlier that dipolar potential varies slowly. Then, we assume that locally the Hamiltonian admits the Lieb-Liniger form because such an interval can be approximated as a waveguide in the experiment from Innsbruck [216]. Therefore, we approximate the last term of the above equations as in [113] but with our definition of interaction parameters:

$$e_{\mathrm{LL}} = N^2(N-1)|\psi|^6 e\left(\frac{2g}{|\psi|^2}\right), \tag{6.16}$$

where $e\left(\frac{2g}{|\psi|^2}\right)$ (denoted in Lieb's work as $e(\gamma)$; here $\gamma = \frac{2g}{|\psi|^2}$) is roughly

$$e(\gamma) = \frac{\pi^2}{6} \frac{\gamma}{\frac{\pi}{3} + \gamma}. \tag{6.17}$$

With that, we rewrite Eq. (6.16) into Eq. (6.7) from the main text

$$e_{\mathrm{LL}} = \frac{gN(N-1)}{2} \frac{|\psi|^6}{|\psi|^2 + \frac{3g}{N\pi^2}}. \tag{6.18}$$

Finally, we obtain the energy functional as a function of $|\psi(x)|^2$ with $\sum_i |\psi(i \cdot d)|^2 d = 1$

$$H = \sum_i e_{\mathrm{LL}}\left(\frac{2g}{|\psi|^2}\right) d + \frac{N(N-1)}{2} \sum_{ij} \psi(i \cdot d)|^2 U_{\mathrm{dd}}((i-j)d)|\psi(j \cdot d)|^2 d^2 \tag{6.19}$$

which can be approximated by an integral

$$\begin{aligned} H = &\int dx\, e_{\mathrm{LL}}\left(\frac{2g}{|\psi|^2}\right) + \frac{N(N-1)}{2} \int dx \int dy\, \psi(x)|^2 U_{\mathrm{dd}}((x-y))|\psi(y)|^2 \\ &\int |\psi(x)|^2 dx = 1 \end{aligned} \tag{6.20}$$

The last approximation comes from our earlier assumptions. In particular, this substitution does not require that $d \to 0$. In the main text, we also added the kinetic energy of the envelope of a state.

Chapter 7

Diagnosing a two-body state of ultracold atoms with light

A diagnosis of a Bose-Einstein condensate is always based on atom-light interactions. One of the most widespread experimental method of investigation of ultracold gases is the absorption imaging. The key role in this technique plays a fact that the absorption rate is proportional to the column density of atoms, or so is tacitly assumed. Absorption imaging opens access to many interesting properties of a gas like density profiles of atomic clouds, higher order correlation functions [200, 217–220] or even a single atom image [221]. Typically a weak pulse is used to avoid multiple scatterings and therefore enhance control over the measurement.

Recently a process of splitting of the Bose-Einstein condensate was analysed [222]. Within the classical field approximation, see for instance [223, 224], it was shown that the statistical properties of the condensate depend on the observation time. Whereas it is possible that these findings are not exactly related to a real quantum measurement with light, a role of spatial and temporal properties of a light pulse in the absorption imaging, to the best of our knowledge, was not analysed in detail.

To shed more light on this problem, we present an oversimplified example of only two atoms located in a spherical harmonic trap. Then, the diagnosis of the system with a light pulse is done through the absorption. Identifying one-photon and two-photon absorption probabilities as a source of a one-particle density distribution and two-body distribution respectively we study the influence of pulse properties on the results.

7.1 Model

Our method of diagnosing the two-body wave function is based on the absorption of sufficiently well collimated light pulses by atoms - both bosons and fermions. The probabilities of one or two photons being absorbed should be measured for different positions of light beams. Out of the estimated likelihoods we may find one - particle density distribution and two - body distribution. In our studies we are going to ignore spontaneous emission.

The total Hamiltonian of the two contact interacting ultracold particles of equal masses $m_1 =$

m_2 absorbing photons from a light beam reads:

$$H = H_{FS} + H_{AF}. \tag{7.1}$$

The term H_{FS} stands for the free system Hamiltonian. It can be written as:

$$\begin{aligned} H_{FS} &= \underbrace{\sum_{i=1}^{2} \left(T_i(\mathbf{r}_i) + V_t(\mathbf{r}_i)\right) + V_I(\mathbf{r}_1 - \mathbf{r}_2)}_{H_S} \\ &\quad + \frac{1}{2}\hbar\omega_0 \sum_{i=1}^{2} \left(|e\rangle_i \langle e| - |g\rangle_i \langle g| \right), \end{aligned} \tag{7.2}$$

where $T_i(\mathbf{r}_i) = -\frac{\hbar}{2m_i}\nabla^2_{\mathbf{r}_i}$ is the kinetic energy of an atom and $V_t(\mathbf{r}_i) = \frac{1}{2}m_i\omega\mathbf{r}_i^2$ a spherical harmonic trapping potential. The short range interaction term for ultracold bosons is expressed by $V_I(\mathbf{r}) = g\delta_{ps}(\mathbf{r})$ with $\delta_{ps}(\mathbf{r})$ standing for the pseudo potential which depends on dimensionality, see [129]. The interactions strength g can be either positive or negative. Its dependence on the 3D scattering length for quasi-1D or quasi-2D trap was found in [130, 131] and verified experimentally in [225]. Note that for two ultra cold fermions in the same spin state $V_I(\mathbf{r}) = 0$. We denote the spatial part of H_{FS} as H_S. The last sum in Eq. (7.2) describes the internal structure of atoms, which is in a form of a simple two-level model [226]. Here $|g\rangle$ indicates the ground state, $|e\rangle$ stands for the excited state and $\hbar\omega_0$ is the energy difference between two states.

We now shortly introduce the interaction term H_{AF}. We assume a weak classical nearly monochromatic beam with an electric field given by

$$\mathbf{E}(\mathbf{r}, t) = E_0 \left(\epsilon(\mathbf{r}, t) e^{i(\mathbf{k}_L \cdot \mathbf{r} - \omega_L t)} + \epsilon^*(\mathbf{r}, t) e^{-i(\mathbf{k}_L \cdot \mathbf{r} - \omega_L t)} \right), \tag{7.3}$$

where E_0 indicates a real-valued magnitude of an amplitude of the electric field, $\mathbf{k}_L$ a wave vector and ω_L an angular frequency of the light. An envelope of a light pulse denoted by $\epsilon(\mathbf{r}, t)$ is spatially and temporally dependent. We further assume that $|\mathbf{k}_L| \cdot \mathbf{r} \ll 1$ over the atom size. Within this, so-called dipole approximation, the atom-field Hamiltonian reads [226]:

$$H_{AF} = -\sum_{i=1}^{2} \widehat{\mathbf{d}}_i \cdot \mathbf{E}(\mathbf{r}_i, t), \tag{7.4}$$

where $\widehat{\mathbf{d}}_i$ is the dipole moment of an atom. For a gaseous medium $\widehat{\mathbf{d}}_i = ed\left(\sigma_+ + \sigma_-\right)$ with d standing for a transition dipole moment of the atom and e for the elementary charge. Here, $\sigma_\pm$ are the ladder operators defined as $\sigma_+ = |e\rangle \langle g|$ and $\sigma_- = |g\rangle \langle e|$. Then:

$$H_{AF} = \hbar\lambda \sum_{i=1}^{2} \left(\sigma_+^i + \sigma_-^i\right) \left(\epsilon(\mathbf{r}_i, t) e^{i(\mathbf{k}_L \cdot \mathbf{r}_i - \omega_L t)} + c.c. \right), \tag{7.5}$$

We assume a weak intensity of the pulse, so that a parameter $\lambda = \frac{dE_0}{\hbar}$ is small as compared to the other terms in the total Hamiltonian. The last step is to simplify Eq. (7.5) by using the Rotating Wave Approximation (RWA) [226]. Firstly, the only considerably strong interactions between

atoms and the field occur close to the resonance, where $\omega_0 \approx \omega_L$. If one considers a unitary transformation of Eq. (7.5) to the Dirac interaction picture, there would be two slowly-oscillating terms with a frequency $\omega_0 - \omega_L$ and two fast-oscillating terms with a frequency $\omega_0 + \omega_L$. Near the resonance the first two dominate the others. Thus, we omit them in the interaction Hamiltonian. Finally, we obtain:

$$H_{AF} = \hbar\lambda \sum_{i=1}^{2} \left(\sigma_+^i e^{i(\mathbf{k}_L \cdot \mathbf{r}_i - \omega_L t)} + \sigma_-^i e^{-i(\mathbf{k}_L \cdot \mathbf{r}_i - \omega_L t)} \right) \tag{7.6}$$

A state vector $\mathbf{\Psi}(\mathbf{r}_1, \mathbf{r}_2, t)$ of two atoms within our model can be written in a general form as:

$$\mathbf{\Psi}(\mathbf{r}_1, \mathbf{r}_2, t) = \begin{pmatrix} \phi(\mathbf{r}_1, \mathbf{r}_2, t) \left| gg \right\rangle \\ \frac{1}{\sqrt{2}} \left(\chi_1(\mathbf{r}_1, \mathbf{r}_2, t) \left| eg \right\rangle + \chi_2(\mathbf{r}_1, \mathbf{r}_2, t) \left| ge \right\rangle \right) \\ \eta(\mathbf{r}_1, \mathbf{r}_2, t) \left| ee \right\rangle \end{pmatrix} \tag{7.7}$$

We want to analyze the time-dependent Shrödinger equation:

$$i\hbar \frac{\partial \mathbf{\Psi}}{\partial t} = H \mathbf{\Psi} \tag{7.8}$$

It can be expressed as a system of equations for unknown functions ϕ, χ_1, χ_2 and η by:

$$\begin{cases} i\hbar\dot{\phi} = (H_S - \hbar\omega_0)\,\phi + \dfrac{\hbar\lambda}{\sqrt{2}} \Big(\epsilon^*(\mathbf{r}_1, t) e^{-i(\mathbf{k_L} \cdot \mathbf{r_1} - \omega_L t)} \chi_1 \\ \qquad\qquad + \epsilon^*(\mathbf{r}_2, t) e^{-i(\mathbf{k_L} \cdot \mathbf{r}_2 - \omega_L t)} \chi_2 \Big) \\ i\hbar\dot{\chi}_1 = H_S \chi_1 + \sqrt{2}\hbar\lambda \Big(\epsilon(\mathbf{r}_1, t) e^{i(\mathbf{k_L} \cdot \mathbf{r}_1 - \omega_L t)} \phi \\ \qquad\qquad + \epsilon^*(\mathbf{r}_2, t) e^{-i(\mathbf{k_L} \cdot \mathbf{r}_2 - \omega_L t)} \eta \Big) \\ i\hbar\dot{\chi}_2 = H_S \chi_2 + \sqrt{2}\hbar\lambda \Big(\epsilon(\mathbf{r}_2, t) e^{i(\mathbf{k_L} \cdot \mathbf{r}_2 - \omega_L t)} \phi \\ \qquad\qquad + \epsilon^*(\mathbf{r}_1, t) e^{-i(\mathbf{k_L} \cdot \mathbf{r}_1 - \omega_L t)} \eta \Big) \\ i\hbar\,\dot{\eta} = (H_S + \hbar\omega_0)\,\eta + \dfrac{\hbar\lambda}{\sqrt{2}} \Big(\epsilon(\mathbf{r}_2, t) e^{i(\mathbf{k_L} \cdot \mathbf{r}_2 - \omega_L t)} \chi_1 \\ \qquad\qquad + \epsilon(\mathbf{r}_1, t) e^{i(\mathbf{k_L} \cdot \mathbf{r}_1 - \omega_L t)} \chi_2 \Big) \end{cases} \tag{7.9}$$

The above system of equations may be solved approximately in the following way. As it was mentioned before we consider a very weak driving to neglect a depletion of the initial state. We also assume that initially two atoms are in the internal ground states, namely that for $t = 0$ a state vector $\mathbf{\Psi}(\mathbf{r}_1, \mathbf{r}_2, 0) = \phi(\mathbf{r}_1, \mathbf{r}_2, 0) \left| gg \right\rangle$. Therefore we assume that during the interaction between the system and the light the state vector remains almost unchanged, that is to say $|\phi| \gg |\chi_1|, |\chi_2| \gg |\eta|$ for the duration of the pulse. Then, introducing the interaction picture by following substitutions $\phi \to \quad e^{i\omega_0 t}\phi$, $\eta \to \quad e^{-iH_S t/\hbar} e^{-i\omega_0 t}\eta$ and $\chi_{1(2)} \to \quad e^{-iH_S t/\hbar}\chi_{1(2)}$ we obtain the

final equations

$$\begin{cases} \phi = e^{-iH_S t/\hbar}\phi(\mathbf{r}_1, \mathbf{r}_2, 0) \\ \dot{\chi}_1 = -i\sqrt{2}\lambda e^{iH_S t/\hbar}\epsilon(\mathbf{r}_1, t)e^{i\mathbf{k_L}\cdot\mathbf{r}_1}e^{-i\Delta t}\phi \\ \dot{\chi}_2 = -i\sqrt{2}\lambda e^{iH_S t/\hbar}\epsilon(\mathbf{r}_2, t)e^{i\mathbf{k_L}\cdot\mathbf{r}_2}e^{-i\Delta t}\phi \\ \dot{\eta} = -i\dfrac{1}{\sqrt{2}}\lambda\Big(e^{iH_S t/\hbar}\epsilon(\mathbf{r}_2, t)e^{i\mathbf{k_L}\cdot\mathbf{r}_2}e^{-i\Delta t}e^{-iH_S t/\hbar}\chi_1 \\ \qquad +e^{iH_S t/\hbar}\epsilon(\mathbf{r}_1, t)e^{i\mathbf{k_L}\cdot\mathbf{r}_1}e^{-i\Delta t}e^{-iH_S t/\hbar}\chi_2\Big) \end{cases} \tag{7.10}$$

where we define a detuning by $\Delta = \omega_L - \omega_0$. One cannot simplify the above equation further because in a general case $\left[\epsilon(\mathbf{r}_i)e^{i\mathbf{k_L}\cdot\mathbf{r}_i}, H_S\right] \neq 0$.

7.2 Solutions

The analytical solutions of the spatial Hamiltonian H_S are well known both for two non-interacting bosons or fermions ($V_I(\mathbf{r}) = 0$) and for two interacting ultra cold bosons [129]. We assume a rectangle pulse envelope. When the light is on $\epsilon(\mathbf{r}, t) = \epsilon(\mathbf{r})$. Thus it is possible to solve Eq. (7.10) analytically. Without loss of generality we choose the initial state as an eigenvector of H_S, namely that:

$$\phi(\mathbf{r}_1, \mathbf{r}_2, 0) = \phi_n(\mathbf{r}_1, \mathbf{r}_2) \tag{7.11}$$

with an index n indicating the n-th eigenvector in a chosen basis. Then, using Dirac notation and a formula $e^{-iH_S t/\hbar} = \sum_i e^{-iE_i t/\hbar}\left|\phi_i\right\rangle\left\langle\phi_i\right|$ with E_i standing for the i-th eigenvalue we find a general solution for χ_1, χ_2 and η as

$$\begin{cases} \phi = e^{-iE_n t/\hbar}\left|\phi_n\right\rangle \\ \chi_1 = -\sqrt{2}\lambda\sum_i \epsilon_{in}\dfrac{\left(e^{i\tilde{\Delta}_{in}t} - 1\right)}{\tilde{\Delta}_{in}}\left|\phi_i\right\rangle \\ \chi_2 = -\sqrt{2}\lambda\sum_i \tilde{\epsilon}_{in}\dfrac{\left(e^{i\tilde{\Delta}_{in}t} - 1\right)}{\tilde{\Delta}_{in}}\left|\phi_i\right\rangle \\ \eta = -\lambda^2\sum_{i,k}\dfrac{\tilde{\epsilon}_{ik}\epsilon_{kn} + \epsilon_{ik}\tilde{\epsilon}_{kn}}{\tilde{\Delta}_{kn}}\times \\ \qquad\left(\dfrac{e^{i\tilde{\Delta}_{ik}t} - 1}{\tilde{\Delta}_{ik}} - \dfrac{e^{i(\tilde{\Delta}_{ik}+\tilde{\Delta}_{kn})t} - 1}{\tilde{\Delta}_{ik} + \tilde{\Delta}_{kn}}\right)\left|\phi_i\right\rangle \end{cases} \tag{7.12}$$

where $\epsilon_{ij} = \left\langle\phi_i\right|\epsilon(\mathbf{r}_1)e^{i\mathbf{k_L}\cdot\mathbf{r}_1}\left|\phi_j\right\rangle$, $\tilde{\epsilon}_{ij} = \left\langle\phi_i\right|\epsilon(\mathbf{r}_2)e^{i\mathbf{k_L}\cdot\mathbf{r}_2}\left|\phi_j\right\rangle$ and obviously $\epsilon_{ij} = \tilde{\epsilon}_{ij}$. Here we define a scalar product by:

$$\left\langle\phi_i\right|\left.\phi_j\right\rangle = \int d\mathbf{r}_1 d\mathbf{r}_2\, \phi_i^*(\mathbf{r}_1, \mathbf{r}_2)\phi_j(\mathbf{r}_1, \mathbf{r}_2). \tag{7.13}$$

The generalized energy difference between i-th and j-th states reads

$$\tilde{\Delta}_{ij} = \Delta_{ij} - \Delta = \frac{E_i - E_j}{\hbar} - \Delta. \tag{7.14}$$

Note that for resonant terms i.e. $\tilde{\Delta}_{ij} = 0$ in any sum of Eq. (7.12) its proper element has to be evaluated by taking a limit $\tilde{\Delta}_{ij} \to 0$. A resonant term behaves as t for χ_1, χ_2 and as t^2 for η. For the clarity of our argumentation hereafter we will take a resonant case with $\Delta = 0$, but our conclusions will hold also for $\Delta \neq 0$ as long as Δ is not too big and RWA holds.

The probabilities of having one or two photons absorbed by atoms are easily defined by

$$P_1(t) = |\chi_1 |eg\rangle + \chi_2 |ge\rangle|^2 = |\chi_1|^2 + |\chi_2|^2 \tag{7.15}$$

and

$$P_2(t) = |\eta |ee\rangle|^2 = |\eta|^2. \tag{7.16}$$

After some straightforward calculations they can be expressed as:

$$P_1(t) = 2\lambda^2 |\epsilon_{nn}|^2 t^2 + 4\lambda^2 \sum_{i \neq n} \frac{|\epsilon_{in}|^2}{\Delta^2{}_{in}} (1 - \cos(\Delta_{in} t)) \tag{7.17}$$

$$P_2(t) = \lambda^4 |\epsilon_{nn}|^4 t^4 + 4\lambda^4 \sum_{\substack{i \neq n \\ k,k'}} \epsilon^*_{ik'} \epsilon^*_{k'n} \epsilon_{ik} \epsilon_{kn} p_{ikk'n}(t), \tag{7.18}$$

where $p_{ikk'n}(t)$ is of order $o(t^4)$ and it is given by:

$$\begin{aligned} p_{ikk'n}(t) = & \frac{1}{\Delta_{k'n}\Delta_{kn}} \left(\frac{e^{i\Delta_{ik}t} - 1}{\Delta_{ik}} - \frac{e^{i(\Delta_{ik}+\Delta_{kn})t} - 1}{\Delta_{ik} + \Delta_{kn}} \right) \\ & \times \left(\frac{e^{-i\Delta_{ik'}t} - 1}{\Delta_{ik'}} - \frac{e^{-i(\Delta_{ik'}+\Delta_{k'n})t} - 1}{\Delta_{ik'} + \Delta_{k'n}} \right) \end{aligned} \tag{7.19}$$

Note that for resonant terms i.e. $\Delta_{ij} = 0$ in any sum of Eq. (7.19) its proper element has to be evaluated by taking a limit $\Delta_{ij} \to 0$. By using Eq. (7.19) it is easy to check that the sum in Eq. (7.18) is a real function of time. A short time characteristic of the probabilities, when $t \ll \Delta_{in}^{-1}$ with i corresponding to the nearest eigenvalue to n, reads:

$$P_1(t) \approx 2\lambda^2 \langle \phi_n | |\epsilon(\mathbf{r}_1)|^2 |\phi_n\rangle t^2, \quad t \to 0 \tag{7.20}$$

$$P_2(t) \approx \lambda^4 \langle \phi_n | |\epsilon(\mathbf{r}_1)|^2 |\epsilon(\mathbf{r}_2)|^2 |\phi_n\rangle t^4, \quad t \to 0. \tag{7.21}$$

The analysis of Eq. (7.17), (7.18), (7.20) and (7.21) reveals an intriguing discrepancy between the short time and the long time behaviour of the probabilities. First of all, the long time probabilities depend on couplings between an actual state of the system and different eigenstates that occur because, for the experimental relevance, beam width must be narrower than a characteristic system width. This fact automatically leads to the conclusion that for longer pulses the information about the actual state of the system is blurred because the atoms move during the measurement. Secondly, although the dominant terms are of the same order in both situations, the coefficients determining their magnitude are not. For the short time the probabilities coefficients are related to the intensity $|\epsilon(\mathbf{r})|^2$. Note that for $P_1(t), \quad t \to 0$ the coefficient in front of t^2 can be rewritten

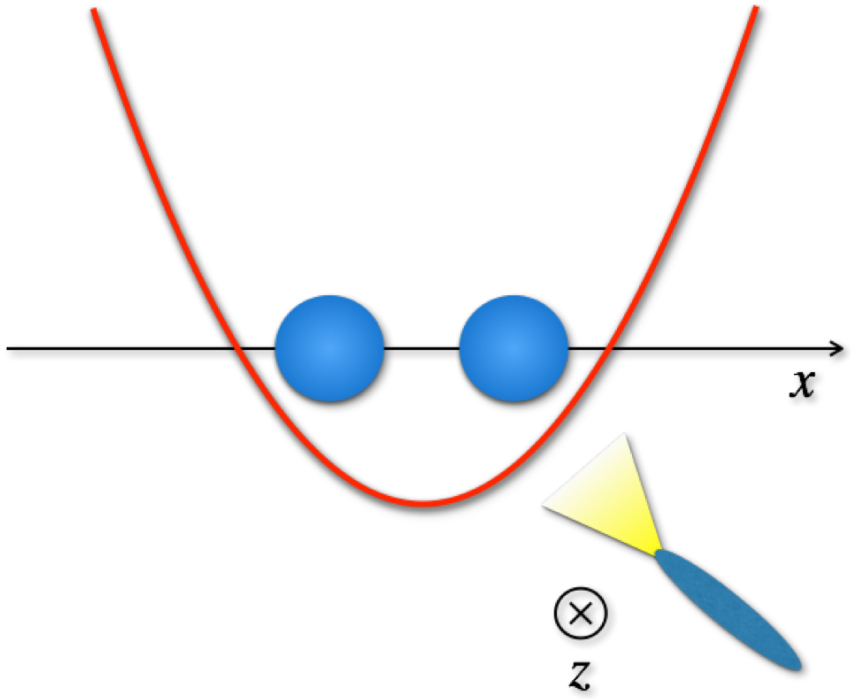

Figure 7.1: Schematic view on a system used in Section 7.3

as $\int d\mathbf{r}\rho(\mathbf{r})\,|\epsilon(\mathbf{r})|^2$ with a one-particle density $\rho(\mathbf{r}) = \int d\mathbf{r}'\,|\phi_n(\mathbf{r},\mathbf{r}')|^2$ which is a very intuitive result. On the other hand the coefficients for the long time depends on the amplitude of the pulse proportional to $\epsilon(\mathbf{r})e^{i\mathbf{k_L}\cdot\mathbf{r}}$ rather than to its intensity alone. In the next section we are going to show the most striking examples of the above differences.

7.3 Results

In this section we present results obtained with our model which are mimicking an experiment diagnosing a quantum state of two ultra cold atoms. We restrict our findings to a quasi-1D system which captures all essential features of our model and provides with a clear picture. In a real experiment it corresponds to cigar-shaped traps with a very strong transverse confinement. We send a probing light pulses along transverse direction z which is related to an electric field

$$\mathbf{E}(\mathbf{r},t) = E_0\left(\epsilon(x)e^{i(k_L z-\omega_L t)} + \epsilon^*(x)e^{-i(k_L z-\omega_L t)}\right). \tag{7.22}$$

with $k_L = |\mathbf{k}_L|$. We may also assume that $1/k_L$ is much bigger than a typical transverse length of a probe so that a driving term $e^{\pm i(k_L z)}$ may be neglected. As the initial state $\phi(x_1,x_2,0)$ we select the ground state both for ideal fermions or bosons and interacting bosons.

7.3.1 One-particle density function

In order to find a one-particle density function we use a single pulse with

$$\epsilon(x;x_0,\sigma) = \frac{1}{\sigma\sqrt{\pi}}e^{-(x-x_0)^2/\sigma^2}. \tag{7.23}$$

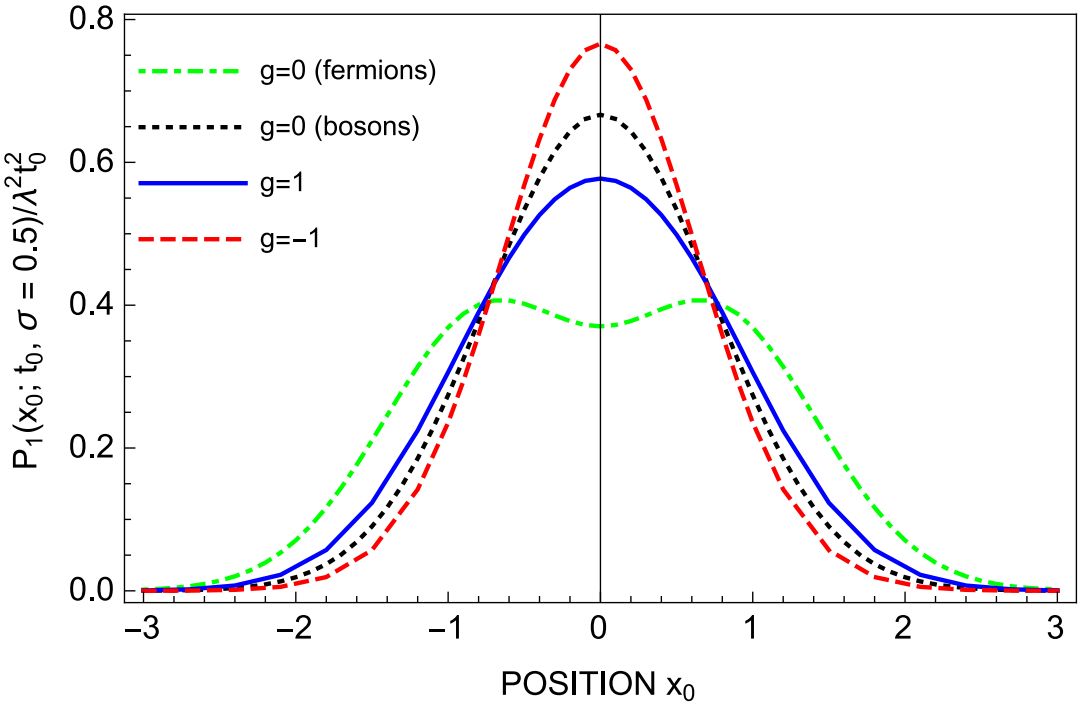

Figure 7.2: One-photon absorption probability $P_1(x_0; t_0, \sigma)/\lambda^2 t_0^2$ as a function of a beam center x_0. A time t_0 was chosen so that Eq. (7.17) and Eq. (7.20) agree with each other i.e. $t_0 = 0.0001\Delta_{10}^{-1}$, where Δ_{10} is the energy difference between the ground and the first excited state. The solid blue line corresponds to two non-interacting bosons, the dashed red line comes from two repulsively interacting bosons, the black dashed line is related to two attractively interacting bosons and the green dashdotted line to two fermions. The oscillatory units are used.

Then, using a short-time characteristic of $P_1(t)$ expressed by Eq. (7.20) we evaluate a probability of one-photon absorption as a function of a position of the pulse center x_0. We compile our results for two non-interacting or interacting bosons and two fermions in Fig. 7.2. As we may note by comparing with the well known analytical solutions of H_S for the ground state the one-photon absorption diagnosis gives a direct access to the one-particle density distribution $\rho(x)$ defined in the preceding section. A clear difference between interacting and non-interacting case is seen as well as between bosons and fermions. A repulsive system distribution is wider than that of an ideal gas, while an attractive system is narrower than the ideal one.

The analysis of Eq. (7.17) shows that using a pulse that is too long may affect a measured one-particle density profile. For pulses with complicated wave fronts the coefficients in the Eq. (7.17) would differ significantly from these of the Eq. (7.20). To illustrate the unwanted field amplitude dependence of the result for long pulses we choose an extreme example of a pulse with cross-section given by

$$\epsilon(x; x_0, \sigma) = \frac{1}{\sigma\sqrt{\pi}} e^{-(x-x_0)^2/\sigma^2} \mathrm{sgn}(x) \tag{7.24}$$

with $\mathrm{sgn}(x)$ staying for the sign function. A comparison between the one-particle density profiles for the non-interacting bosons for two different pulse durations $t_0 = 0.0001\Delta_{10}^{-1}$ and $t_0 = \Delta_{10}^{-1}$,

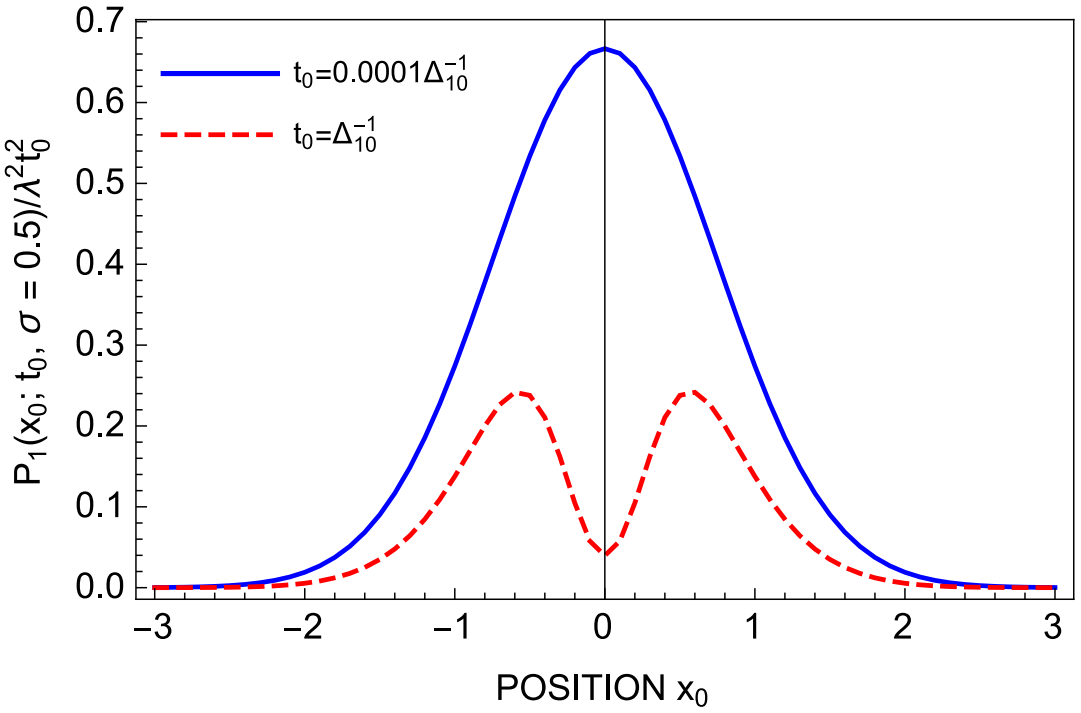

Figure 7.3: One-photon absorption probability $P_1(x_0; t_0, \sigma)/\lambda^2 t_0^2$ as a function of a beam center x_0 for two non-interacting bosons. The solid blue line corresponds to time $t_0 = 0.0001\Delta_{10}^{-1}$, whereas the red dashed line to time $t_0 = \Delta_{10}^{-1}$. The oscillatory units are used.

where Δ_{10} is related to the energy difference between the ground and the first excited state, is presented in Fig. 7.3. For the result based on Eq. (7.17) we truncate the sum at $i = 20$ ensuring that adding another eigenstate would not change the result up to 1% accuracy. A striking difference can be observed. The density profile obtained after a measurement with a long pulse has nothing in common with the actual one-particle density. It is a clear indication that a diagnosis of a few-body quantum state can be highly biased for longer pulses.

7.3.2 Two-body wave function

Measuring a two-photon absorption probability a two-body wave function can be diagnosed. To achieve that one has to use a pulse with a double-focused envelope, namely with

$$\epsilon(x; x_1, x_2, \sigma) = \frac{1}{\sigma\sqrt{\pi}} \left(e^{(x-x_1)^2/\sigma^2} + e^{(x-x_2)^2/\sigma^2} \right). \tag{7.25}$$

Then a coefficient in Eq. (7.21) reads

$$\begin{aligned} &\langle \phi_G | \, |\epsilon(x; x_1, x_2, \sigma)|^2 \, |\epsilon(y; x_1, x_2, \sigma)|^2 \, | \phi_G \rangle \approx \\ &\quad \Big\langle \phi_G | 2 \, |\epsilon(x; x_1, \sigma)|^2 \, |\epsilon(y; x_2, \sigma)|^2 + |\epsilon(x; x_1, \sigma)|^2 \times \\ &\qquad |\epsilon(y; x_1, \sigma)|^2 + |\epsilon(x; x_2, \sigma)|^2 \, |\epsilon(y; x_2, \sigma)|^2 \, | \phi_G \Big\rangle \end{aligned} \tag{7.26}$$

with $|\phi_G\rangle$ denoting the ground state of H_S. Here we neglect the interference terms like

$$e^{(x-x_1)^2/\sigma^2} e^{(x-x_2)^2/\sigma^2}$$

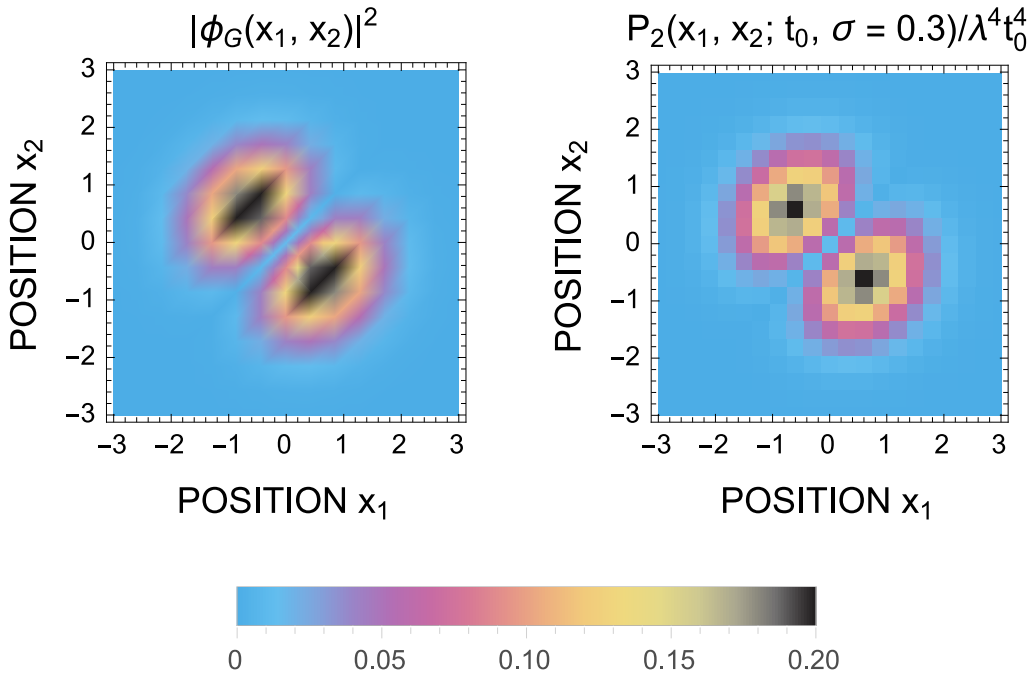

Figure 7.4: Two-photon absorption probability $P_2(x_1, x_2; t_0, \sigma)/\lambda^4 t_0^4$ for two interacting bosons with $g = 6$ as a function of a beam positions x_1 and x_2 for $t_0 = 0.0001\Delta_{10}^{-1}$ after subtracting a single beam two-photon absorption (right). The oscillatory units are used. Left plot shows the analytical solution of $|\phi_G(x_1, x_2)|^2$ for $g = 6$.

that in experiment can be realized either by ensuring $|x_1 - x_2| > 3\sigma$ or by introducing a phase difference between two pulses and averaging over many measurements. The last two terms of a sum in the above equation are corresponding to processes where two photons were absorbed at the same space point. The probability of such a process should be measured independently and then subtracted from the total result of the two-photon absorption. The easiest way to notice that is by assumption that $|\epsilon(x; x_1, \sigma)|^2 \approx \delta(x - x_1)$ which makes $\langle\phi_G| \, |\epsilon(x; x_1, x_2, \sigma)|^2 \, |\epsilon(y; x_1, x_2, \sigma)|^2 \, |\phi_G\rangle \approx 2\,|\phi_G(x_1, x_2)|^2 + |\phi_G(x_1, x_1)|^2 + |\phi_G(x_2, x_2)|^2$.

We sum up our considerations with an example of two repulsive bosons with interaction strength $g = 6$. The total two-photon absorption probability $P_2(t)$ was found for $t_0 = 0.0001\Delta_{10}^{-1}$ and for several beam positions x_1 and x_2. Then we subtract from it the probabilities of a single pulse two-photon absorption. Finally we compare our findings with the analytical solution for $\phi_G(x, y)$ which is plotted in Fig. 7.4. It is a straightforward observation that we reconstructed the actual two-body wave function density with our model.

Analogously to the previous subsection the results for a long pulse in a time domain when Eq. (7.18) holds may lead to a wrong two-body wave function. One more time we use the example of the highly modified wave front with

$$\epsilon(x; x_1, x_2, \sigma) = \frac{1}{\sigma\sqrt{\pi}} \left(e^{(x-x_1)^2/\sigma^2} + e^{(x-x_2)^2/\sigma^2} \right) \mathrm{sgn}(x). \tag{7.27}$$

The resulting two-photon probability absorption $P_2(t)/\lambda^4 t^4$ for $t_0 = 0.0001\Delta_{10}^{-1}$ and $t_0 = \Delta_{10}^{-1}$

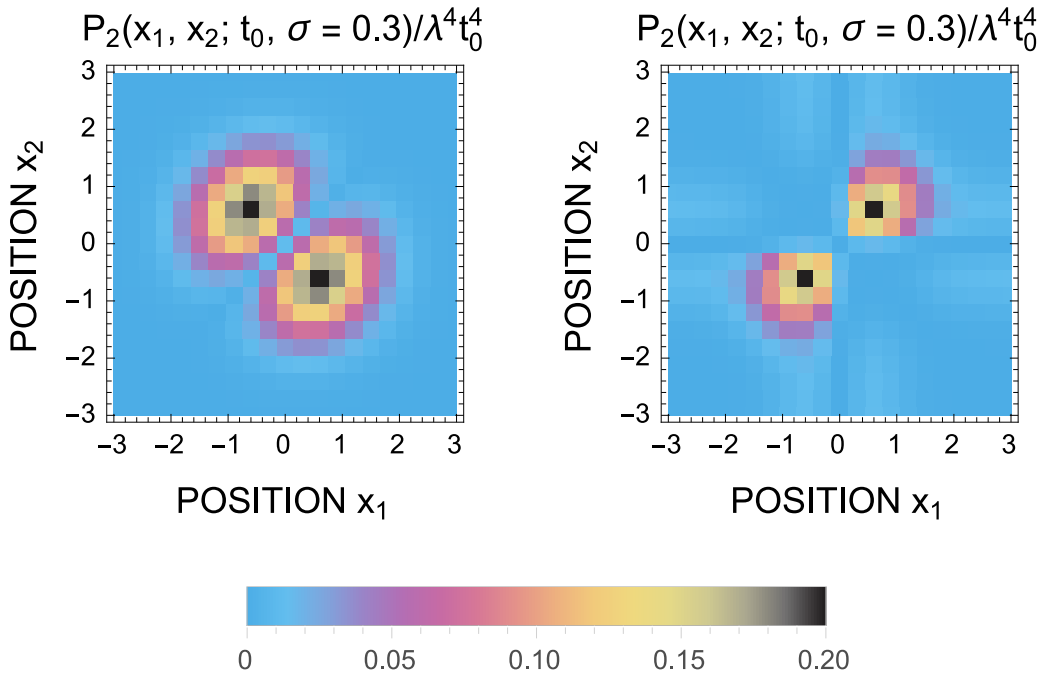

Figure 7.5: Two-photon absorption probability $P_2(x_1, x_2; t_0, \sigma)/\lambda^4 t_0^4$ for two interacting bosons with $g = 6$ as a function of a beam positions x_1 and x_2 for $t_0 = 0.0001\Delta_{10}^{-1}$ (left) and $t_0 = \Delta_{10}^{-1}$ (right) after subtracting a single beam two-photon absorption. The oscillatory units are used.

for two interacting bosons with $g = 6$ as a function of beam positions can be found in Fig. 7.5. For the result based on Eq. (7.18) we truncate the sum at $i = 20$ ensuring that adding another eigenstate would not change the result up to 1%. accuracy. Our findings stress the fact that a pulse duration in an experimental diagnosis should be chosen very carefully.

7.4 Conclusions

In conclusions, we studied a simple model of diagnosing a two-body state with light for interacting or non-interacting bosons and fermions. We demonstrated that results of an experiment based on our theory would crucially depend on a pulse duration. For sufficiently short pulses, we estimate with our measurement the actual one-particle density function and the two-body wave function. For longer pulses a hypothetical experimental findings would be highly biased. The main reason for that is that the calculated probabilities of one-photon or two-photons absorptions are related to the intensity of the light beam for sufficiently short time, whereas for longer time they depend on the amplitude of a pulse. The structure of Eq. (7.17) and Eq. (7.18) can be understood that the probability of the absorption in a space point is strongly blurred by free evolution of the initial state. Note that the solutions found in the preceding sections are valid if only we use a weak beam i.e. $\lambda \ll 1$ and consider time t much shorter than $1/\omega_0$. To make our predictions more realistic, the spontaneous emission should be included.

In principle, our results may be easily generalized to systems containing more particles. If we

are interested in the second-order correlation function it is still a two-photon absorption problem. The only difference lays in combinatorics. On the other hand, considering higher order processes within analogous approach would allow to investigate an experimental procedure of diagnosing higher-order correlation functions from the many-body perspective.

Chapter 8

Conclusions and outlook

Recently, we have been observing amazing progress in controlling and preparing ultracold systems with highly magnetic atoms in various configurations of trapping potential with an anisotropy change at hand. Modern experiments easily explore three-dimensional scenarios with isotropic traps as well as the one-dimensional world with highly anisotropic cigar-shaped traps. With experimental implements like in Innsbruck lab, we are now closer to examine the physics of small systems with a few atoms and stronger interactions between them allowing simulations of even more complicated theories from various field of physics with a crucial contribution from non-local forces. The mean field approaches describe such systems only in the limit of vanishing interactions. Therefore, new theoretical tools are of need, whose devising remains a challenging task. On the other hand, measuring different properties of the few-body system requires an improved understanding of the methods usually utilized with ultracold gases. Our efforts stretched on many different theoretical approaches give new insights to all of these problems. We summarize the main achievements of this thesis and present possible extensions of our work in the following way.

- We have studied the properties of atom-atom interaction in case of two dipolar atoms in a harmonic trap. We have predicted the experimental possibility of pumping the system from the s-wave to the d-wave relative motion. Our results have been already extended for the case with an external magnetic field [222] and with electric dipoles [227] within the same approach as we have proposed in this thesis. On the other hand, the eigenvalues of a system consisting of two dipolar atoms moving in a cylindrical trap depend on their polarisation. The authors of [32] suggested that one can use this fact to determine the value of the scattering length in the system and proposed a very simplified theoretical model of such measurement. With our methods, we can generalize our results from the isotropic trap to the cylindrical trap providing a more accurate description of the process.

- We have examined dipolar atoms in one dimension for different polarizations. Accordingly, we were able to investigate the influence of the interplay of local and non-local interactions on the ground state and low-lying excitations of the system in different scenarios.

- We have shown that some Dicke states, which are solutions of the ideal gas problem, encode

hallmark features of dark solitons in a weakly repulsive system of bosons. However, one needs larger systems to consider in order to find correspondence between the recent discovery of dipolar dark solitons within the MF and the underlying many-body problem. This comes from the fact, that small healing lengths require large interactions for a few-body system making their description beyond the weakly interacting limit crucial for the MF foundations. We plan to achieve larger systems by using a new approach devised in [228].

- We have found numerically exactly the roton state for small one-dimensional systems with stronger interactions beyond the Bogoliubov approximation, but still far weaker than in superfluid Helium case. We have studied spatial properties of the roton which are accessible in experiments. Two immediate possibilities of extending our work appear. First of all, by going to a bit larger system with a bit weaker interactions respectively, we would like to study the case, where the roton minimum has the same energy as the ground state becoming a meta-stable state. It would open a possibility to explore the supersolid state from the many-body perspective. Note, that spatial structures found in this thesis are similar to the ones recently measured in three different labs. [36–38]. Second of all, in the case of repulsive interactions type-I as well as type-II interactions are expected for atoms moving on the circumference of a ring. It is an open question of whether type-II excitations also exist in the spectrum for the rotonic case.

- We have discovered a novel droplet-soliton transition in the one-dimenisonal system without advocating for LHY corrections and for stronger interactions than in [107]. It would be a natural step to determine the character of the transition: is it a crossover or a phase transition? In future, we plan to answer this question by chemical potential analysis as the function of a number of atoms and f_{dd}.

- We have proposed a microscopic model of a two-body wave function diagnosis and analyze the influence of the pulse duration on the absorption imaging. Within the same approach, we would like to generalize our results on the measurement of the higher-order correlations functions. It would be a physical realization of the symmetry breaking process introduced in [124, 125, 139].

Bibliography

[1] S. Giorgini, L. P. Pitaevskii, and S. Stringari, Rev. Mod. Phys. **80**, 1215–1274 (2008).

[2] Bose, Zeitschrift für Physik **26**, 178–181 (1924).

[3] W. Natanson, *On the statistical theory of radiation* (Imprimerie de l'Université, 1911).

[4] W. Natanson, *On the Energy-content of material Bodies* (Imprimerie de l'Université, 1912).

[5] A. Einstein, Sitzber. Kgl. Preuss. Akad. Wiss **3**, 1925 (1925).

[6] L. Tisza, Nature **141**, 913 (1938).

[7] F. London, London **141**, 643 (1938).

[8] A. Griffin, D. W. Snoke, and S. Stringari, *Bose-einstein condensation* (Cambridge University Press, 1996).

[9] C. N. Cohen-Tannoudji, Rev. Mod. Phys. **70**, 707–719 (1998).

[10] W. D. Phillips, Rev. Mod. Phys. **70**, 721–741 (1998).

[11] S. Chu, Rev. Mod. Phys. **70**, 685–706 (1998).

[12] E. A. Cornell and C. E. Wieman, Rev. Mod. Phys. **74**, 875–893 (2002).

[13] W. Ketterle, Rev. Mod. Phys. **74**, 1131–1151 (2002).

[14] W. Ketterle, S. Inouye, M. R. Andrews, J. Stenger, H.-J. Miesner, and D. M. Stamper-Kurn, Nature **392**, 151–154 (1998).

[15] A. J. Leggett, Rev. Mod. Phys. **73**, 307–356 (2001).

[16] I. Bloch, J. Dalibard, and W. Zwerger, Rev. Mod. Phys. **80**, 885–964 (2008).

[17] L. Pitaevskii and S. Stringari, *Bose-Einstein condensation and superfluidity*, Vol. 164 (Oxford University Press, 2016).

[18] A. Acín, I. Bloch, H. Buhrman, T. Calarco, C. Eichler, J. Eisert, D. Esteve, N. Gisin, S. J. Glaser, F. Jelezko, S. Kuhr, M. Lewenstein, M. F. Riedel, P. O. Schmidt, R. Thew, A. Wallraff, I. Walmsley, and F. K. Wilhelm, New Journal of Physics **20**, 080201 (2018).

[19] K. Góral, K. Rzążewski, and T. Pfau, Phys. Rev. A **61**, 051601 (2000).

[20] S. Yi and H. Pu, Physical review letters **97**, 020401 (2006).

[21] M. Vengalattore, S. Leslie, J. Guzman, and D. Stamper-Kurn, Physical review letters **100**, 170403 (2008).

[22] Y. Kawaguchi, H. Saito, K. Kudo, and M. Ueda, Physical Review A **82**, 043627 (2010).

[23] A. Griesmaier, J. Werner, S. Hensler, J. Stuhler, and T. Pfau, Phys. Rev. Lett. **94**, 160401 (2005).

[24] Q. Beaufils, T. Zanon, R. Chicireanu, B. Laburthe-Tolra, E. Maréchal, L. Vernac, J.-C. Keller, and O. Gorceix, Phys. Rev. A **78**, 051603 (2008).

[25] M. Lu, N. Q. Burdick, S. H. Youn, and B. L. Lev, Phys. Rev. Lett. **107**, 190401 (2011).

[26] Y. Tang, N. Q. Burdick, K. Baumann, and B. L. Lev, New J. Phys. **17**, 045006 (2015).

[27] K. Aikawa, A. Frisch, M. Mark, S. Baier, A. Rietzler, R. Grimm, and F. Ferlaino, Phys. Rev. Lett. **108**, 210401 (2012).

[28] T. Koch, T. Lahaye, J. Metz, B. Fröhlich, A. Griesmaier, and T. Pfau, Nature physics **4**, 218 (2008).

[29] T. Lahaye, C. Menotti, L. Santos, M. Lewenstein, and T. Pfau, Reports on Progress in Physics **72**, 126401 (2009).

[30] C. Trefzger, C. Menotti, B. Capogrosso-Sansone, and M. Lewenstein, Journal of Physics B: Atomic, Molecular and Optical Physics **44**, 193001 (2011).

[31] M. Lewenstein, A. Sanpera, and V. Ahufinger, *Ultracold Atoms in Optical Lattices: Simulating quantum many-body systems* (OUP Oxford, 2012).

[32] S. Baier, M. J. Mark, D. Petter, K. Aikawa, L. Chomaz, Z. Cai, M. Baranov, P. Zoller, and F. Ferlaino, Science **352**, 201–205 (2016), http://science.sciencemag.org/content/352/6282/201.full.pdf .

[33] M. Schmitt, M. Wenzel, F. Böttcher, I. Ferrier-Barbut, and T. Pfau, Nature **539**, 259–262 (2016).

[34] L. Chomaz, S. Baier, D. Petter, M. J. Mark, F. Wächtler, L. Santos, and F. Ferlaino, Phys. Rev. X **6**, 041039 (2016).

[35] L. Chomaz, R. Bijnen, D. Petter, G. Faraoni, S. Baier, J. Becher, M. Mark, F. Wächtler, L. Santos, and F. Ferlaino, Nat. Phys. **14**, 442 (2018).

[36] L. Tanzi, E. Lucioni, F. Famà, J. Catani, A. Fioretti, C. Gabbanini, R. N. Bisset, L. Santos, and G. Modugno, Phys. Rev. Lett. **122**, 130405 (2019).

[37] F. Böttcher, J.-N. Schmidt, M. Wenzel, J. Hertkorn, M. Guo, T. Langen, and T. Pfau, Phys. Rev. X **9**, 011051 (2019).

[38] L. Chomaz, D. Petter, P. Ilzhöfer, G. Natale, A. Trautmann, C. Politi, G. Durastante, R. M. W. van Bijnen, A. Patscheider, M. Sohmen, M. J. Mark, and F. Ferlaino, Phys. Rev. X **9**, 021012 (2019).

[39] G. E. Astrakharchik and Y. E. Lozovik, Phys. Rev. A **77**, 013404 (2008).

[40] A. Einstein and W. J. de Haas, Verh. Dtsch. Phys. Ges. **17**, 152–170 (1915).

[41] O. Penrose and L. Onsager, Phys. Rev. **104**, 576–584 (1956).

[42] L. Pitaevskii, Sov. Phys. JETP **13**, 451–454 (1961).

[43] E. P. Gross, Il Nuovo Cimento (1955-1965) **20**, 454–477 (1961).

[44] D. Frantzeskakis, Journal of Physics A: Mathematical and Theoretical **43**, 213001 (2010).

[45] D. D. J. Korteweg and D. G. de Vries, The London, Edinburgh, and Dublin Philosophical Magazine and Journal of Science **39**, 422–443 (1895), https://doi.org/10.1080/14786449508620739 .

[46] E. Bour, J. Ecole Imperiale Polytechnique **19**, 1–48 (1862).

[47] J. Frenkel and T. Kontorova, Izvestiya. Akademii Nauk SSR, Seriya Fizicheskaya **1**, 137–149 (1939).

[48] Y. S. Kivshar and B. Luther-Davies, Physics Reports **298**, 81–197 (1998).

[49] V. E. Zakharov and A. Shabat, Zh. Eksp. Teor. Fiz. **61**, 118 (1971).

[50] V. E. Zakharov and A. Shabat, Zh. Eksp. Teor. Fiz. **64**, 1627 (1973).

[51] S. Burger, K. Bongs, S. Dettmer, W. Ertmer, K. Sengstock, A. Sanpera, G. V. Shlyapnikov, and M. Lewenstein, Phys. Rev. Lett. **83**, 5198–5201 (1999).

[52] J. Denschlag, J. E. Simsarian, D. L. Feder, C. W. Clark, L. A. Collins, J. Cubizolles, L. Deng, E. W. Hagley, K. Helmerson, W. P. Reinhardt, *et al.*, Science **287**, 97–101 (2000).

[53] P. Engels, I. Coddington, P. C. Haljan, V. Schweikhard, and E. A. Cornell, Phys. Rev. Lett. **90**, 170405 (2003).

[54] K. Pawłowski and K. Rzażewski, New Journal of Physics **17**, 105006 (2015).

[55] M. J. Edmonds, T. Bland, D. H. J. O'Dell, and N. G. Parker, Phys. Rev. A **93**, 063617 (2016).

[56] T. Bland, K. Pawłowski, M. J. Edmonds, K. Rzążewski, and N. G. Parker, Phys. Rev. A **95**, 063622 (2017).

[57] T. Bland, *Elementary and topological excitations in ultracold dipolar Bose gases*, Ph.D. thesis, Newcastle University (2018).

[58] J. Allen and A. Misener, Nature **141**, 75 (1938).

[59] P. Kapitza, Nature **141**, 74 (1938).

[60] L. Landau, Phys. Rev. **60**, 356–358 (1941).

[61] L. Landau, Journal of Physics **5**, 71 (1941).

[62] L. Landau, Journal of Physics **11**, 91 (1947).

[63] P. L. Kapitza, Phys. Rev. **60**, 354–355 (1941).

[64] V. Peshkov, Journal of Physics **10**, 389 (1946).

[65] R. P. Feynman, Phys. Rev. **94**, 262–277 (1954).

[66] R. P. Feynman and M. Cohen, Phys. Rev. **102**, 1189–1204 (1956).

[67] D. Henshaw and A. Woods, Physical Review **121**, 1266 (1961).

[68] D. E. Galli, E. Cecchetti, and L. Reatto, Phys. Rev. Lett. **77**, 5401–5404 (1996).

[69] V. Apaja and M. Saarela, Phys. Rev. B **57**, 5358–5361 (1998).

[70] J. L. Epstein and E. Krotscheck, Phys. Rev. B **37**, 1666–1679 (1988).

[71] B. E. Clements, H. Godfrin, E. Krotscheck, H. J. Lauter, P. Leiderer, V. Passiouk, and C. J. Tymczak, Phys. Rev. B **53**, 12242–12252 (1996).

[72] B. E. Clements, E. Krotscheck, and C. J. Tymczak, Phys. Rev. B **53**, 12253–12275 (1996).

[73] R. Rota, F. Tramonto, D. E. Galli, and S. Giorgini, Phys. Rev. B **88**, 214505 (2013).

[74] R. M. Wilson, *Manifestations of the Roton in Dipolar Bose-Einstein Condensates*, Ph.D. thesis, University of Colorado at Boulder (2011).

[75] L. Santos, G. V. Shlyapnikov, and M. Lewenstein, Phys. Rev. Lett. **90**, 250403 (2003).

[76] D. H. J. O'Dell, S. Giovanazzi, and G. Kurizki, Phys. Rev. Lett. **90**, 110402 (2003).

[77] J. L. Bohn, R. M. Wilson, and S. Ronen, Laser Phys. **19**, 547–549 (2009).

[78] U. R. Fischer, Phys. Rev. A **73**, 031602 (2006).

[79] S. Ronen, D. C. Bortolotti, and J. L. Bohn, Phys. Rev. Lett. **98**, 030406 (2007).

[80] R. M. Wilson, S. Ronen, J. L. Bohn, and H. Pu, Phys. Rev. Lett. **100**, 245302 (2008).

[81] J. L. Bohn, R. M. Wilson, and S. Ronen, Laser Phys. **19**, 547–549 (2009).

[82] N. Parker, C. Ticknor, A. Martin, and D. O'Dell, Phys. Rev. A **79**, 013617 (2009).

[83] R. M. Wilson, S. Ronen, and J. L. Bohn, Phys. Rev. Lett. **104**, 094501 (2010).

[84] R. Nath and L. Santos, Phys. Rev. A **81**, 033626 (2010).

[85] M. Klawunn, A. Recati, L. Pitaevskii, and S. Stringari, Phys. Rev. A **84**, 033612 (2011).

[86] A. Martin and P. Blakie, Phys. Rev. A **86**, 053623 (2012).

[87] P. Blakie, D. Baillie, and R. Bisset, Phys. Rev. A **86**, 021604 (2012).

[88] M. Jona-Lasinio, K. Łakomy, and L. Santos, Phys. Rev. A **88**, 013619 (2013).

[89] R. Bisset, D. Baillie, and P. Blakie, Phys. Rev. A **88**, 043606 (2013).

[90] R. Bisset and P. Blakie, Phys. Rev. Lett. **110**, 265302 (2013).

[91] M. Jona-Lasinio, K. Łakomy, and L. Santos, Phys. Rev. A **88**, 025603 (2013).

[92] J. P. Corson, R. M. Wilson, and J. L. Bohn, Phys. Rev. A **87**, 051605 (2013).

[93] P. Blakie, D. Baillie, and R. Bisset, Phys. Rev. A **88**, 013638 (2013).

[94] S. S. Natu, L. Campanello, and S. D. Sarma, Phys. Rev. A **90**, 043617 (2014).

[95] D. Petrov, Phys. Rev. Lett. **115** (2015), 10.1103/physrevlett.115.155302.

[96] H. Kadau, M. Schmitt, M. Wenzel, C. Wink, T. Maier, I. Ferrier-Barbut, and T. Pfau, Nature **530**, 194–197 (2016).

[97] I. Ferrier-Barbut, H. Kadau, M. Schmitt, M. Wenzel, and T. Pfau, Phys. Rev. Lett. **116**, 215301 (2016).

[98] F. Wächtler and L. Santos, Phys. Rev. A **93**, 061603 (2016).

[99] F. Wächtler and L. Santos, Phys. Rev. A **94**, 043618 (2016).

[100] D. Baillie, R. M. Wilson, R. N. Bisset, and P. B. Blakie, Phys. Rev. A **94**, 021602 (2016).

[101] A. R. P. Lima and A. Pelster, Phys. Rev. A **84**, 041604 (2011).

[102] A. R. P. Lima and A. Pelster, Phys. Rev. A **86**, 063609 (2012).

[103] R. Ołdziejewski and K. Jachymski, Phys. Rev. A **94** (2016), 10.1103/physreva.94.063638.

[104] F. Böttcher, M. Wenzel, J.-N. Schmidt, M. Guo, T. Langen, I. Ferrier-Barbut, T. Pfau, R. Bombín, J. Sánchez-Baena, J. Boronat, *et al.*, arXiv preprint arXiv:1904.10349 (2019).

[105] D. S. Petrov and G. E. Astrakharchik, Phys. Rev. Lett. **117**, 100401 (2016).

[106] K. Jachymski and R. Ołdziejewski, Phys. Rev. A **98**, 043601 (2018).

[107] D. Edler, C. Mishra, F. Wächtler, R. Nath, S. Sinha, and L. Santos, Phys. Rev. Lett. **119**, 050403 (2017).

[108] B. B. Baizakov, F. K. Abdullaev, B. A. Malomed, and M. Salerno, Journal of Physics B: Atomic, Molecular and Optical Physics **42**, 175302 (2009).

[109] P. Courteille, R. S. Freeland, D. J. Heinzen, F. A. van Abeelen, and B. J. Verhaar, Phys. Rev. Lett. **81**, 69–72 (1998).

[110] T. Giamarchi, *Quantum physics in one dimension*, Vol. 121 (Clarendon press, 2003).

[111] F. Franchini, *An introduction to integrable techniques for one-dimensional quantum systems*, Vol. 940 (Springer, 2017).

[112] A. Imambekov, T. L. Schmidt, and L. I. Glazman, Rev. Mod. Phys. **84**, 1253 (2012).

[113] E. H. Lieb and W. Liniger, Phys. Rev. **130**, 1605–1616 (1963).

[114] E. H. Lieb, Phys. Rev. **130**, 1616–1624 (1963).

[115] J.-S. Caux and P. Calabrese, Phys. Rev. A **74**, 031605 (2006).

[116] F. Meinert, M. Panfil, M. J. Mark, K. Lauber, J.-S. Caux, and H.-C. Nägerl, Phys. Rev. Lett. **115**, 085301 (2015).

[117] P. P. Kulish, S. V. Manakov, and L. D. Faddeev, Theoretical and Mathematical Physics **28**, 615–620 (1976).

[118] M. Ishikawa and H. Takayama, Journal of the Physical Society of Japan **49**, 1242–1246 (1980), https://doi.org/10.1143/JPSJ.49.1242 .

[119] R. Kanamoto, L. D. Carr, and M. Ueda, Phys. Rev. Lett. **100**, 060401 (2008).

[120] R. Kanamoto, L. D. Carr, and M. Ueda, Phys. Rev. A **81**, 023625 (2010).

[121] E. Kaminishi, R. Kanamoto, J. Sato, and T. Deguchi, Phys. Rev. A **83**, 031601 (2011).

[122] O. Fialko, M.-C. Delattre, J. Brand, and A. R. Kolovsky, Physical review letters **108**, 250402 (2012).

[123] J. Sato, R. Kanamoto, E. Kaminishi, and T. Deguchi, Phys. Rev. Lett. **108**, 110401 (2012).

[124] A. Syrwid and K. Sacha, Physical Review A **92**, 032110 (2015).

[125] A. Syrwid, M. Brewczyk, M. Gajda, and K. Sacha, Physical Review A **94**, 023623 (2016).

[126] J. Sato, R. Kanamoto, E. Kaminishi, and T. Deguchi, New Journal of Physics **18**, 075008 (2016).

[127] E. Kaminishi, T. Mori, and S. Miyashita, "Construction of quantum dark soliton in one-dimensional bose gas," (2018), arXiv:1811.00211 .

[128] S. De Palo, E. Orignac, R. Citro, and M. Chiofalo, Phys. Rev. B **77**, 212101 (2008).

[129] T. Busch, B.-G. Englert, K. Rzążewski, and M. Wilkens, Found. Phys. **28**, 549–559 (1998).

[130] M. Olshanii, Phys. Rev. Lett. **81**, 938–941 (1998).

[131] T. Bergeman, M. G. Moore, and M. Olshanii, Phys. Rev. Lett. **91**, 163201 (2003).

[132] S. Sinha and L. Santos, Phys. Rev. Lett. **99**, 140406 (2007).

[133] F. Deuretzbacher, J. C. Cremon, and S. M. Reimann, Physical Review A **81**, 063616 (2010).

[134] F. Deuretzbacher, J. Cremon, and S. Reimann, Physical Review A **87**, 039903 (2013).

[135] B. Mottelson, Phys. Rev. Lett. **83**, 2695–2698 (1999).

[136] I. Hamamoto and B. Mottelson, Nuclear Physics A **507**, 65 – 78 (1990).

[137] C. Lanczos, *An iteration method for the solution of the eigenvalue problem of linear differential and integral operators* (United States Governm. Press Office Los Angeles, CA, 1950).

[138] M. Płodzień, D. Wiater, A. Chrostowski, and T. Sowiński, arXiv preprint arXiv:1803.08387 (2018).

[139] J. Javanainen and S. M. Yoo, Phys. Rev. Lett. **76**, 161–164 (1996).

[140] R. Bach and K. Rzążewski, Phys. Rev. Lett. **92**, 200401 (2004).

[141] N. Metropolis, A. W. Rosenbluth, M. N. Rosenbluth, A. H. Teller, and E. Teller, The journal of chemical physics **21**, 1087–1092 (1953).

[142] Y. Castin and R. Dum, Phys. Rev. A **57**, 3008–3021 (1998).

[143] M. Greiner, O. Mandel, T. Esslinger, T. W. Hänsch, and I. Bloch, Nature **415**, 39–44 (2002).

[144] M. Greiner, O. Mandel, T. W. Hänsch, and I. Bloch, Nature **419**, 51–54 (2002).

[145] W. S. Bakr, A. Peng, M. E. Tai, R. Ma, J. Simon, J. I. Gillen, S. Folling, L. Pollet, and M. Greiner, Science **329**, 547–550 (2010).

[146] F. Serwane, G. Zurn, T. Lompe, T. B. Ottenstein, A. N. Wenz, and S. Jochim, Science **332**, 336–338 (2011).

[147] M. Köhl, K. Günter, T. Stöferle, H. Moritz, and T. Esslinger, J. Phys. B: At., Mol. Opt. Phys. **39**, S47–S56 (2006).

[148] K. Gawryluk, M. Brewczyk, K. Bongs, and M. Gajda, Phys. Rev. Lett. **99**, 130401 (2007).

[149] Y. Kawaguchi, H. Saito, and M. Ueda, Phys. Rev. Lett. **96**, 080405 (2006).

[150] K. Kanjilal, J. L. Bohn, and D. Blume, Phys. Rev. A **75**, 052705 (2007).

[151] S. Ronen, D. C. E. Bortolotti, D. Blume, and J. L. Bohn, Phys. Rev. A **74** (2006), 10.1103/physreva.74.033611.

[152] A. Petrov, E. Tiesinga, and S. Kotochigova, Phys. Rev. Lett. **109**, 103002 (2012).

[153] T. M. Hanna, E. Tiesinga, W. F. Mitchell, and P. S. Julienne, Phys. Rev. A **85**, 022703 (2012).

[154] E. L. Bolda, E. Tiesinga, and P. S. Julienne, Phys. Rev. A **66**, 013403 (2002).

[155] D. Blume and C. H. Greene, Phys. Rev. A **65**, 043613 (2002).

[156] M. Abramowitz and I. A. Stegun, *Handbook of Mathematical Functions, With Formulas, Graphs, and Mathematical Tables,* (Dover Publications, Incorporated, 1974).

[157] Http://functions.wolfram.com/05.10.16.0007.01.

[158] P. O. Fedichev, Y. Kagan, G. V. Shlyapnikov, and J. T. M. Walraven, Phys. Rev. Lett. **77**, 2913–2916 (1996).

[159] F. K. Fatemi, K. M. Jones, and P. D. Lett, Phys. Rev. Lett. **85**, 4462–4465 (2000).

[160] G. Thalhammer, M. Theis, K. Winkler, R. Grimm, and J. H. Denschlag, Phys. Rev. A **71**, 033403 (2005).

[161] S. Blatt, T. L. Nicholson, B. J. Bloom, J. R. Williams, J. W. Thomsen, P. S. Julienne, and J. Ye, Phys. Rev. Lett. **107**, 073202 (2011).

[162] L. Landau, Phys. Z. Sowjetunion **2**, 46–51 (1932).

[163] C. Zener, Proc. R. Soc. A **137**, 696–702 (1932).

[164] T. Maier, H. Kadau, M. Schmitt, A. Griesmaier, and T. Pfau, Opt. Lett. **39**, 3138 (2014).

[165] R. Oł dziejewski, W. Górecki, K. Pawłowski, and K. Rzażewski, "Roton in a many-body dipolar system," (2018), arXiv:1801.0658 .

[166] R. Kanamoto, L. D. Carr, and M. Ueda, Phys. Rev. A **79**, 063616 (2009).

[167] L. D. Carr, C. W. Clark, and W. P. Reinhardt, Phys. Rev. A **62**, 063611 (2000).

[168] Z. Wu and E. Zaremba, Phys. Rev. A **88**, 063640 (2013).

[169] A. J. Leggett and F. Sols, Foundations of Physics **21**, 353–364 (1991).

[170] M. R. Andrews, C. G. Townsend, H.-J. Miesner, D. S. Durfee, D. M. Kurn, and W. Ketterle, Science **275**, 637–641 (1997).

[171] Y. Castin and J. Dalibard, Phys. Rev. A **55**, 4330–4337 (1997).

[172] Y. Castin and C. Herzog, Comptes Rendus de l'Academie des Sciences de Paris **2**, 419 (2001).

[173] B. Lücke, M. Scherer, J. Kruse, L. Pezzé, F. Deuretzbacher, P. Hyllus, O. Topic, J. Peise, W. Ertmer, J. Arlt, L. Santos, A. Smerzi, and C. Klempt, Science **334**, 773–776 (2011).

[174] X.-Y. Luo, Y.-Q. Zou, L.-N. Wu, Q. Liu, M.-F. Han, M. Khoon Tey, and L. You, Science **355**, 620 (2017).

[175] R. H. Dicke, Phys. Rev. **93**, 99–110 (1954).

[176] D. Bohm, Phys. Rev. **85**, 180–193 (1952).

[177] D. Bohm, Phys. Rev. **85**, 166–179 (1952).

[178] A. Benseny, G. Albareda, A. S.Sanz, J. Mompart, and X. Oriols, EPJ D **68**, 286 (2014).

[179] A. Syrwid and K. Sacha, Phys. Rev. A **96**, 043602 (2017).

[180] S. S. Shamailov and J. Brand, Phys. Rev. A **99**, 043632 (2019).

[181] G. E. Astrakharchik, J. Boronat, I. L. Kurbakov, and Y. E. Lozovik, Phys. Rev. Lett. **98**, 060405 (2007).

[182] F. Mazzanti, R. E. Zillich, G. E. Astrakharchik, and J. Boronat, Phys. Rev. Lett. **102**, 110405 (2009).

[183] D. Hufnagl, E. Krotscheck, and R. E. Zillich, Journal of Low Temperature Physics **158**, 85 (2009).

[184] F. Cinti, P. Jain, M. Boninsegni, A. Micheli, P. Zoller, and G. Pupillo, Phys. Rev. Lett. **105**, 135301 (2010).

[185] S. Baier, D. Petter, J. Becher, A. Patscheider, G. Natale, L. Chomaz, M. Mark, and F. Ferlaino, arXiv:1803.11445 (2018).

[186] O. Fialko, M.-C. Delattre, J. Brand, and A. R. Kolovsky, Phys. Rev. Lett. **108**, 250402 (2012).

[187] R. A. Doganov, S. Klaiman, O. E. Alon, A. I. Streltsov, and L. S. Cederbaum, Phys. Rev. A **87**, 033631 (2013).

[188] J. Von Stecher, C. H. Greene, and D. Blume, Phys. Rev. A **77**, 043619 (2008).

[189] D. Blume, Rep. Prog. Phys. **75**, 046401 (2012).

[190] J. Christensson, C. Forssén, S. Åberg, and S. Reimann, Phys. Rev. A **79**, 012707 (2009).

[191] S. Klaiman, A. U. Lode, A. I. Streltsov, L. S. Cederbaum, and O. E. Alon, Phys. Rev. A **90**, 043620 (2014).

[192] M. Imran and M. Ahsan, Adv. Sci. Lett. **21**, 2764–2767 (2015).

[193] R. Beinke, S. Klaiman, L. S. Cederbaum, A. I. Streltsov, and O. E. Alon, Phys. Rev. A **92**, 043627 (2015).

[194] V. Bolsinger, S. Krönke, and P. Schmelcher, J. Phys. B: At., Mol. Opt. Phys. **50**, 034003 (2017).

[195] V. Bolsinger, S. Krönke, and P. Schmelcher, Phys. Rev. A **96**, 013618 (2017).

[196] P. Jeszenszki, A. Y. Cherny, and J. Brand, Phys. Rev. A **97**, 042708 (2018).

[197] S. Kotochigova, Rep. Prog. Phys. **77**, 093901 (2014).

[198] S. Fölling, F. Gerbier, A. Widera, O. Mandel, T. Gericke, and I. Bloch, Nature **434**, 481–484 (2005).

[199] M. Schellekens, R. Hoppeler, A. Perrin, J. V. Gomes, D. Boiron, A. Aspect, and C. I. Westbrook, Science **310**, 648–651 (2005).

[200] J. Esteve, J.-B. Trebbia, T. Schumm, A. Aspect, C. I. Westbrook, and I. Bouchoule, Phys. Rev. Lett. **96**, 130403 (2006).

[201] T. Jeltes, J. M. McNamara, W. Hogervorst, W. Vassen, V. Krachmalnicoff, M. Schellekens, A. Perrin, H. Chang, D. Boiron, A. Aspect, *et al.*, Nature **445**, 402–405 (2007).

[202] W. Dür, G. Vidal, and J. I. Cirac, Phys. Rev. A **62**, 062314 (2000).

[203] L. Pezzé and A. Smerzi, Phys. Rev. Lett. **102**, 100401 (2009).

[204] F. Haas, J. Volz, R. Gehr, J. Reichel, and J. Estève, Science **344**, 180–183 (2014), http://science.sciencemag.org/content/344/6180/180.full.pdf .

[205] R. N. Bisset, D. Baillie, and P. B. Blakie, Phys. Rev. A **83**, 061602 (2011).

[206] R. N. Bisset, D. Baillie, and P. B. Blakie, Phys. Rev. A **86**, 033609 (2012).

[207] C. Ticknor, Phys. Rev. A **85**, 033629 (2012).

[208] M. J. Edmonds, T. Bland, R. Doran, and N. G. Parker, New Journal of Physics **19**, 023019 (2017).

[209] I. Ferrier-Barbut, M. Wenzel, F. Böttcher, T. Langen, M. Isoard, S. Stringari, and T. Pfau, Phys. Rev. Lett. **120**, 160402 (2018).

[210] C. R. Cabrera, L. Tanzi, J. Sanz, B. Naylor, P. Thomas, P. Cheiney, and L. Tarruell, Science **359**, 301–304 (2018), https://science.sciencemag.org/content/359/6373/301.full.pdf .

[211] P. Cheiney, C. R. Cabrera, J. Sanz, B. Naylor, L. Tanzi, and L. Tarruell, Phys. Rev. Lett. **120**, 135301 (2018).

[212] G. E. Astrakharchik and B. A. Malomed, Phys. Rev. A **98**, 013631 (2018).

[213] E. B. Kolomeisky, T. J. Newman, J. P. Straley, and X. Qi, Phys. Rev. Lett. **85**, 1146–1149 (2000).

[214] G. Lang, F. Hekking, and A. Minguzzi, SciPost Phys. **3**, 003 (2017).

[215] H. Yao, D. Clément, A. Minguzzi, P. Vignolo, and L. Sanchez-Palencia, Phys. Rev. Lett. **121**, 220402 (2018).

[216] F. Meinert, M. Panfil, M. J. Mark, K. Lauber, J.-S. Caux, and H.-C. Nägerl, Phys. Rev. Lett. **115**, 085301 (2015).

[217] J. Grondalski, P. M. Alsing, and I. H. Deutsch, Opt. Express **5**, 249–261 (1999).

[218] E. Altman, E. Demler, and M. D. Lukin, Phys. Rev. A **70**, 013603 (2004).

[219] S. Fölling, F. Gerbier, A. Widera, O. Mandel, T. Gericke, and I. Bloch, Nature **434**, 481–484 (2005).

[220] M. Greiner, C. Regal, J. Stewart, and D. Jin, Phys. Rev. Lett. **94**, 110401 (2005).

[221] E. W. Streed, A. Jechow, B. G. Norton, and D. Kielpinski, Nat. Commun. **3**, 933 (2012).

[222] T. Górski and K. Rzążewski, J. Phys. B: At., Mol. Opt. Phys. **48**, 035303 (2015).

[223] E. Witkowska, M. Gajda, and K. Rzążewski, Phys. Rev. A **79**, 033631 (2009).

[224] M. Brewczyk, M. Gajda, and K. Rzazewski, in *Quantum Gases: Finite Temperature and Non-Equilibrium Dynamics.*, edited by N. Proukakis, S. Gardiner, M. Davies, and M. Szymańska (London: Imperial College Press, 2013) pp. 191–202.

[225] E. Haller, M. J. Mark, R. Hart, J. G. Danzl, L. Reichsöllner, V. Melezhik, P. Schmelcher, and H.-C. Nägerl, Phys. Rev. Lett. **104**, 153203 (2010).

[226] P. Knight and G. Gerry, *Introductory Quantum Optics* (Cambridge University Press, 2005).

[227] W. Górecki and K. Rzążewski, EPL **116**, 26004 (2016).

[228] W. Golletz, W. Górecki, R. Ołdziejewski, and K. Pawłowski, arXiv preprint arXiv:1905.04604 (2019).